Master's thesis

NTNU
Norwegian University of Science and Technology
Faculty of Natural Sciences
Department of Materials Science and Engineering

Marius Larsen

Densification of charcoal by thermal decomposition of methane

Master Thesis

Master's thesis in Materials Science and Engineering
Supervisor: Merete Tangstad
Co-supervisor: Maria Wallin

June 2022

NTNU
Norwegian University of
Science and Technology

Marius Larsen

Densification of charcoal by thermal decomposition of methane

Master Thesis

Master's thesis in Materials Science and Engineering
Supervisor: Merete Tangstad
Co-supervisor: Maria Wallin
June 2022

Norwegian University of Science and Technology
Faculty of Natural Sciences
Department of Materials Science and Engineering

NTNU
Norwegian University of
Science and Technology

Preface

This report describes the effect of certain physical properties of charcoal, as a result of densification through decomposition of methane at elevated temperatures. This assignment is done during the spring of 2022, under the course TMT4905, which is the masters assignment of materials science and engineering.

I would like to thank my supervisor Merete Tangstad and my co-supervisor Maria Wallin for the possibility to work with this project, and for allowing me to participate on different conferences, both domestic and abroad. The opportunity for me to get new contact and to see how other companies and institutions do their work and research has been a highly valuable experience for me, and for that I am grateful. I would also like to thank Merete Tangstad for all the constructive supervisor-meetings we have had, for having great discussions about the subject and a lot of advice, feedback and support. I would also like to thank Hamideh Kaffash, who was my co-supervisor prior to this masters-assignment, for great support and guidance in some of the experimental methods. I would like to thank Yingda Yu, for guidance when it comes to SEM. I would also like to thank Pål Skaret, who assisted me with the compression-testing. I would like to thank Nicholas Smith-Hanssen for all the assistance with the induction furnace, among other things. I would also like to thank Elin Harboe Albertsen for all the times she helped me with the pycnometry-experiments and the BET-experiments. Finally I would like to thank my family and fellow students who helped me through this period with great discussions and advice.

Abstract

(English)

In this project, the densification of charcoal through the use of methane decomposition was examined. In total 6 sample sets, each with an weight of about 350 g were analysed. The different degrees of carbon-deposition that was examined was 10.3 , 11.1, 24.0 and 29.7 wt%, in addition to raw charcoal and charcoal heated with only argon-gas. The results of the densification-experiments showed that the amount of densification was depending on both reaction-temperature and distribution of particle-size, and the results also pointed towards a linear relationship between the purging-time of methane and the amount of deposited carbon, under the same temperature and size-conditions. The analysis and comparison of fraction of methane-conversion showed that 5 out of 7 of the experiments done above 1070 °C had a conversion-value above 35 %. Testing of both the compression-strength and abrasive strength showed that the heating-process with only argon had a greater effect towards increased strength compared to the methane decomposition-reaction. Porosity-testing with absolute and apparent density showed a small trend towards decreased porosity as the amount of deposited carbon increased, and that the density of the deposited carbon is lower than for

the charcoal. The porosity-results done with SEM and ImageJ showed a big standard deviation for the different degrees of densification, but it also showed indications of more porosity in the centre of the samples compared to on the surface. The balance regarding energy and material-flow showed a loss of 1,3% of materials during the densification-process and an electric energy-requirement of 0,52 kwh /kg C input in the furnace when the methane is purging for about 3 hours.

(Norsk)

I dette prosjektet ble densifisering av trekull gjennom dekomponering av metan undersøkt. Totalt ble 6 prøvesett analysert, hver med en vekt på ca 350 g. De ulike gradene av densifisering var 10.3 , 11.1 , 24.0 og 29.7 vkt% (vektprosent), i tillegg til ubehandlet trekull og trekull som var blitt oppvarmet med kun argon-gass. Resultatene av densifiseringseksperimentene viste at mengden densifisering var avhengig av både reaksjons-temperatur og størrelsesfordeling, og resultatene pekte i retning et lineært forhold mellom tid med gasstrømning av metan og mengde deponert karbon, under like temperatur- og størrelsesforhold. Analysen og sammenligningen av andel konvertert metan viste at 5 av 7 eksperiment som hadde reaksjonstemperatur over 1070°C, hadde en konverteringsandel som var høyere enn 35 %. Testing av både kompresjonsstyrke og slipestyrke viste at oppvarmingsprosessen med argon hadde mer effekt på økning av styrke enn selve dekomponeringen av metan. Testing av porøsitet gjennom beregning med absolutt tetthet og tilsynelatende tetthet viste en svak nedgang i porøsitet med stigende grad av dekomonering av karbon, og det viste også at tettheten til det deponerte karbonet var lavere enn tettheten til det ubehandlede trekullet. Testing av porøsitet gjennom SEM og ImageJ viste et stort standardavvik for de ulike gradene av densifisering, men det viste også indikasjoner på en høyere porøsitetsverdi i sentrum av prøven i forhold til på overflaten. Til sist viste energi- og materialbalansen at 1,3 % av materialer går tapt og at det kreves tilførsel av elektrisk energi på 0,52 kwh/ kg karbon innsatt i ovnen når det kjøres forsøk med metan i om lag 3 timer.

Contents

1 Introduction

1.1 Background and motivation

Carbon plays an unique role when it comes to the metal-industry. This is manly due to its great abilities to reduce extracted metal-oxides into pure metal-compounds. As of today, one of the most frequently used carbonaceous materials for metal production is metallurgical coke. One of the big issues and disadvantages to the use of this material, is the relative high amount of CO_2-emission during the industrial process. A very hot topic among researchers nowadays is to try to find a sustainable and more environmental-friendly substitute for such materials, and many studies point towards several alternatives.

One of these alternatives is charcoal. Charcoal is made up of carbonization of wood, and one of the great benefits to using charcoal is that it has a relatively low emission related to production and use [27]. However, using charcoal for industrial purposes such as for metal-production may have some disadvantages and limitations. One of those is that the density of charcoal is significantly lower than for metallurgical coke, which means that a greater amount of charcoal may have to be used to get the same results as for metallurgical coke. This is highly related to the fact that the structure of charcoal is much more affected by pores, and therefore the strength of the material is also lower than for many other carbonaceous materials [19]. These are some the issues that requires

more attention before charcoal can be able to substitute more polluting carbonaceous materials on the market.

1.2 Aim and scope of the work

This work will examine the densification of charcoal by the use of methane decomposition at elevated temperatures. The aim of this project is to see if there are some clear developments on certain physical properties as the densification-time goes on. The physical properties that are planned investigating are density, different types of material-strength, porosity and specific surface area. In addition, there will be a material- and energy-balance calculated for the decomposition-reaction to see how much energy and material is lost/gained related to the industry.

2 Theory/Literature

2.1 Charcoal - Production and properties

Charcoal is a black, porous, carbonaceous residue that results from exposing a specific type of biomass to a pyrolytic process. This process is a high-temperature heating process, with restricted access to oxygen. A typical pyrolysis-reaction of cellulose can be shown as the following reaction [Grønli and Antal jr 2003][2]

$$C_6H_{10}O_5 \rightarrow 3,74C + \ 2,65H_2O + 1,17CO_2 + 1,08CH_4 \tag{2.1}$$

The bio-material is converted to a form of carbon during the pyrolytic process. This is related to the disappearance of various types of volatiles and other substances as a result of evaporation. The most important point is that the removal occurs either as gases or as other volatiles in the smoke. The proportion of volatiles in the feedstock material has a significant impact on whether or not the generated charcoal burns cleanly. Charcoals with a high fraction of volatiles burn at a low temperature and produce a smoky flame, whereas charcoals with a low fraction of volatiles burn considerably more cleanly and are often difficult to ignite[Oyedun et al. 2012] [32].

There are various ways and definitions to what is the ideal temperature for the pyrolytic process, with respect to temperature-ranges. Decomposition of hemicellulose and cellulose, which are important producers of volatiles in the feedstock, takes place at temperatures of $200 - 260°C$ and $240 - 350°C$, respectively, whereas lignin decomposes at a temperature of $280 - 500°C$. According to the work of Oyedun and co-workers [Oyedun et al. 2012][32] , the ideal temperature range for

charcoal production is in the temperature range of about $450 - 500°C$. Antal jr. and Grønli's publications also support this claim, which is illustrated in Figure 1:

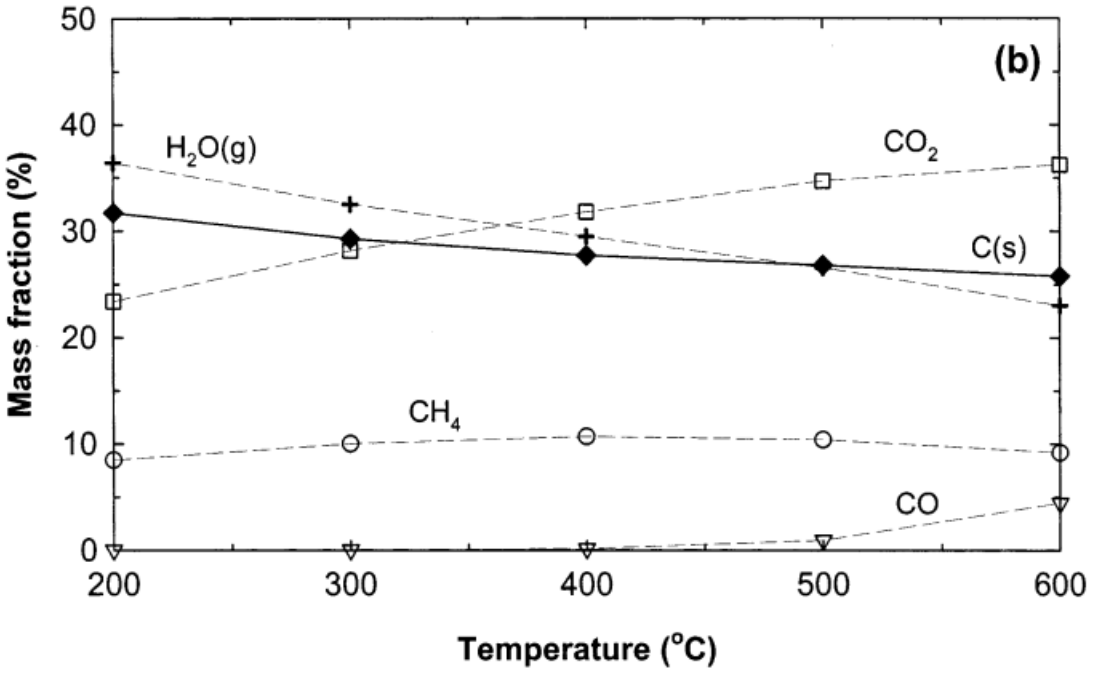

Figure 1: Effects of temperature on the products of cellulose pyrolysis. The results in this figure are produced as a result of thermochemical equilibrium calculations at a fixed pressure at 1 MPa. [Antal Jr 2003] [2]

As one can see in the graph, there is a relatively steep decline at temperatures lower than $400°C$, but according to the authors, this is only of theoretical interest. The reason for this is that at such low temperatures, carbonization rates are so slow that they are regarded unimportant.

There are many important production parameters when it comes to the production of charcoal from biomass. The parameters can have great impact of both chemical and the physical properties of the produced charcoal. Examples of such parameters are **peak temperature** and **moisture** [Antal Jr 2003][2].

2.1.1 Peak temperature

The peak temperature is defined as the highest temperature reached throughout the carbonization process, according to Grønli and Antal jr. [Antal Jr 2003][2], and this temperature may have a significant effect on both the volatile matter and the characteristics of the produced charcoal. The mechanical properties have been demonstrated to be affected by peak temperature. According

to Blankenhorn with others, the dynamic elastic modulus decreases with increasing temperature, reaching a minimum value at 330°C , followed by an equal increase until the temperature reaches around 900°C [Blankenhorn et al. 1972][4].

There are numerous articles that claim that when the peak temperature rises, the compressive strength of the charcoal decreases. According to the mentioned report by Blankenhorn, certain types of wood-materials, such as softwood (e.g. spruce or pine), are more fragile than hardwoods (e.g. alder or birch) [Grønli et al. 1996] [10]. Surrup and co-workers [Surrup et al. 2019] [40] found that when the pyrolytic temperature rises, the char yield decreases. This experiment was carried out at temperatures ranging from $500 - 1300$°C. However, the paper proposes a solution to this problem, which is to include recirculated tar in a co-existing pyrolysis process along with the primary process. At 700 , 900 and 1100 °C, this resulted in a 4% increase in char yield.

The structure of the various types of pores in the material appears to be affected by temperature. According to MacKay and Roberts' articles, the processing of microporosity happens at roughly 500°C. To exceed this temperature will result in an increase in the volume of the micropores. Graphitic or ribbon development has been observed at 400°C, and a further increase in the temperature has been observed to increase the apparent diameter of the areas of the material that are crystalline. This process will lead to an expansion of the edge-groups in the material, which again indicates the formation of the microporous structure at temperatures below 500°C [MacKay and Roberts 1981] [24]. According to the same publication, a further increase from $500 - 700$°C will increase the micropore-volume, mainly because of the removal of non-crystalline components that blocks the pore-entrances. From 700°C there is no significant change in the microporous structure.

The electrical resistance of the charcoal is also affected by temperature. Coutinho's research with coworkers includes, among other things, a measurement of electrical resistivity in biocarbon electrodes (BCE) as a function of heat temperatures, as seen in the picture below (Figure 2). The BCE is made from eucalyptus wood, which is a clean and renewable source of feedstock, as seen in the diagram. The graph demonstrates that the material acts as a non-conductor material until it reaches around 800°C, and that increasing the temperature over 800°C results in more or less constant resistance, which is employed in commercial graphite electrodes [Coutinho et al. 2000][6].

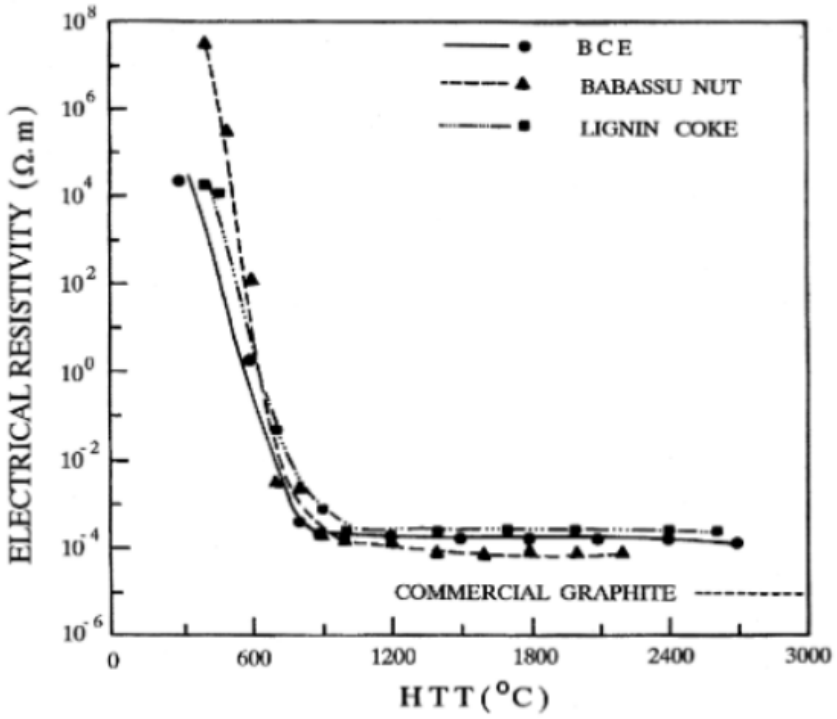

Figure 2: Electrical resistivity as a function of HTT(heating temperature) [6]

There has also been publications investigating the influence of temperature and flow-rate of argon-gas with respect to the synthesis of charcoal from aquatic biomass (duckweed) [Muradov et al. 2012][30]. One of the project's main goals was to look into the long-term relationship between char yield and various pyrolytic parameters, such as temperature and argon-flow-rate, where the argon was utilized as a sweep-gas. The current temperature and argon-flow ranges were 400°C-700°C and 36-150 cm^3min^{-1}, respectively, and the results are shown below (Figure 3)

It is worth noting that the duckweed samples were pre-dried overnight at 120°C, so the influence of moisture may be ignored . The yield in Figure 3b drops from 36-60 cm^3min^{-1}, while increasing the flow-rate causes the yield to stabilize at roughly 46-48 %, but the highest yield of bio-char appears to be in the lower area of the provided temperature-range in Figure 3a . According to the authors, the rapid fall in yield at lower temperatures (from 400°C-500°C) could be due to an increase in the volatilization-rate of organic compounds, which is causing some of the char-related compounds to be released faster. Partially gasified char is likewise ruled out as a viable explanation by the authors. Based on the results above, the main conclusion can be that the ideal conditions for maximum char-yields is at 400°C at a sweeping flow-rate at 60 cm^3min^{-1}.

The flow-rate of inert gas and the temperature is also studied in the publication of Lua and co-

workers [Lua 2006] [23]. In this article, the production of activated carbon from oil-palm-shells are investigated. This article is as mentioned focusing on the influence of temperature and inert gas flow-rate, in addition to holding time and heating-rate. With a temperature-interval of 400°C-900°C, the holding times is varying from 0.5 - 3 hours, the inert gas flow-rate varying from 50-300 cm^3min^{-1} and the heating-rate is varying from $5-50°C/min$.The results are shown in Figure 4 and Figure 5. It is shown in Figure 4 that an increase in pyrolytic temperature leads to a decrease in the volatile content, and it also leads to a decrease in the char-yield and the yield of the activated carbon. This is the same tendencies as shown in the results published by Muradov [30]. Since all the current temperatures are above the evaporation-temperature, there is no clear development when it comes to moisture-content. This means that the effect can rather be neglected. According to the results in Figure 5 an increase in all of the three chosen parameters will lead to an higher rate of release of volatiles. This will obviously lead to a decrease in volatile-content.The rate of decrease seems to be approximately the same for each of the parameters.

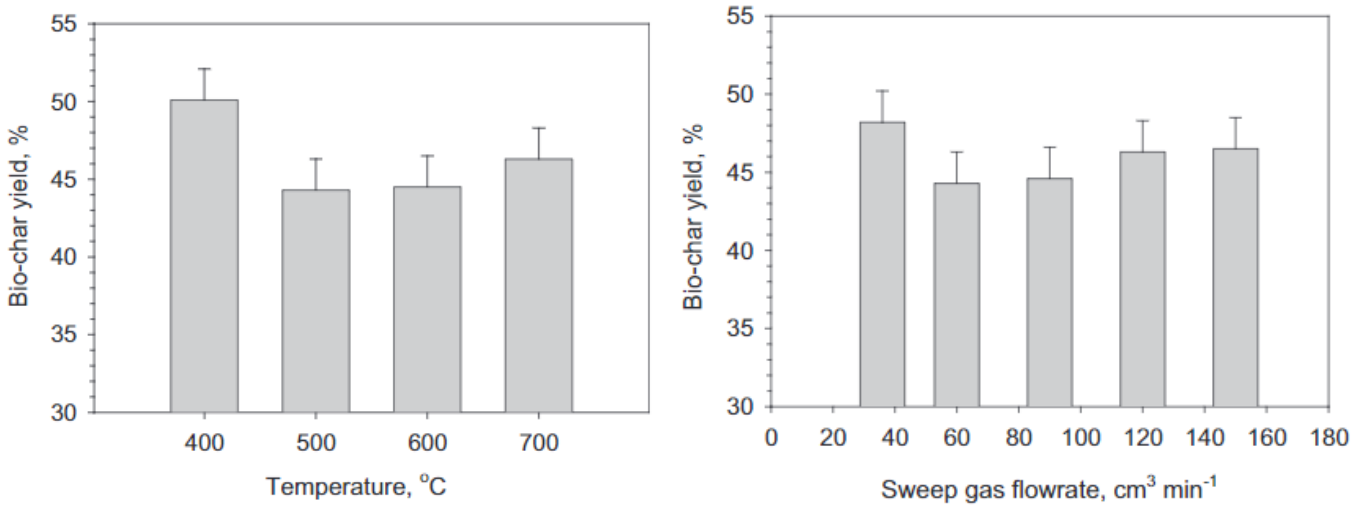

Figure 3: Correlation between biochar-yield from duckweed-pyrolysis with respect to a) Temperature and b)Ar flowrate [30] In fig a) there was a constant flow rate of Argon at 60 $cm^3 min^{-1}$ while in fig b) there was a constant temperature at 120°C

Temperature (°C)	Char					Activated carbon (dry basis)			
	M (%)	*V* (%)	FC (%)	Ash (%)	Yield (%)	*V* (%)	FC (%)	Ash (%)	Yield (%)
400	5.11	32.52	60.45	1.92	49.97	7.22	90.35	2.43	30.47
500	6.43	22.47	69.11	1.99	40.64	6.62	90.87	2.51	27.12
600	7.52	15.99	73.99	2.50	36.61	5.70	90.74	3.56	26.88
700	8.52	9.38	79.10	3.00	31.19	5.76	90.64	3.60	26.31
800	9.57	7.11	79.20	4.12	29.83	5.72	90.57	3.71	25.85
900	6.60	6.85	80.68	5.87	28.74	5.68	90.48	3.84	25.37

M: moisture content; *V*: volatile content; FC: fixed carbon. Pyrolysis conditions: hold time = 2 h; nitrogen flow rate = 150 cm^3/min; heating rate = 10 °C/min.

Figure 4: The table is showing the temperatures effect on moisture (M), volatiles(V), fixed carbon(FC),ash-content and yield for both the char and the activated carbon in [23]

Varying hold time	Volatile content	Varying N_2 flow rate	Volatile content	Varying heating rate	Volatile content
600-0.5-150-10	18.56	600-2-50-10	17.59	600-2-150-5	17.06
600-1-150-10	17.43	600-2-100-10	16.86	600-2-150-10	15.99
600-1.5-150-10	16.67	600-2-150-10	15.99	600-2-150-15	14.43
600-2-150-10	15.99	600-2-200-10	15.32	600-2-150-30	13.89
600-2.5-150-10	13.13	600-2-250-10	14.41	600-2-150-40	13.11
600-3-150-10	12.06	600-2-300-10	13.25	600-2-150-50	12.87

Figure 5: The table is showing the influence of temperature,holding-time,flow-rate and heating-rate on the volatile-content of the char

Publications indicates that the heating rate of the pyrolytic reaction has a substantial effect on the charcoal-properties, in particular on the charcoal-yield. Mackay and Roberts [Mackay/Roberts 1982] [24] publications shows an increase in the char-yield from 22% to 32% for redwood when the heating-rate is reduced from 200°C/min to 1°C/min. The reason for this development is , according to these authors, that decreased heating-rate gives the dehydration-reaction more time to develop, which again results in an increased char-yield.

2.1.2 Moisture content

The content of moisture in the biomass is a parameter that affects the charcoal yield strongly. This is verified by several publications. According to Mok and Antal jr, a linear correlation exists between the moisture-content and the yield of charcoal. An increase in moisture-content also decreases the maximum pyrolytic temperature in the charcoal production[Mok and Antal Jr. 1992][26]. These experiments were performed to test whether water acts as an autocatalytic agent in the formation of charcoal or not. The results went in favor of the auto-catalytic properties of water.

The impact of moisture-content prior to the pyrolytic process has also been done research on. Shimazu and Sterling [Shimazu and Sterling 1966] [35] concluded that cellulose that is moist by being immersed in liquid water at elevated pressures, has a better resistivity to thermal break-down than dry samples.The cellulose in these experiments were from extracted cotton, and these materials were exposed to pressure-test at (100°C and 150°C) for a duration of 5 hours, with and without moisture. The dry samples broke down much faster than the moist samples, for both temperatures. One possible explanation for this, according to Shimazu and Sterling, is that the free radicals that are generated due to the heating-process, is quickly quenched because of the abundantly availability of water [35].

2.2 Decomposition of methane

2.2.1 Thermodynamic analysis

When exposed to temperatures at around $1100 - 1200°C$ methane is able to decompose as shown in the following reaction [Abbas and Wan Daud 2010][1]:

$$CH_{4(g)} \rightarrow C_{(s)} + 2H_{2(g)} \tag{2.2}$$

The reaction is very endothermic ($\Delta H° = 75{,}6$ kJ/mol at 25°C) and requires much energy. This decomposition-reaction can also be done in the proximity of a carbonaceous sample-material, for example charcoal. The result is that the charcoal becomes densified by the produced carbon, which also acts as a catalyzing factor for the decomposition-reaction itself. This brings the required temperature down to $1000 - 1100°C$ [1].

When the decomposition of the methane takes place, a chemical equilibrium between the different gases inside the furnaces (H_2 and CH_4) is achieved. The equilibrium constant of the decomposition reaction (K) can be defined as follows:

$$K = \frac{p_{H_2}^2 a_C}{p_{CH_4}} \tag{2.3}$$

Where p_{H_2} and p_{CH_4} represents the partial pressure of the hydrogen and the methane gas, respectively. The a_C is the activity of solid carbon and can be assumed to be equal to 1. The equilibrium constant can be found as a function of temperature by using thermodynamical values, and Figure 6 shows the calculated values of the equilibrium constant as a function of decomposition temperature

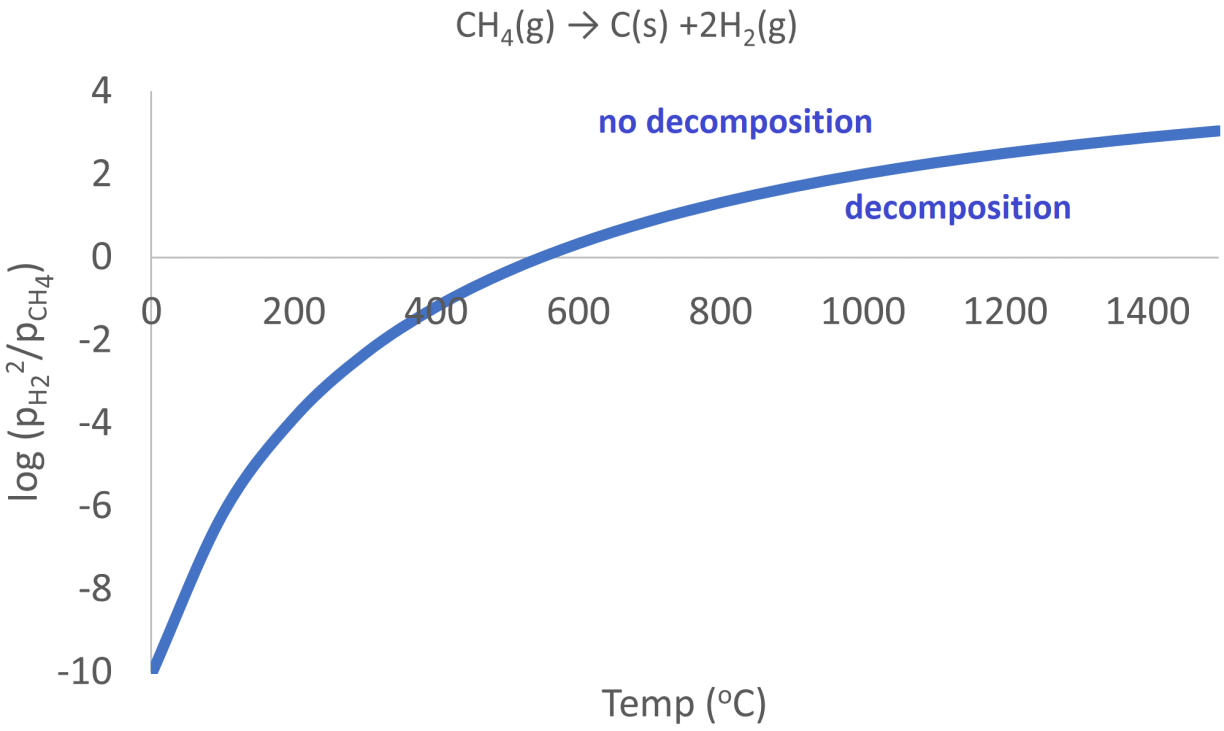

Figure 6: The figure is showing the partial pressure of methane and hydrogen as a function of temperature at chemical equilibrium.

An increase in the partial pressure of methane will according to Le Chateliers principle drive the reaction towards more decomposition, while the increase of both partial pressure of hydrogen or total pressure will drive the reaction towards retardation, that is no decomposition. From this we can see that the graph in Figure 6 represents a borderline in this way.

If one uses the fact that:

$$p_{H_2} + p_{CH_4} = 1 \tag{2.4}$$

And, as mentioned, that :

$$K = \frac{p_{H_2}^2}{p_{CH_4}} \tag{2.5}$$

It is then possible to find a theoretical value of the partial pressure of methane when you know the reaction temperature (which is calculated from the K) This expression is a second degree-polynomial equation:

$$p_{CH_4}^2 + (-2 - K(T))p_{CH_4} + 1 = 0 \tag{2.6}$$

And when one knows the value of the partial pressure, it is also possible to calculate the theoretical

value of the methane-decomposition-ratio if one knows the volume of the container in which the reaction happens.

2.2.2 Reaction mechanisms and catalytic materials

Methane (CH_4) is a chemical compound that can achieve relatively high bond-energy between the different molecules. The methane molecule has a tetrahedral structure which is made up of four C-H-bonds through sp^3-hybridization, and some reportings claim that the C-H bonding-energy can be as high as 435 kJ/mol [Schwarz 2011][34]. This strong bonding is one of the reasons that the decomposition of methane requires either a catalyst-material in the proximity, or high-temperature environments (above 400°C).

The produced carbon that comes from the methane decomposition often comes out of the reaction as carbon black (CB). Carbon black can also come as a product of incomplete combustion of natural gases, among others, and an example of such a reaction is:

$$\mathrm{C_nH_m} + \tau_{\mathrm{o2}}\mathrm{O_2} \rightarrow \tau_{\mathrm{co2}}\mathrm{CO_2} + \tau_{\mathrm{H2}}\mathrm{H_2} + \tau_{\mathrm{H2O}}\mathrm{H_2O} + \tau_{\mathrm{C}}\mathrm{C} \tag{2.7}$$

where τ_x represents the rate of the component x in the furnace process. Carbon black is used for many applications, for example as a reinforcing filler in the rubber industry [9]. The catalytic decomposition of methane (CDM) is a relatively complicated reaction which can be divided into different steps [Fan 2021] [8]:

1. Chemisorption of methane on the active site of the catalyst. If the catalyst is metal-based, the carbon atoms reacts with unsaturated metal atoms to form M-C-bonds.

2. The C-H bond in the chemisorbed methane are broken. This happens according to the following steps:

$$\mathrm{CH_4(g)} \rightarrow \mathrm{CH_3(a)} + \mathrm{H(a)} \tag{2.8}$$

$$\mathrm{CH_3(g)} \rightarrow \mathrm{CH_2(a)} + \mathrm{H(a)} \tag{2.9}$$

$$\mathrm{CH_2(g)} \rightarrow \mathrm{CH(a)} + \mathrm{H(a)} \tag{2.10}$$

$$\mathrm{CH(g)} \rightarrow \mathrm{C(a)} + \mathrm{H(a)} \tag{2.11}$$

   The notations g and a represents respectively gaseous and adsorbed species, and the first equation is most often the equation that requires the most energy.

3. The adsorbed hydrogen-atoms forms together as molecules according to the following equation:

$$2\mathrm{H(a)} \rightarrow \mathrm{H_2(g)} \tag{2.12}$$

4. Accumulation of the adsorbed carbon-atoms. The adsorbed carbon-atoms diffuse into the proximity-materials under the promotion of a concentration-gradient. Once the saturation-levels are reached, deposition is allowed to take place.

The deposition of carbon is often related to the development of carbon nanomaterials. This development is very much dependent of the properties of the catalyst-foundation material. An example of this is that because the morphology can vary a lot for the different catalyst, there are a great variation in the morphology for the developed carbon-structures as well.

Through the history there has been a great variety of different types of catalyst that has proven to be very effective regarding to this reaction. This includes both metal-based and carbon-based materials.

Even though there are great thermodynamic benefits using a catalyzing material for the CDM, there are also some major challenges when performing such experiments. One such challenge is deactivation, which happens because the already deposited carbon is creating a barrier between the methane-gas and the reacting catalyst-surface. Other potential challenges are: great amounts of unreacted methane in the effluents, emissions regarding the regeneration and recovery of catalyst material, and that the carbon products may have low purity.

Among the catalyst materials, there are one main group in particular that may be able to solve the challenge of deactivation because of deposition. This group is the carbon-based materials. Carbon-based materials normally requires a higher operating temperature when performing the CDM, compared to the metal-based catalysts. This is because of the higher activation-energy. On the other hand, these types of catalysts are relatively cheap and are much more able to resist high temperatures than the catalysts that are metal-based. Another advantage of using carbon-based catalysts is that these materials are immune to the sulfur-poison of the methane-gas, which means that the industrial step of pre-removal of sulfur from the methane gas can be skipped. This will result in a highly adaptable raw-material.

Among the different carbon-based materials, it has been reportings of a great deal of variation in the catalytic activity. In the works done by Muradov [Muradov 2001] [28], it was used several types of carbon-materials as a catalytic material for methane decomposition. Here it was reported that the materials that had a more disordered morphology and atomic structure, such as carbon black and activated carbon, had greater catalytic activity compared to for example graphite or diamond powder, where there was more order in the atomic structure. An increased disorder in the atomic arrangement may lead to an increased amount of actives cites in the atomic structure, which may explain why so much more methane were able to absorb onto the material compared

to the ordered structures.

Another factor that tend to change the catalytic activity of the methane decomposition is the surface area of the catalyst. These variations can be relatively big, however this is only valid for the initial stage of the decomposition process. The reason for this is that as the time goes by, the surface properties will more or less be the same, since its covered by the same material (deposited carbon). In 2019, Haruki Nishii and others published a report showing the differences in the initial catalytic activity on carbons with different structures (activated carbon, carbon black, meso-porous carbon and carbon nanofiber) [Nishii 2019][31] . One of the structural properties that was measured and compared was the surface area. The figure below (Figure 7) is gathered from the mentioned report and shows the methane conversion ratio (%) as a function of specific surface area (m^2g^{-1}). The figure shows a more or less proportional relationship between the surface area and the conversion ratio. An exception to this development is shown for the mesoporous carbon with its decreased conversion ratio in spite of increased surface area compared to carbon black. This may be explained by other factors than the surface area. Figure 8 shows how the methane conversion-ratio changes with time for the relevant materials in the report. According to what is shown in the figure, the different values for the conversion-ratio tends to decrease rapidly in the initial phase, due to blockage of the pores, and then converges to a value of approximately 17 % [31].

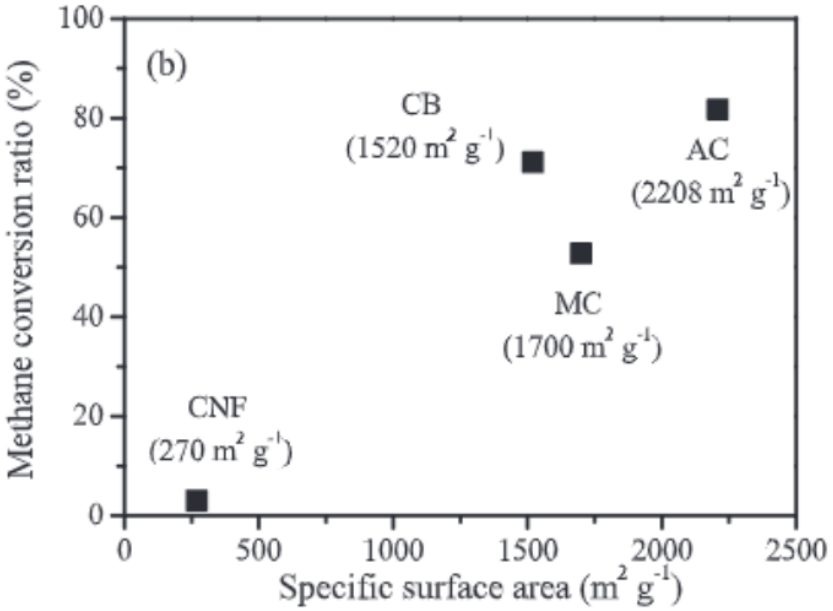

Figure 7: Methane conversion ratio as a function of the specific surface area for the investigated materials: CNF (carbon nanofiber), CB (carbon black), MC (mesoporous carbon) and AC (activated carbon)

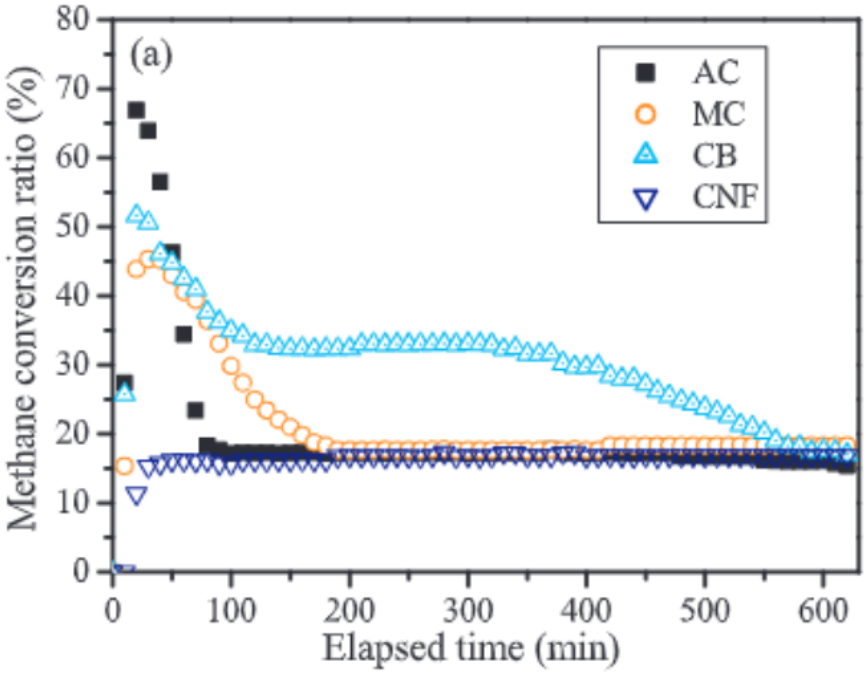

Figure 8: Plot showing the change of methane conversion ratio as a function of elapsed time for the investigated materials: CNF (carbon nanofiber), CB (carbon black), MC (mesoporous carbon) and AC (activated carbon)

The effect of catalytic activity was also examined by Muradov, Smith and T-Raissi, when they performed experiments on a variety of carbon-catalytic materials, among them several kinds of carbon black and activated carbon [Muradov 2005][29]. The work included comparison of catalytic activity with regard to surface area, surface groups, impurities and there were also done examination to how strong the catalytic activity is for carbons that are made from decomposition of other types of hydrocarbons. When it comes to the latter, the authors found concluded that the deposited carbon made from methane decomposition was not a good catalytic material in itself, which is the reason that decomposition of methane with such a material does not behave "autocatalytic". By using small pulses of hydrocarbon-gases during methane-decomposition experiments, the authors were able to monitor the change in the decomposition-rate to see if the different gases had an impact. The conclusion was that carbon derived from cracking of aromatic hydrocarbons, such as benzene, had the greatest catalytic activity, followed by acetylene and ethylene, while methane was relatively poor.

The authors also compared other parameters during the mentioned publication. As in many other publications, they were able to confirm the correlation between the surface area and the decomposition-rate, which is shown in Figure 9

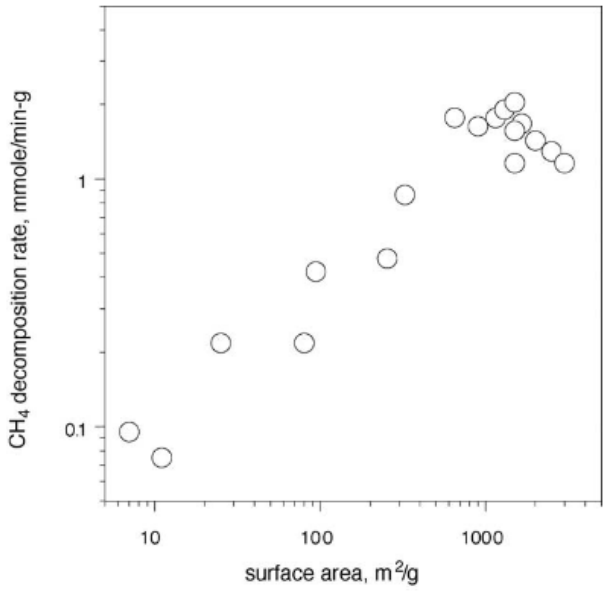

Figure 9: Methane decomposition-rate as a function of surface area.

2.3 Relevant litterature

Abbas and co-workers has performed some research regarding the different parameters in thermal decomposition of a palm-shell carbon-based activated carbon (ACPS). The experiment was done under atmospheric pressure and the temperature-values was in the range of $750-850°$C. One of the main conclusions in this article was that they were able to measure the catalytic activity of methane decomposition in the proximity of the ACPS, and a deactivation energy (E_0) of 177KJmol^{-1}. To achieve and calculate this specific value, an Arrhenius plot was used of lnk_d against 1/T, where k_d is the catalyst deactivation rate constant and T is the temperature (i Kelvin). This lead to the following expression for the slope (s):

$$s = \frac{-E_0}{R} \tag{2.13}$$

Where R is the molar gas constant (8.31JK^{-1}mol^{-1}). The table below (Figure 10) shows an overview of the experimental and calulated parameters. Some of these parameters were used to calculate k_d.

Experiment no.	ACPS weight (g)	Temperature (°C)	Methane flow rate (L min^{-1})	VHSV (hr^{-1})	Residence time (min)	Initial H_2%	Initial CH_4%	Initial CH_4fractional conversion	R_o (mmol $(g_{cat.}\ min)^{-1}$)
1	20	850	0.7	1764	0.034	47.9	49.8	0.319	0.4849
2	40	850	0.7	882	0.068	62.5	34.9	0.458	0.3473
3	80	850	0.7	441	0.136	77	21.2	0.617	0.2295
4	120	850	0.7	294	0.204	81.6	16.7	0.686	0.1693
5	40	850	0.23	294	0.204	83.1	13.2	0.671	0.172
6	40	850	0.34	441	0.136	78.3	22	0.636	0.227
7	40	850	0.7	882	0.068	62.5	34.9	0.458	0.3473
8	40	850	1.4	1764	0.034	57.9	41.5	0.407	0.5918
9	40	850	0.7	882	0.068	62.5	34.9	0.458	0.3473
10	40	825	0.7	882	0.068	60.9	37.6	0.436	0.3227
11	40	800	0.7	882	0.068	50.9	48.7	0.34	0.245
12	40	775	0.7	882	0.068	39.1	59.5	0.242	0.181

Figure 10: Summary of the experimental conditions and the main findings [Abbas and Wan Daud 2010] [1] VHSV stands for volume hourly space velocity and R_0 stands for initial rate of methane decomposition.

The same article studied the effect of diffusional limitations on the decomposition-process. The authors found a dramatic change in surface area and micropore-volume of deactivated ACPS compared to fresh ACPS, and this indicated that the decomposition was mainly carried out in the micropores of the material [Abbas and Wan Daud 2010] [1].

In 2014, an article regarding decomposition of methane during oxide reduction with natural gas was published by Halvor Dalaker and Pål Tetile [7]. This article focused on the thermodynamical conditions for when methane was used as a reducing agent to different kinds of oxides. One of the main goals for the authors was to find out if it was a correlation between the temperature upon methane cracking (methane decomposition) and the carbon-affinity for the oxide-component. Four different oxides were used (Al_2O_3, MgO, SiO_2 and CaO), in addition to an experiment in an empty alumina-crucible. Although there were some uncertainties due to noise in the signals, the authors were able to determine some clear cracking-temperatures for methane in the proximity of SiO_2 (770°C), CaO (810°C), MgO (820°C) and for the empty crucible (950°C). These points were determined by plotting the concentration-values of methane and hydrogen gas as a function of temperature. As a part of the study, the authors also included the possibility that the formations of acetylene and ethylene took place, and shown in the respective reactions below:

$$2CH_4 \rightarrow C_2H_2 + 3H_2 \tag{2.14}$$

$$2CH_4 \rightarrow C_2H_4 + 2H_2 \tag{2.15}$$

The figure below consist of a plot that shows for the different carbide-formations of the relevant

metal-oxides in addition to the formations of acetylene and ethylene. These values are plotted as a function of temperature. The formations of carbide are included since they are a good indicator for the conditions for deposition of carbon due to methane decomposition.

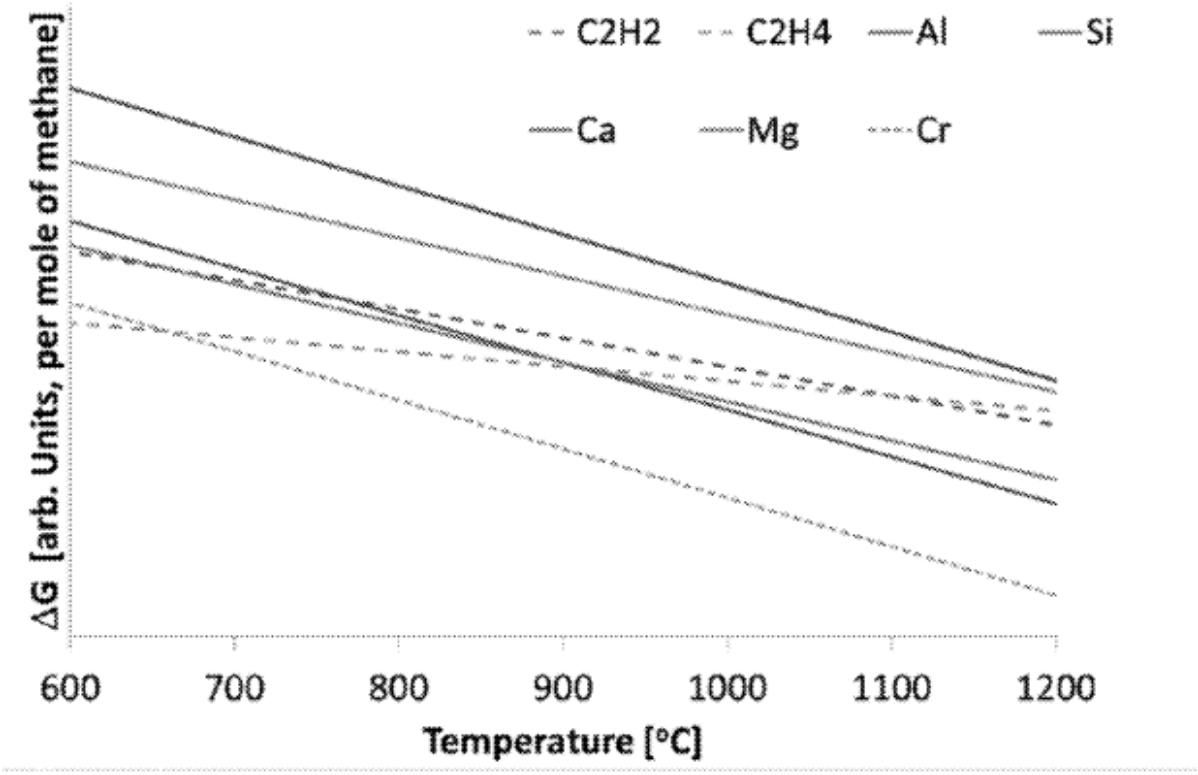

Figure 11: -values for the formation of the different metal-carbides together with the -values for the formation of ethylene and acetylene as a function of temperature.

The concluding points of this article was that the degree of meta-stability that could be achieved was not correlating with the carbon-affinity of the different metallic oxides. It was also concluded that in order to use methane as a good reducing agent to different metal-oxides, one had to make sure that the methane-oxide-reaction was more energetically favourable compared to the formation of acetylene and ethylene, according to Figure 11.

The thermodynamic conditions of the decomposition of methane was also studied by Marquardt and co-workers in the proximity of different carbonaceous materials [Marquardt et al. 2020] [25]. Several experiments were compared, and all the different methods and thermodynamical parameters and materials are shown in the table below (Figure 12):

–	Ref.	Carbon type C	Measurement method	Given quantity	T in K
a	[51]	Coke	Electrochemical	G_C^f, H_C^f, $\Delta S_{C-graphite}$	955–1245
b	[52]	Amorphous Carbon	–	H_C^f	–
c	[53]	Coke (10 types)	Methane decomposition equilibrium	$\Delta^R G_{TDM,C}$, H_C^f	1073–1273
d1	[54]	Filamentous/ Nickel carbide	Methane decomposition equilibrium on Ni based catalyst	$\ln(K_p)$	662–792
d2	[54]	Filamentous/ Iron carbide	Methane decomposition equilibrium on Fe based catalyst	$\ln(K_p)$	887–1037
e	[55]	Filamentous/ Nickel carbide	Methane decomposition equilibrium on Ni based catalyst	$\ln(K_p)$	673–873
f	[56]	Filamentous/ Nickel carbide	Methane decomposition equilibrium on Ni based catalyst	$\ln(K_p)$	773–848
g1	[57]	Nanofibers	Combustion calorimetry	H_C^f	298
g2	[57]	MWCNT	Combustion calorimetry	H_C^f	298
h	[58]	MWCNT	Electrochemical	G_C^f, H_C^f, $\Delta S_{C-graphite}$	820–920
i	[59]	SWCNT	Combustion calorimetry/ Calculation	H_C^f, $\Delta S_{C-graphite}$	1084
j	[60]	SWCNT	Electrochemical/ Calculation	H_C^f	750–1015

Figure 12: Overview of the different materials used in the publications of Marquardt and co-workers. The numbers in the second column represents citations of all the compared experiments. [25]

Some of the most important results of the article are shown in the two figures below (Figure 13a and Figure 13b) According to the figure, there is a small increase in the reaction-enthalpy with increasing temperature for all materials. When it comes to methane-conversion, this increase is far much bigger with rising temperature. According to Figure 13b the methane-conversion is highest for the multi-walled carbon nanotubes (MWCNT) at the relevant temperature-range, while coke has the lowest [25].

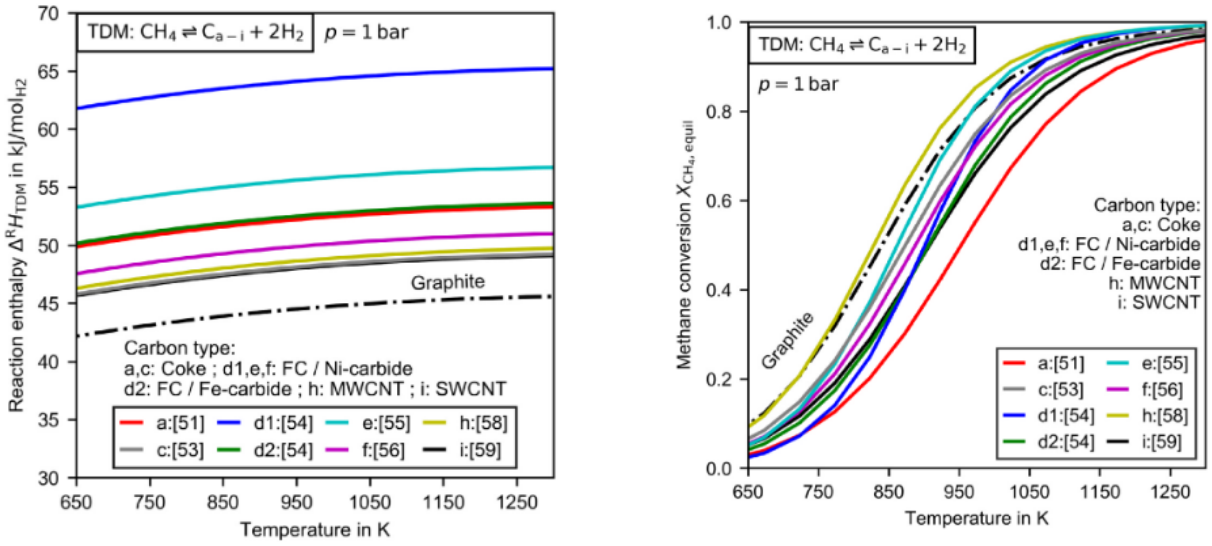

(a) **(b)**

Figure 13: The figures show a schematically representation of the reaction-enthalpy (a) and the fraction of methane-conversion (b) against temperature for the different carbonacous materials used in the study of Marquardt [25]

The experiments that are planned to be performed as a part of this master-thesis has also been done by other master-students and professors and researchers. In the publications of Khaffash and Tangstad [Khaffash and Tangstad 2021] [19], three different sets of charcoals , with some variations in volatile-fraction, fixed-carbon-fraction and ash-fraction , were submitted to methane-purging in an induction furnace at 1100°C for 90 minutes, and the increased effect in weight, compression-strength and porosity were measured. The proximity analysis and the composition of the three different charcoal-sets is shown in Table 1 together with the porosity and density-measurements. As shown below, there is a great increase in the compressive strength for all sets of charcoals that is submitted to densification. Figure 17 andFigure 18 show that porosity seems to decrease for all three sets of charcoal. The results below shows that the increased weight due to methane purging is 13-15 % as a result of 90 minutes of methane-purging. Similar experiments has also been done in the summer-report 2021 and the specialization-project for 2021, both done by Larsen [21] [22]. In these projects charcoal were densified through methane-decomposition at approximately 1100°C for respectively 1, 2 and 3 hours, and the development with time was measured for weight-change, compression strength and porosity. In the summer-project it was found that 1h of densification resulted in an increase of 7,1% in the weight due to carbon-deposition, while densification for 2 and 3 h both resulted in an increased weight of about 18,5%. In the specialization-project, the author were able to detect an increased wt% as high as 16,8 % after 3 hours. There were

also taken images with SEM (Scanning Electron Microscopy) to see the change in the amount of deposited carbon and to see the change in the pore-structure. The SEM-images for raw sample and sample with 1h of densification is shown in Figure 19. Figure 21 and Figure 20 shows the different values of respectively the skeletal and the apparent densities of the examined charcoal, which was used to calculate the porosity in the specialization-project. Densification experiments was also performed by Solhaug as a part of her summer- and specialization-projects in 2021[37] [36]. In the specialization-project, which was about testing the CO_2-reactivity of densified charcoal that went through different kinds of K-impregnation. The overview of the relevant results, both when it comes to densification-results (Figure 14), compression-results (Figure 15 and Figure 16) and porosity (Figure 17 and Figure 18) is shown in the figures below. Also included are the relevant SEM-images (Figure 19) and density measurements (Figure 20 and Figure 21) by Larsen. The last thing that is included is a table showing the amount of carbon in the purged methane which is deposited on the charcoal in the specialization-project by Larsen (Table 2) .

Material	Charcoal A	Charcoal B	Charcoal C	Metallurgical coke
Proximate analysis (wt%, dry basis)				
Volatile	13,08	16,75	15,79	0,9
Fixed carbon	85,17	80,50	81,60	88,20
Ash	1,75	2,75	2,61	10,90
Ultimate analysis (wt%, dry basis)				
C	85,5	83	83,58	87,7
H	1,95	3,14	2,4	0,21
N	$< 0,5$	0,26	0,21	1,75
O	10,4	10,8	11,2	$< 0,1$
S	n.s.	n.s.	n.s.	n.s.
Physical characteristics				
Porosity (%)	68	80	74	44-55
Density (g/ cm^3)	0,5	0,44	0,56	0,9-1,1

Table 1: The table shows the proximate analysis, the ultimate analysis and the porosity and density of the three types of charcoal used in the experiments of Kaffash and Tangstad, in addition to the same data for metallurgical coke [19]

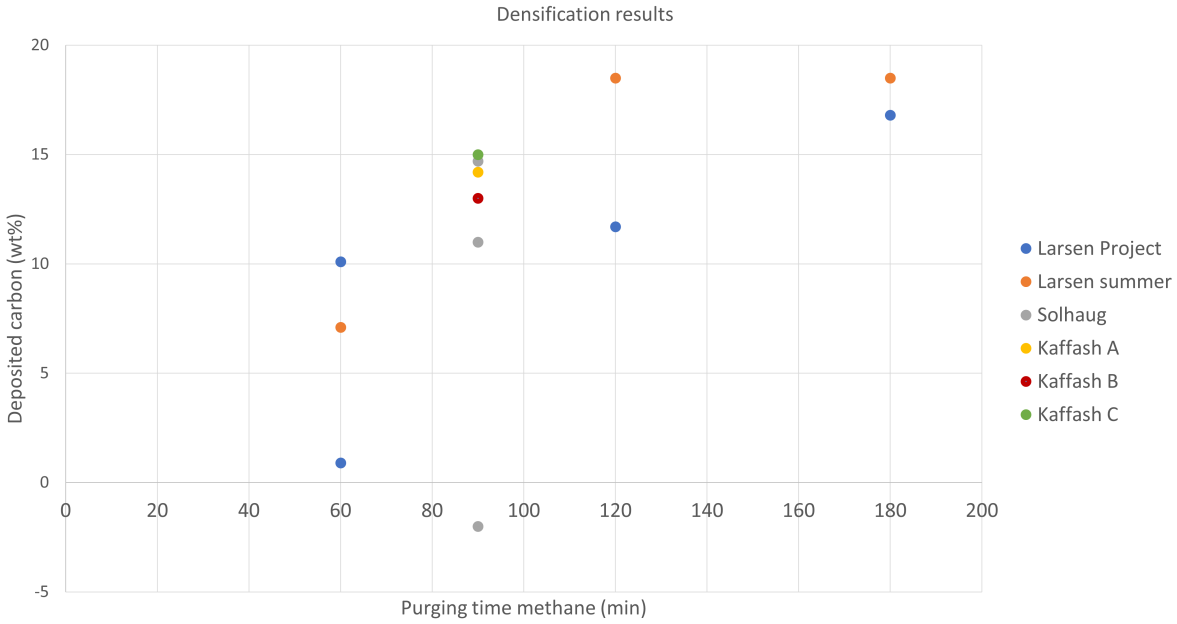

Figure 14: An overview of the results of the different densification-experiments performed by Kaffash, Solhaug and Larsen

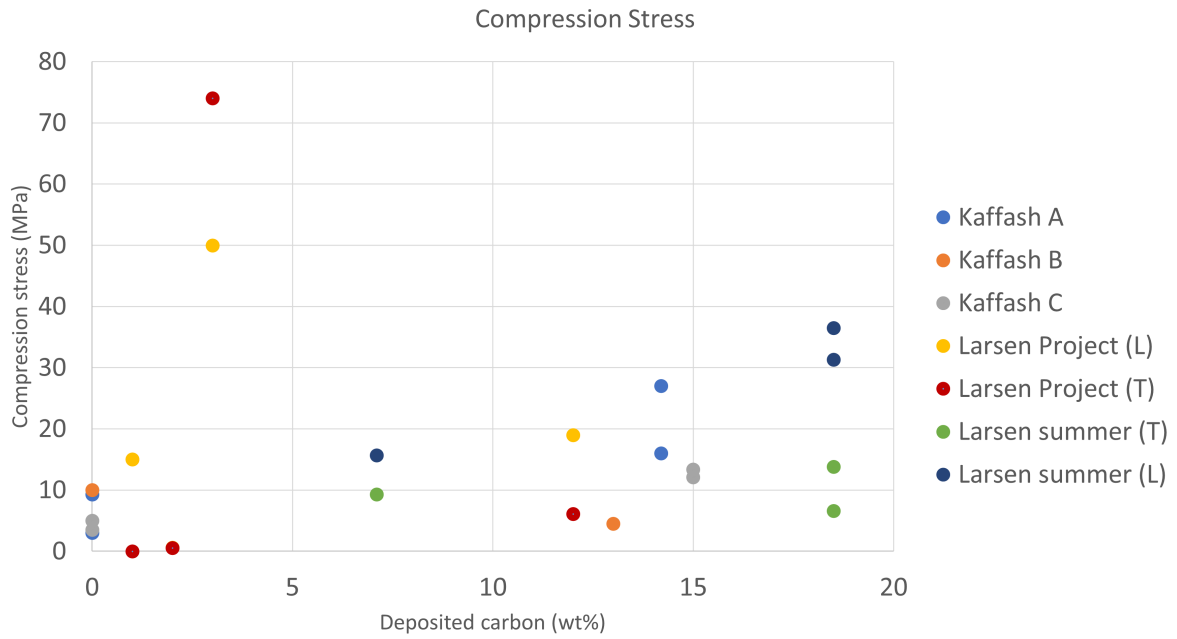

Figure 15: Overview of the different results of compression-testing for the experiments of both Larsen and Kaffash. The letters T and L is respectively reffering to compression stress performed perpendicular and paralell to the fiber-direction in the material.

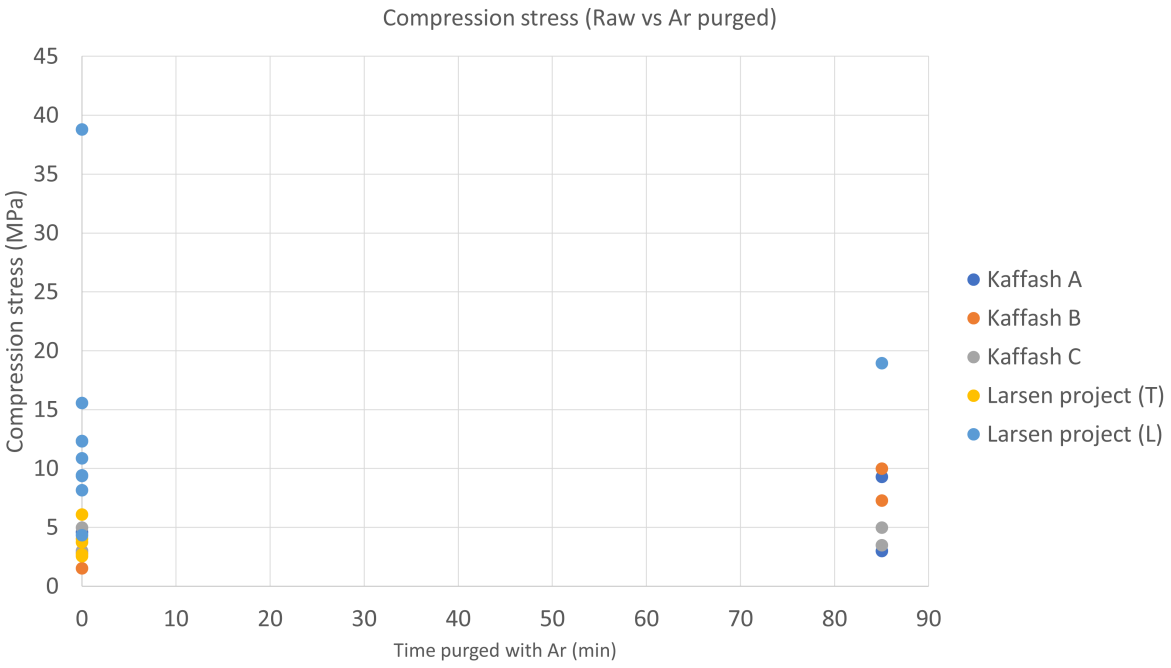

Figure 16: A comparison of the different compression-results for raw material and Ar-purged material for the experiments of both Larsen and Kaffash

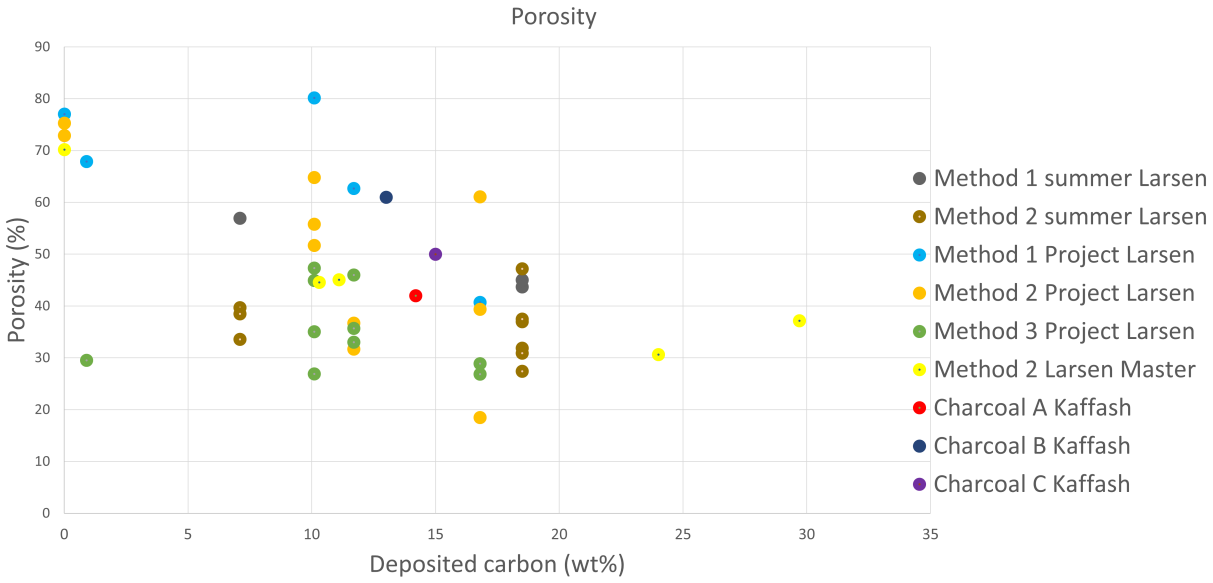

Figure 17: An overview of the different values of porosity from the experiments of both Larsen and Kaffash

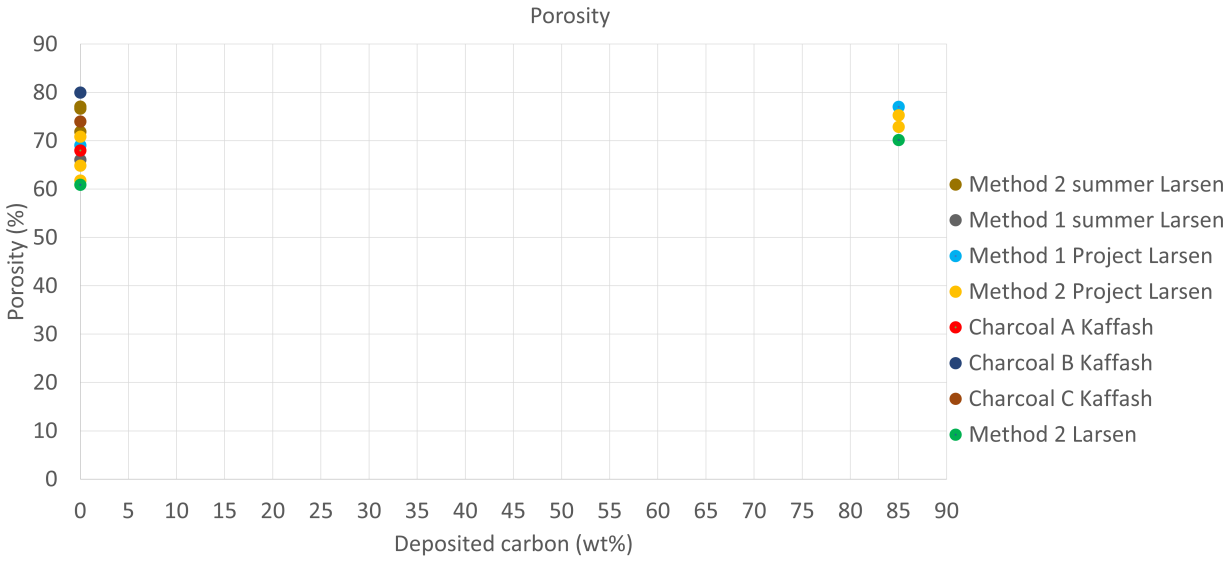

Figure 18: An overview of the different values of porosity from the experiments of both Larsen and Kaffash

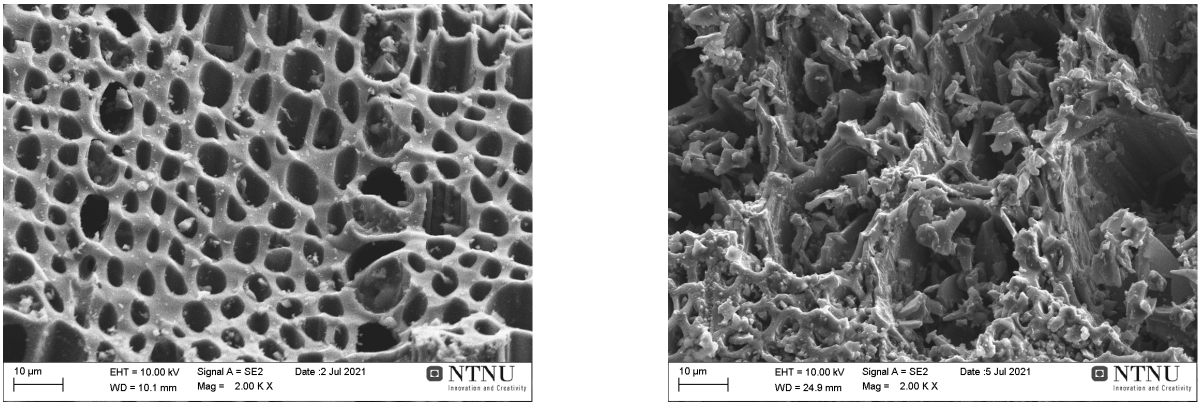

(a) Raw charcoal **(b)** 1h densification

Figure 19: SEM-images of the charcoal and the 1h densified charcoal

Sample	1h	2h	3h	1h(2)
Average purging-temp (°C)	1055,3	1022,0	1052,7	1092,3
Increased weight due to CH_4-purge (wt%)	0,9	11,7	16,8	10,1
Amount of reacted methane (mol)	0,25	3,08	4,83	2,91
Amount of purged methane (mol)	7,13	14,75	22,04	7,37
Conversion-fraction of methane (%)	3,5	20,89	21,91	39,53

Table 2: Table showing important parameters regarding the calculation of the fraction of methane-conversion for the specialization-project by Larsen [22]

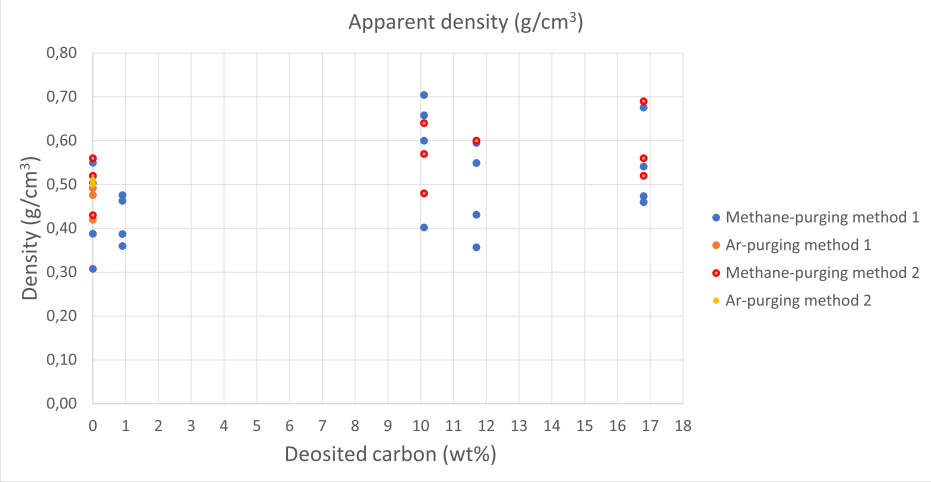

Figure 20: Overview of the results of apparent density in the specialization-project by Larsen[22]

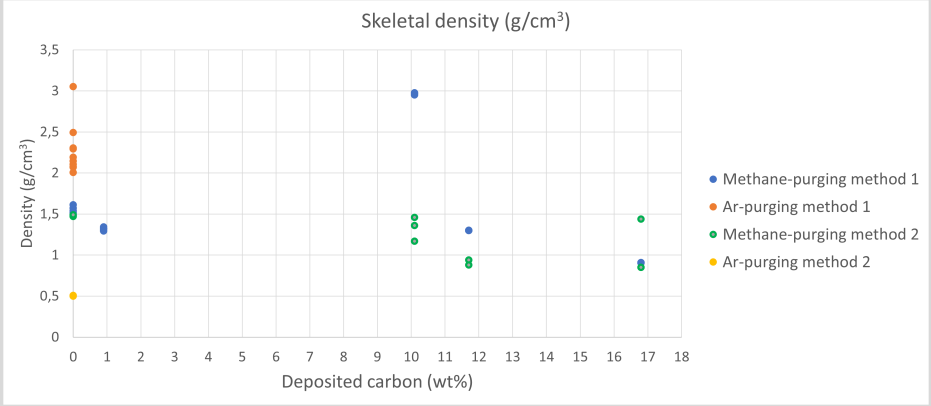

Figure 21: Overview of the results of skeletal density in the specialization-project by Larsen[22]

Thermal decomposition of methane is not the only alternative when it comes to trying to solve the problems with low density/high porosity for the charcoal material compared to other carbonaceous

materials. In 2016, a publication was made by Hussein, Larachi, Ziegler and Alamdari. The work attempted to explore the effect of heat treatment and acid washing on the reactivity and the physical properties and structures on charcoal. The industrial aim was to see if the resulting charcoal was competitive with petroleum coke when it comes to anode manufacturing [12]. The theory behind this idea was that the acid-washing and the heat treatment would favor the growth of the more ordered structures in the material, at the expense of the more amorphous structures and areas. The tested charcoal was heated under inert conditions with different temperatures, acid-washed with different concentrations, and exposed to a combination of both acid-washing and heat treatment. Figure 22 shows the specific surface area of the charcoal as a function of heating temperature. The BET adsorption experiments were done with both N_2- and CO_2- gas, which is shown respectively as the black and grey graph in the figure. According to the authors, the reason for the higher values for the CO_2-experiments is that the sample have high amounts of micropores, that is missed by the N_2-gas. The decrease in the surface area at the elevated temperature also fitted well with another publication [Kercher and Nagle 2003] [20], that concluded that this was due to the continuous growth of graphene sheets. Figure 23 shows the effect the heating temperature has on the real density of the material. The real density was measured by using a gas pyncometer with Helium as the inert gas, which penetrates the pores without a chemical reaction.

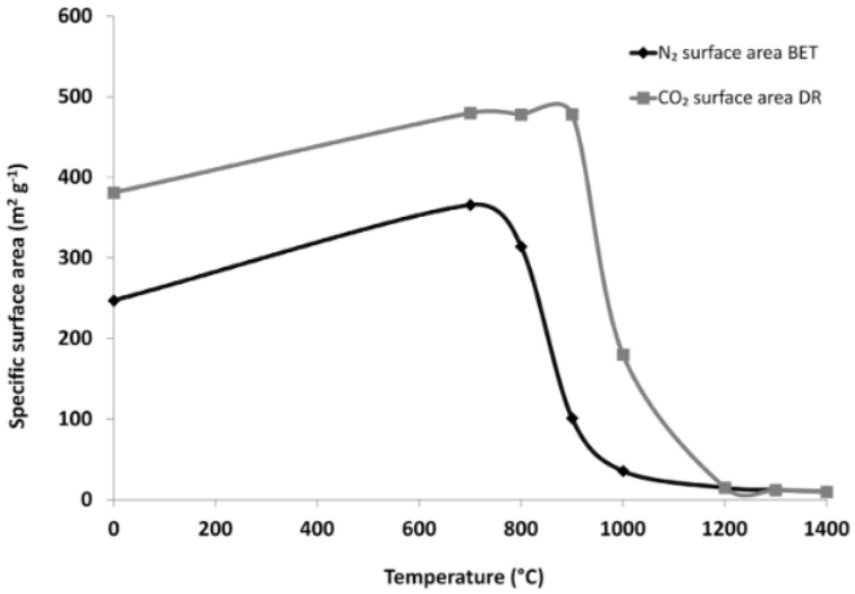

Figure 22: Specific surface area as a function of heating temperature for two different BET-experiments [12]

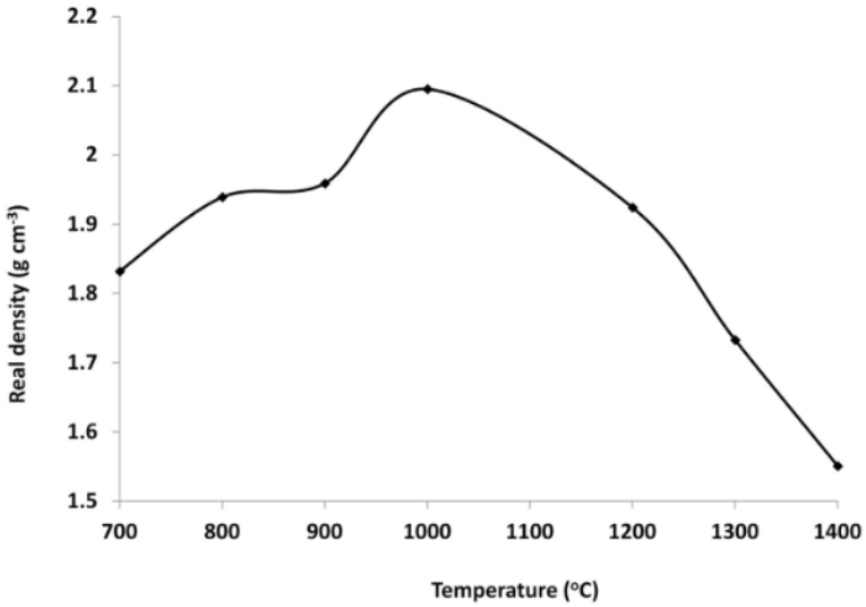

Figure 23

In 2007 Suelves with others [39] published a work regarding the catalytic properties of several carbonaceous materials, where the mass gain, surface area, initial rate and the catalytic efficiency were evaluated, among other things. The catalytic properties were investigated with respect to the thermo-catalytic decomposition of methane. 5 sets of carbon black and 1 set of activated carbon was tested, and the results of the deposited mass as a function of time are shown in Figure 24. According to the figure, the activated carbon has a relatively high deposition rate at the beginning, but its clear that the BP 2000 carbon black has the most deposited carbon overall before deactivation takes place.

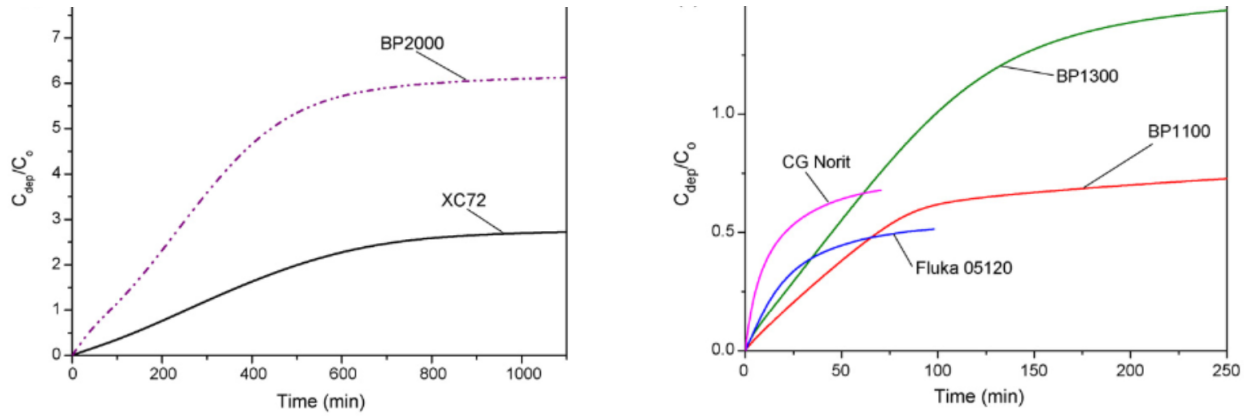

(a) **(b)**

Figure 24: Gram of carbon deposited per gram of initial catalytic material as a function of deposition time elapsed. The GC Norit is the only activated carbon material, while the rest are carbon blacks. T=900°C

Another interesting point from the works of Suelve and partners is shown in Figure 25 . The figure shows a decreasing trend for the surface area as the amount of deposition goes on, while there is a linear and increasing relationship between the deposited amount and the total pore volume.

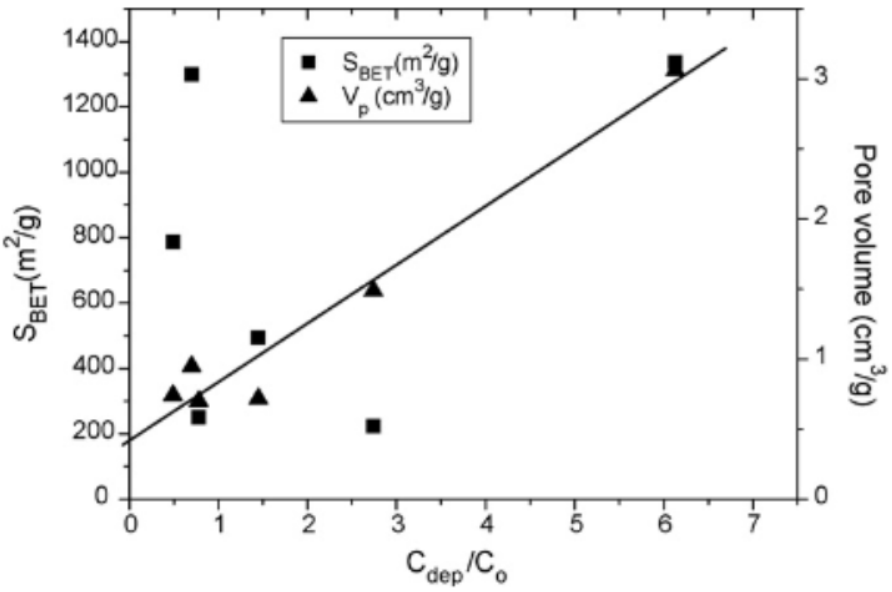

Figure 25: Specific surface area and total pore volume as a function of deposited carbon per gram of initial catalyst material [39]

In another publication, done by Villacampa with partners [Villacampa et.al 2003] [41], the decomposition of methane was investigated and evaluated with Ni-Al_2O_3 as the catalytic material. The effect of reaction temperature was investigated, along with many other parameters. Two interesting findings in this publication are the carbon deposition and the carbon formation rate as a function of time and methane-concentration (Figure 26) and reaction temperature (Figure 27). As one can see from the figures, the initial carbon formation rate increases with increasing methane-concentration, but the change of the rate is more rapid when the concentrations are lower. An increase in the concentration also increases the deactivation rate at the same time. An increase in the operating temperature also favors the formation of both carbon filaments and encapsulated coke. At really high temperatures the catalyst deactivation effect is more marked than of the nucleation and growth of carbon filaments, and this is the reason that the amounts of carbon formed at high temperatures are relatively low, according to the authors.

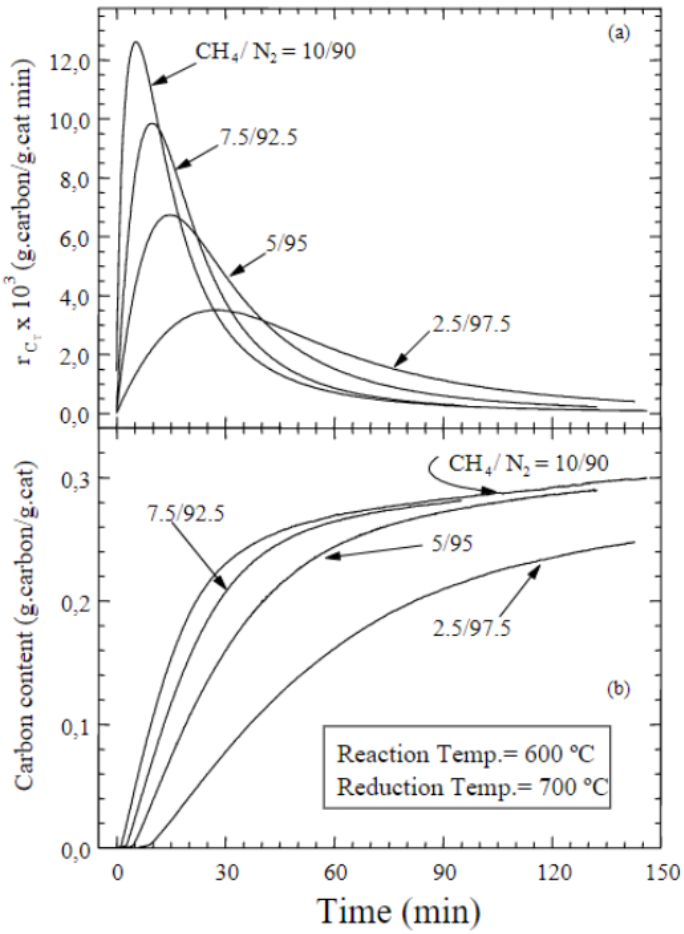

Figure 26: The figure shows the influence of the partial pressure of methane on the carbon formation rate (a) and the carbon content[41]

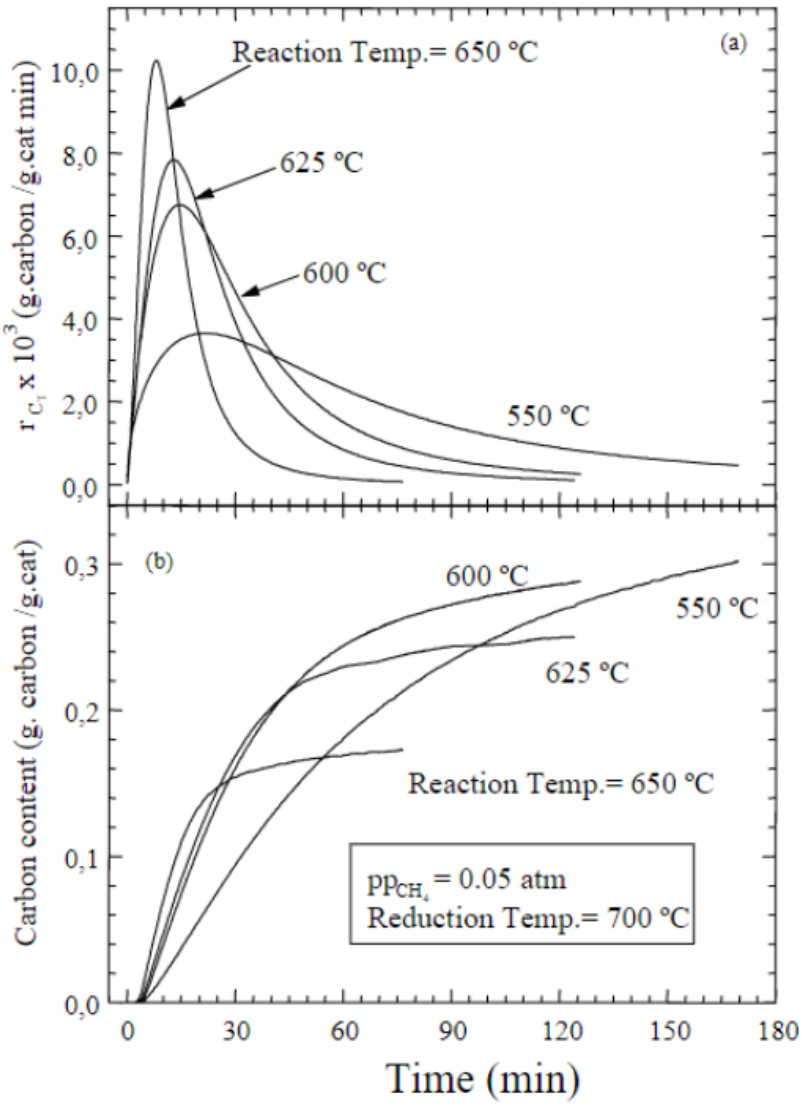

Figure 27: The figure shows the influence of the reaction temperature (in °C) on the carbon formation rate (a) and the carbon content[41]

3 Experimental

The main goal of this article is to examine some physical properties of charcoal when exposed to heat-treatment and densification due to decomposition of methane. The charcoal was distributed in a specific size-range, and characterized with respect to strength, both compressive and abrasive. The porosity was also measured, both by measurement of densities and by the use of SEM-images. The specific surface-area and pore-dimensions were measured by the use of BET and BJH, in addition to a CT-scan of some of the samples. The following chapter provides an insight in the different methods of characterization, as well as the heat-treatment and densification-process.

3.1 Preparation of materials

For each sample-set , 350 g charcoal were collected. Some information about this charcoal is shown in the table below () and the information was provided by Vegard Andersen at NTNU. The original size-distribution of the batch of charcoal was 5-25 mm. In order to get an equal size-distribution among all the samples, various amounts of raw charcoal were sifted using Retsch AS200Tap analytical sieve shaker (Figure 28) to the size-distribution of 10-13,2 mm.

Figure 28: Picture of the experimental setup of the sieving-process

	Value	Unit
Proximate analysis		
Moisture NTNU	4,7	wt%
Moisture ALS	1,4	wt%
Fix C (d)	79	% DW
Volatiles (d)	17,7	% DW
Ash (d)	3,32	% DW
Ultimate analysis		
C (d)	83	% DW
N (d)	0,39	% DW
O (d)	9,6	% DW
H (d)	3,71	% DW
S (d)	$< 0,1$	% DW

Table 3: The table shows the results of the proximate analysis and the ultimate analysis that was performed on the charcoal by ALS in Sweden prior to this master-thesis. DW = Dry Weight and (d) denotes dry

3.2 Densification

Six sets of charcoal, which had a mass of approximately 350 g each, were collected to be exposed to different kinds of heat-exposure. Each of these samples contained particles where the size distribution is described in the subsection above (10-13,2mm). Each sample-set were then distributed with a sample-splitter, to prevent big variations in the upcoming results because of variations in the different locations of the box that the charcoal were collected from in the very beginning. The sample-splitter that was used in this experiment is shown in Figure 32. Five of the sample-sets were placed in an induction furnace for heat-treatment and densification with CH_4. The remaining sample were left untreated. Figure 29 shows an example of how each sample-set was distributed with respect to the different characterization-methods.

The mentioned five sets were placed in a crucible made out of steel for densification. A thermocouple was also placed in the crucible to monitor the temperature. The thermocouple was placed precisely in the middle of the crucible to give an exact information about the overall temperature in the crucible during the experiments. An overview of the experimental setup is shown in Figure 31

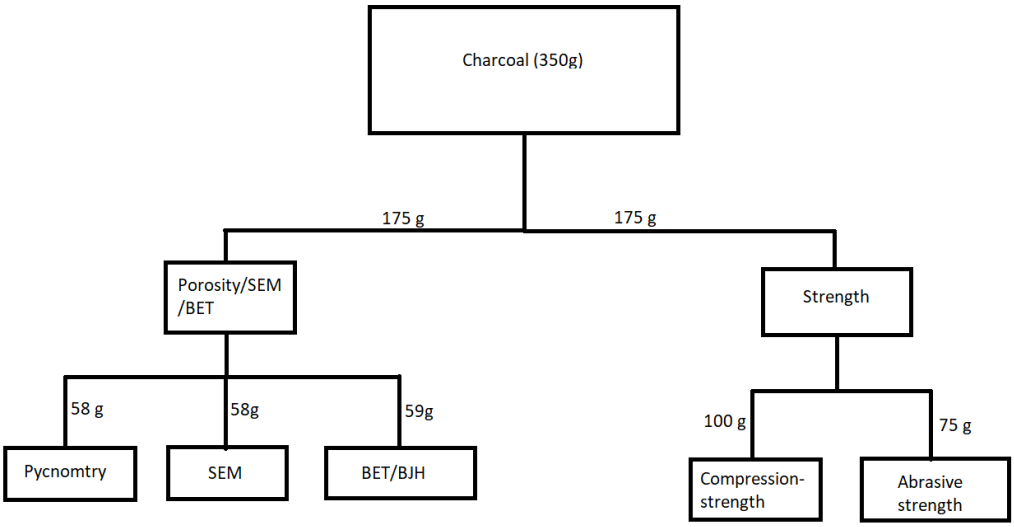

Figure 29: Overview of the sample-splitting process for 1h of densification with methane. The method of splitting was the same for all the samples, although there were some variations in the mass-distribution between the different samples.

(a) **(b)**

Figure 30: Pictures of the sample-splitter used for distributing the different samples within each sample-set

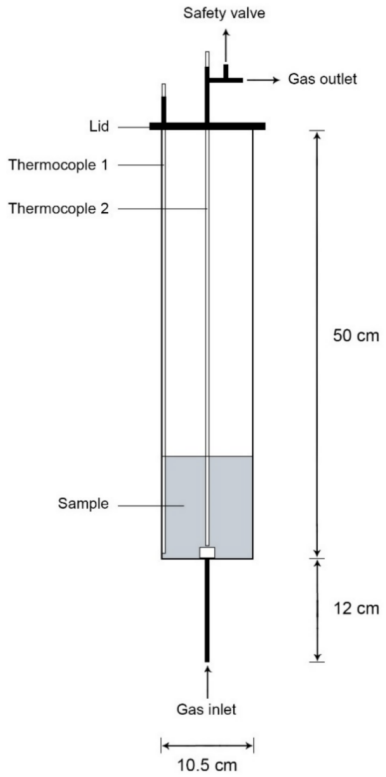

Figure 31: Experimental setup for the densification process.The illustration is published in the work of Khaffash,Surrup and Tangstad : Densification of Biocarbon and Its Effect on CO_2 Reactivity (2021)[18]

The crucible and the thermocouple was then placed in the furnace and all the necessary wires and tubes for in- and outgases were connected. The furnace was connected to a computer with software, which were used to measure and regulate the temperature and the different flow-rates of the gases. The furnace were first scheduled to heat up to a temperature of about 500°C. This took about 25 minutes. One of the samples were heated up to the temperature of 1100 °C, with the purging of argon-gas. The remaining four samples were also exposed to this treatment, but in addition they were exposed to purging of methane for respectively 1,2 and 3 hours. The reason that there were four sample-sets is that the experiment scheduled for 1 hour of methane-purging had to be repeated due to inflow-problems of methane and pressure-issues during the first try. After this, the methane-gas were switched off. The furnace was then cooled down to room temperature, which took about an hour. The samples were then left in the furnace to the next morning to cool down. The final step was to take the charcoal out of the furnace and measure the weight, to the nearest gram.

The table below (Table 4) is an example of how the densification-experiments were run. The table

shows the schedule for 1h of purging with methane. The entire schedule is divided in sessions (rows). The second column represents the terminal temperature, that is the temperature is expected to develop towards this value, but no further. The third column represents the change in temperature per minute. As mentioned before, the methane is supposed to decompose at 1100 °C, and the reaction is endothermic. As a consequence, the temperature will have a tendency to decrease slightly during the session. Because of this the Ramp SP was set to 3 °C/min to compensate for the temperature-loss.

Time [HH:MM:SS]	Temp SP[°C]	Ramp SP [°C/min]	Ar-flow [L/min]	CH_4-flow [L/min]
00:25:00	500	20	3	0
00:60:00	1100	10	3	0
00:60:00	1100	3	0	3
00:60:00	25	0	3	0

Table 4: Schedule of the 1h-densification-process. The other tests are run similarly, but with different holding-times at the maximum temperature.

3.3 Fraction of methane-conversion

The fraction of produced carbon that is reacted and was attached to the charcoal was calculated by the help of schematic overviews of the temperature and the flow-rates of the purging-gases with respect to the elapsed time. In order to calculate the total amount of methane-volume ($V_{CH_4,tot}$) that flows into the crucible, the average flow-rate of methane-purging ($F_{CH_4,av}$) has to be calculated over the total methane-purging time (t_{CH_4}):

$$V_{CH_4,tot} = F_{CH_4,av} \cdot t_{CH_4} \tag{3.1}$$

The corresponding mass of methane can be calculated as:

$$m_{CH_4,purge} = V_{CH_4,tot} \cdot \rho_{CH_4} \tag{3.2}$$

where ρ_{CH_4} is the density of methane ($6{,}57 \cdot 10^{-4}$ g/cm^3 at 25°C and 1 atm). The amount of methane (in mol) is found by the following equation:

$$n_{CH_4,purge} = \frac{m_{CH_4,purge}}{M_{CH_4}} \tag{3.3}$$

Where M_{CH_4} is the molar mass of methane (16,0 g/mol [3]). To find the amount of methane that has reacted with the charcoal, the mass of deposited carbon m_C has to be used, and the amount

of carbon can be calculated as :

$$n_C = \frac{m_C}{M_C} \tag{3.4}$$

Where M_C = 12,01 g/mol. From the stoichiometry of the methane decomposition-reaction, it is clear that $n_{CH_4} = n_C$. Therefore it can be written that:

$$n_{CH_4,reacted} = \frac{m_C}{M_C} \tag{3.5}$$

The fraction of converted methane (X_{CH_4}) is then finally calculated from the following equation:

$$X_{CH_4} = \frac{n_{CH_4,reacted}}{n_{CH_4,purge}} \cdot 100 \tag{3.6}$$

With a unit of % The calculations performed in the subsection is done in the same way as was done in the specialization-project by Larsen [Larsen 2021] [22].

3.4 Abrasive strength

In order to measure the charcoals abrasive properties as a function of densification, the different samples were exposed to a drumming process with the Hanover drum as shown in **??**. Each drumming-process lasted for 30 minutes, and the speed was adjusted to 40 rounds per minute. The inside of the drum has a diameter of 21 cm, a depth of 10 cm, and consists of four wings, which is shown in Figure 32b Each drumming process was followed up by a 15 minutes long sieving-process. From the sieving-process it was possible to distribute the resulting material into the following sizes:

- 0-1,25mm
- 1,25-3,75mm
- 3,75-4,75mm
- 4,75-6,7mm
- 6,7-10mm
- 10-13,2mm

(a) **(b)**

Figure 32: The picture shows the experimental setup (a) as well as the inside of the used drum

3.5 Porosity: Gas pycnometry

To measure the porosity with this method, one has to take into account two different types of density, which is apparent density and absolute density. The porosity is then calculated with respect to these two parameters.

The apparent density, or often envelope density, is the most conventional way of measuring density. This density can be defined as the mass of an object divided by its volume where the volume includes that of its pores and small cavities [15]. This type of density was measured by manually measure the mass and volume of specimen-cubes, by the use of a mm-scaled ruler and a weight (to the nearest 0,001 g).

The absolute, skeletal or sometimes called true density does not include the pores and cavities in the material. In this method of porosity, the absolute density was measured by the use of gas-pycnometry. The apparatus used for this experiment is named Accupyc II 1340 (Figure 33) , which is a two-chamber gas displacement pycnometry system. What happens in this system is that the chamber with the material sample is first filled with inert gas (in this case Helium). This chamber is called the sample-chamber. If the system is sealed and the equilibrium-pressure is reached, the occupying amount of gas-volume is then released to a second chamber and measured there. Based on the known value of the sample-chamber and the volume of the inert gas, it is possible to calculate a precise volume of the sample material, since the inert gas penetrates into the pore of the material. By measuring the sample-mass in advance, it is possible to calculate the absolute density based on this[14]. The machine normally runs with 5-10 iterations per sample, in order to get as low uncertainty as possible. During the experiments, the lower limit for the equilibrium-rate was set to 0,005 psig/min, which was the value that had to be reached to get a new density-value for each iteration. When the sample that had just been heated with argon-gas at 1100 °C was tested, pressure-fail occurred. According to consulting discussions with Eli Harboe Albertsen at the department of materials science (IMA) and Henrik Wielechowski at Phoenix laboratory equipment, it was concluded that the pressure-fail probably occurred due to moisture or that the helium-particles got physically adsorbed at the charcoal-surface. Because of this, the lower limit for the equilibrium-rate was increased to 0,025 psig/min. This resulted in a successfully experiment, but with relatively higher standard deviation.

Porosity (p) can be defined as the ratio between the pore volume (V_p) and the total bulk-volume (V_b) in the material. With its unit in percent, the following expression for porosity can be used.[11]:

$$p = \frac{V_p}{V_b} \cdot 100 \tag{3.7}$$

One can define the total bulk volume as $V_b = V_p + V_m$ where V_m is the volume of the actual material. Then the porosity can be reformulated to the following equation:

$$p = (1 - \frac{V_m}{V_b}) \cdot 100 \tag{3.8}$$

By turning the fraction upside-down and multiplying with the same sample-mass both over and under, we get the following expression:

$$p = (1 - \frac{\frac{m}{V_b}}{\frac{m}{V_m}}) \cdot 100 \tag{3.9}$$

If one re-defines into densities, one gets the final expression for porosity:

$$p = (1 - \frac{\rho_b}{\rho_m}) \cdot 100 \tag{3.10}$$

Where ρ_b represent the apparent density and ρ_m represent the absolute density. Both parameters have g/cm^3 as units.

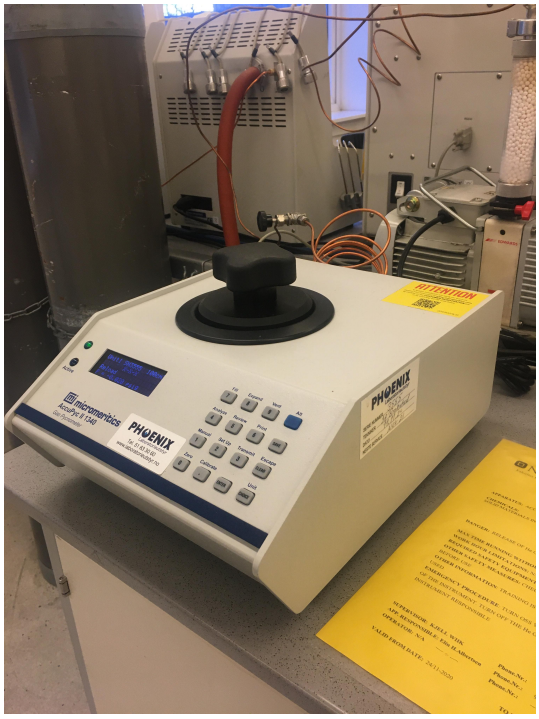

Figure 33: Picture of Accupyc II 1340, which is the apparatus used for the gas-pycnometry experiments

3.6 Compression testing

To measure the compressive strength, the samples were brought to the cutting-lab and shaped into cubes with dimensions ranging from 0,5-1cm, as shown in Figure 34.This was done to be able to measure clear and distinct surface areas, which was going to be exposed to the compression-stress equipment. The compression-test were performed at the compression-lab at room E-112, with a Zwick/Roell Z2.5 material testing machine. The samples were placed in a small bowl, and exposed to compression-forces by a $1,7 \cdot 1,7\ cm^2$ area crosshead, which runs at a speed of about 2 mm/min. The software which is connected to the machine gave out force-values in N, and by dividing with the surface area, we were able to compute the compression-stress-value for each sample, both paralell and perpendiclar to the fibers in the material.

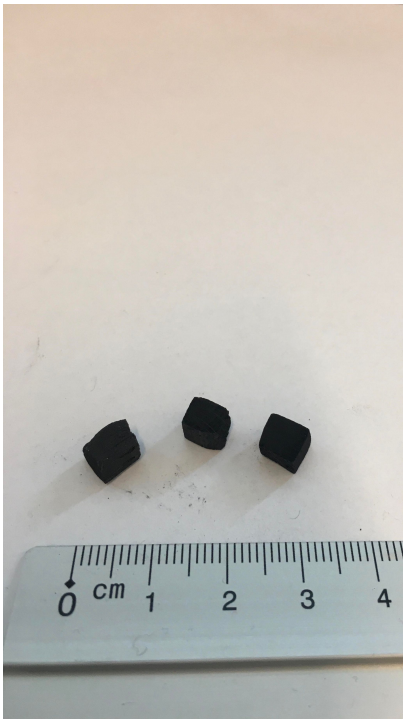

Figure 34: Examples of testing cubes for compression strength

3.7 Surface characterization: BET-analysis

In order to measure surface-properties of the densified charcoal, the different samples were scheduled to be examined with the micrometrics 3Flex, which is a high-performance adsorption analyzer, and can be used to calculate surface-area, pore size and pore volume of powders and particulate materials [16]. The device is shown in the left figure below (Figure 35a), and what happens in this process is that the sample material gets exposed to low pressure of "adsorptive" gas, and as the gas-pressure is increasing, so does the amount of adsorbed gas-atoms at the surface, until a monolayer is formed. This is used to calculate the BET surface area. An increased pressure of gas will lead to the penetration and filling of smaller and smaller pores. For more practical purposes, the entire filling-process is performed within low temperatures, normally around the boiling point of liquid nitrogen [33]. This explains the function of the big cylindrical container in Figure 35a; to contain the liquid nitrogen.

Prior to the adsorption-process, its crucial that the sample surface is free from moisture and other volatile species. Therefore the samples were heated and evacuated with the Degas SmartPrep System, which is showed in Figure 35b. This was done the day before the actual adsorption experiments, to make sure that the samples were as well prepared as possible.

The entire characterization-process is described chronological below, which is according to the

official procedure in the lab:

- First the mass of the test tube was measured, both empty and with the sample material in it. This was done to be able to monitor the change weight during the degas-reaction. The test tube tube was rather narrow (approximately 1 cm in diameter) so it naturally lead to a limited size of the sample materials.
- Degasing-process. The testing tube was attached to the port, together with a metallic heat-jacket around the pipe. The machine was set to "vac" and the degasing temperature was set to 250 °C. The sample was set to degas overnight.
- For the adsorption experiments, the container had to be filled up with liquid nitrogen approximately 30 minutes before use to stabilise the temperature. The container was filled up until 5 cm from the top of the flask. The sample tubes was then mounted to the respective ports in the adsorption-device together with the flask of nitrogen. At the end the protective shield was hung up in front of the test tubes.
- After all the practical was done, the software settings were adjusted to show a full BET-analysis, and a report were made. From everything was mounted and set up, it took approximately 6-7 hours before the results were ready.

The outputs that are used to calculate the specific surface area, is gained in the form of a BET surface plot. This is a linear plot with the following expression:

$$\frac{1}{\mathrm{Q}(\mathrm{P_0}/\mathrm{P}) - 1} = \frac{1}{\mathrm{Q_m C}} + \frac{\mathrm{C} - 1(\mathrm{P}/\mathrm{P_0})}{\mathrm{Q_m C}} \tag{3.11}$$

Where $(\mathrm{P}/\mathrm{P_0})$ is the relative pressure, Q_m is the monolayer capacity (cm^3/g), Q is the quantity adsorbed (cm^3/g), and C is a constant. According to a linear equation y =ax + b, where the relative pressure is the variable x, one can be able to calculate the intersection with the y-axis (i) and the slope of the curve (s):

$$\mathrm{s} = \frac{\mathrm{C} - 1}{\mathrm{Q_m C}} \tag{3.12}$$

$$\mathrm{i} = \frac{1}{\mathrm{Q_m C}} \tag{3.13}$$

There is then possible to find an expression for Q_m based on the intersect and the slope:

$$\mathrm{Q_m} = \frac{1}{\mathrm{s} + \mathrm{i}} \tag{3.14}$$

From this it is possible to calculate the specific surface area (S) by using the following formula

[Hwang and Barron 2011] [13] :

$$S = \frac{Q_m L_{av} A_m}{M_v} \tag{3.15}$$

where L_{av} is the Avogadros number, A_m is the molecular cross-sectional area and Mv is the molar volume (22414 ml)

(a) 3Flex **(b)** SmartPrep degas system

Figure 35: The pictures shows the instrumental setup of the BET-experiment (a) and the degasing-process done the day before (b).

Unfortunately, only one of the sample-sets of charcoal managed to be examined with results, while all the other test were interrupted due to a leakage-error. Although it is not confirmed, it could be due to the same reason for the errors in the testing with gas-pycnometry, with adsorbed nitrogen which does not return, and that the machine interpret this as a leakage.

3.8 Scanning electron microscopy and picture analysis

Scanning electron microscopy (SEM) was used both for qualitative comparison of the different degrees of densification, but also for measurement of the porosity. The measuring of porosity was done using a computer software called "ImageJ". This software measures the fraction of black

(pores) compared to the fraction of white (material surface) in a micrograph, which becomes the calculated porosity. It was therefore important with a relative high amount of contrast when the images are taken.

The images was taken with Zeiss-Ultra 55 FEG SEM (Figure 36). The electron voltage was set to 10 kV, and the detector used in the characterization was for secondary-electron(SE)-signals. Such signals are generated by inelastic scattering mechanisms, and one of the most common reasons is that loosely bound valence-electrons are ejected from the structure. The kinetic energy of the ejected electrons are produced when the primary electron hits the sample [Inkson 2016] [17]. Secondary electrons are much more abundant than backscattered electrons, for instance, and SE-imaging is the most basic imaging when one wants to investigate the shapes of a specimen.

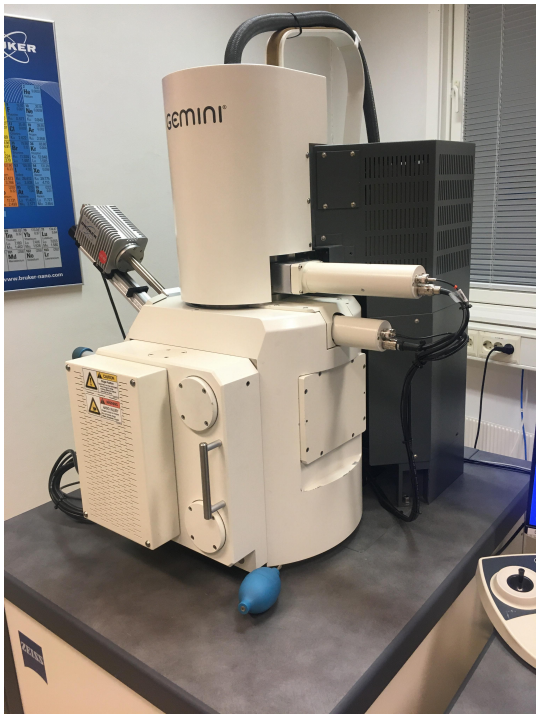

Figure 36: Zeiss-Ultra 55 FEG SEM

ImageJ is a software used for processing of images, and that is Java-based. The software is incorporated with a number of useful tools for image processing, such as histogram manipulations and standard image filters (mean, median etc.). It also provides a set of image segmentation algorithms, such as mixture modeling, maximum entropy and color-based threshold [5]. The latter is especially important when it comes to the measurement of porosity, which is also going to be applied in this experiment.

The experimental procedure for measuring the porosity is described chronological below:

- First the chosen micrograph had to be opened and saved in the software.
- Preparation of image. The setup named "particle analysis" was chosen. The chosen imaged was cropped in order to highlight the correct area, and then it was converted to an 8-bit image.
- Threshold adjustment. The threshold for particle detection was adjusted so that the phase of interest (the pores) was coloured red, while the rest was coloured white. The adjustment was made by the use of slide bars at the side of the page (image), and when one hits the "apply"-button the image turned black and white, showing the contrasts of the pores and the rest of the material.
- Image analysis. In order to be able to calculate the porosity by calculating the fraction of pores in the image, the setup "analyze particles" was chosen in the menu. The final outcome of the analysis was three windows: the first was showing the numerical values in the different areas of the image, the second window showed a list of the values of the porosities, and the third window was a summary.
- The last process was iterated a few times until the value of the fraction/porosity was reliable enough.

4 Results

4.1 Densification results

Figure 37, Figure 38, Figure 39, Figure 40 and Figure 41 shows the development of the temperature and the gas flow during each of the experiments, with both argon and methane. As shown in Figure 38, the planned one hour experiment, the total amount of methane gas supplied to the process were a bit shorter than expected due to technical challenges, but the reaction temperature was within the acceptable limits. Because of this the experiment were repeated once more, with better results. All of the experiments were scheduled to be performed under reaction temperatures at 1100 °C. One can see from most of the figures that there was a small deviation in temperature compared to what was expected, but that this is considered good enough. A substantial exception is the experiment that was scheduled for 3 hours of methane-purging. As one can see, there is some difference between the furnace control temperature and the measure temperature of the thermocouple in Figure 41, so it may be not so clear as to determine if this is due to some error with the equipment, or if the reaction temperature is too low.

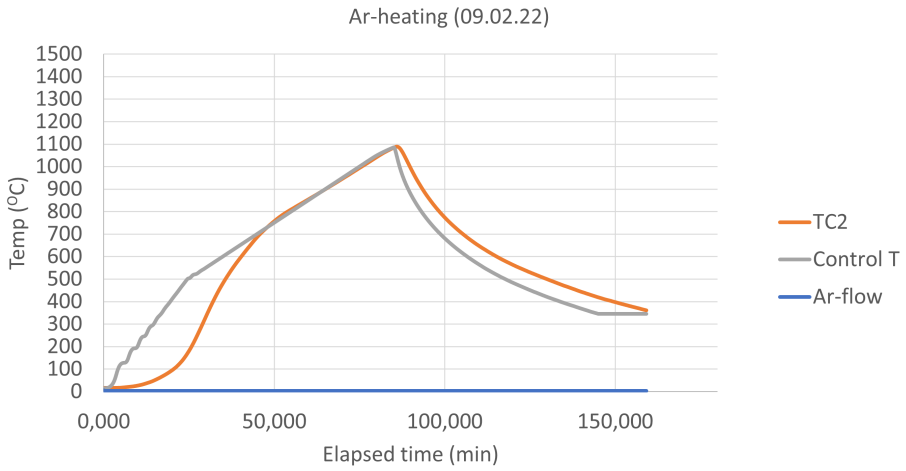

Figure 37: The figure shows experimental temperature and gas flow as a function of time of the Ar-purged sample

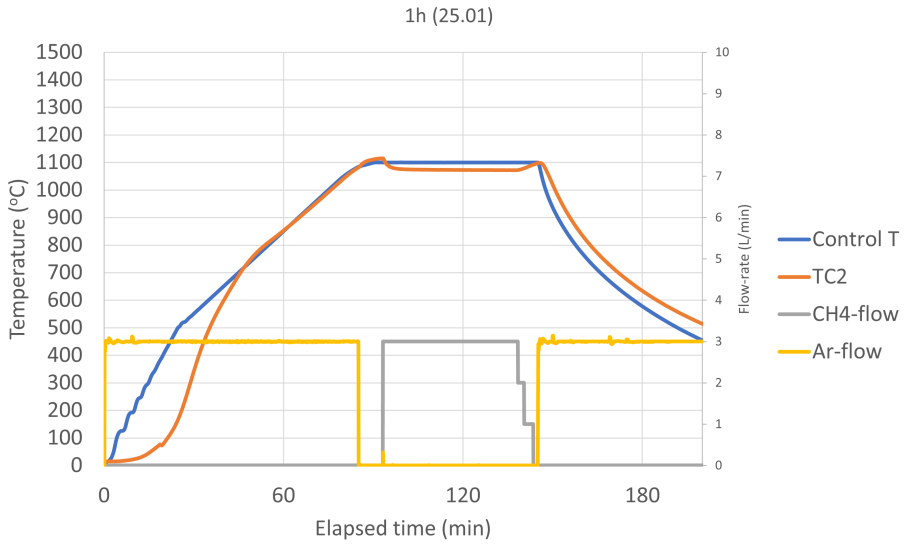

Figure 38: The figure shows experimental temperature and gas flow as a function of time of the sample purged with methane for 1h (10,3 wt% deposition)

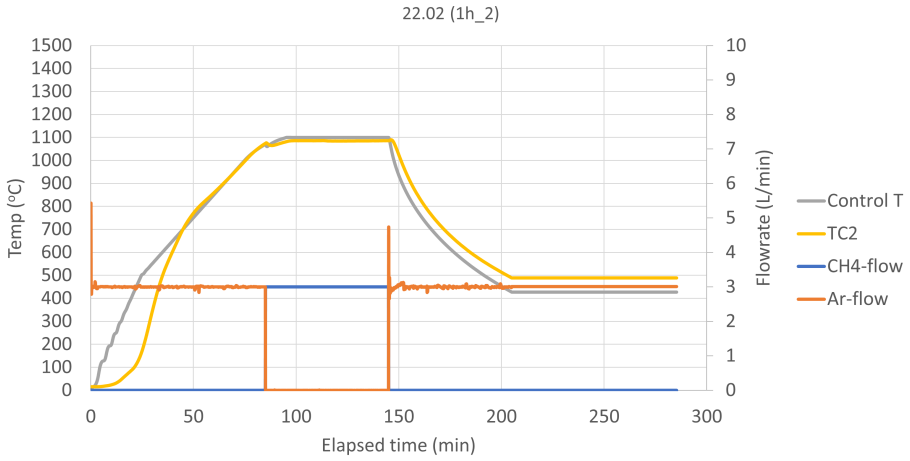

Figure 39: The figure shows experimental temperature and gas flow as a function of time of the sample purged with methane for 1h (11,1 wt% deposition

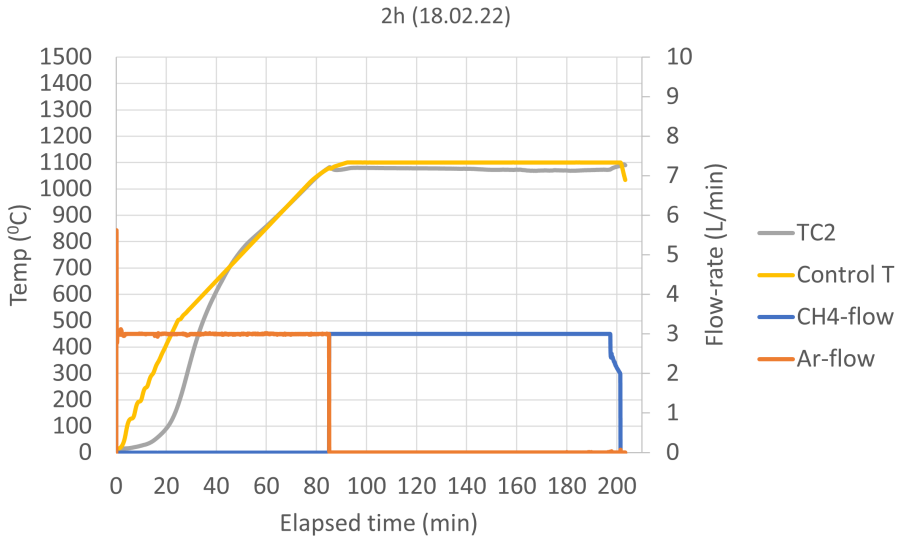

Figure 40: The figure shows experimental temperature and gas flow as a function of time of the sample purged with methane for 2h (24,0 wt% deposition

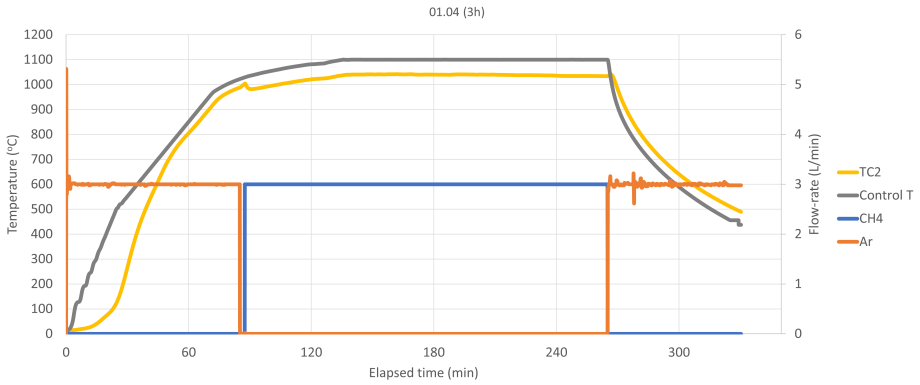

Figure 41: The figure shows experimental temperature and gas flow as a function of time of the sample purged with methane for 3h (29,7 wt% deposition

If one looks at Figure 42 one can see that the amount of deposited carbon increases with purging time of methane. Despite that the reaction temperature varies from 1031-1083°C, there is almost a linear relationship between the purging time and carbon-deposition. This is illustrated by the line in the figure. As one can see, the experiment with the temperature of approximately 1074°C is a bit above the line, as well as the experiment with a reaction temperature of about 1031°C is placed a bit under the line. This suggests that the relationship would have been almost perfect linear if all the experiments have had the same temperature. Another interesting result in this figure is that there is possible to achieve a deposition as high as 29,7 wt% after approximately 3 hours. This value would have been even higher, as mentioned, had it not been for the low temperature.

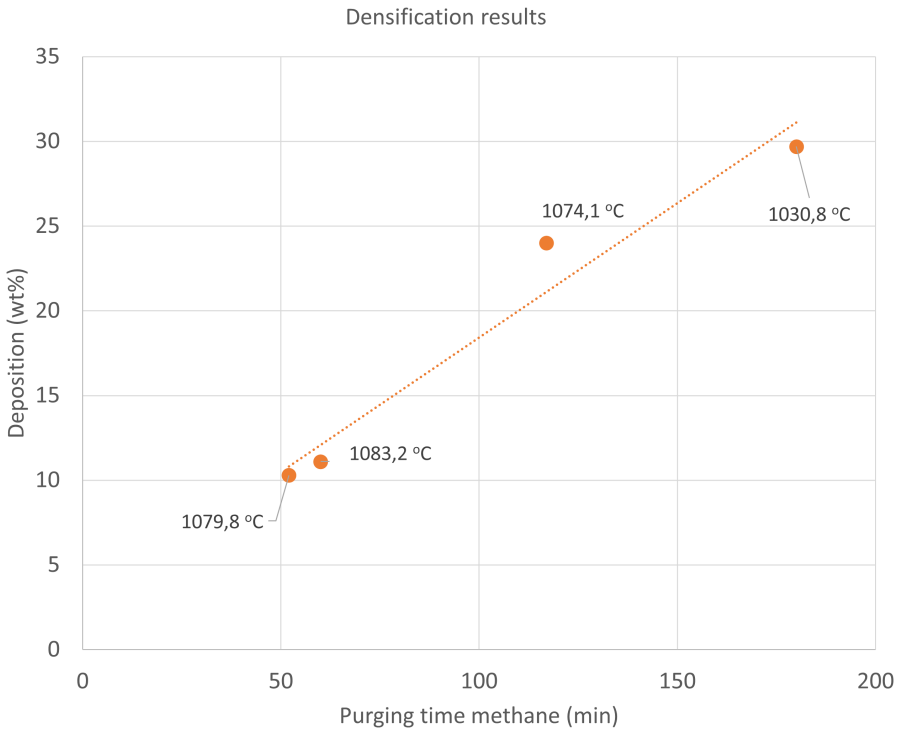

Figure 42: The figure shows an overview of the densification experiments, with different degrees of C-deposition as a function of purging time with methane, in addition to a trend-line showing the approximate linear relationship. The average-temperature is also included for each experiment.

However, if one takes a look at the results in Figure 43, one can see that the fraction of converted methane lies within the range of 40-50 %. One can also see that lower average reaction temperature and higher total reaction-time tends to lead to a lower fraction of conversion. However, if one look at the experiment at 60 min purging-time and 1083°C, this one has a conversion-value at 43%. This shows that this trend is not too significant. One can also notice that the experiment with the largest purging-time has the lowest average reaction-temperature. Because of this there may

be difficult to separate the parameters of high purging-time and low reaction-temperature. What else is shown in this figure is that the methane conversion-fraction tends to rise with the rising reaction-temperature in most cases. One exception is the experiment done with the highest reaction temperature, which shows a bit lower fraction of conversion than the others in the same area of temperature. Why this is the case can be unclear, but one of the reasons may be some irregularities with the furnace during operation.

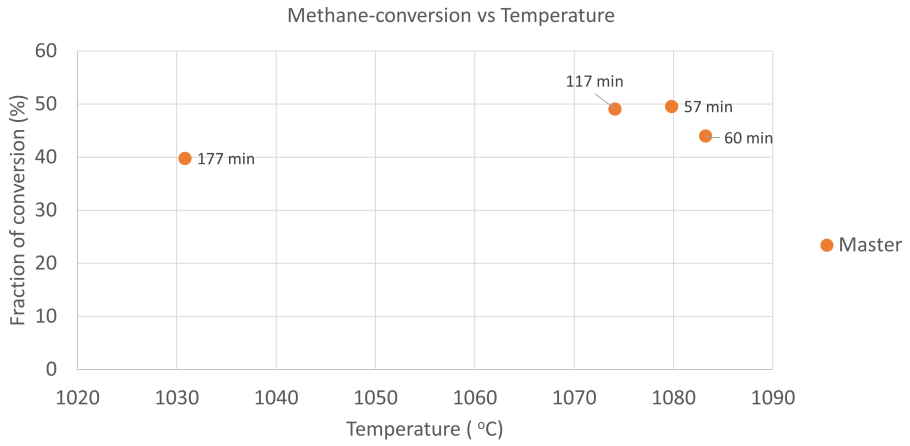

Figure 43: The figure shows an overview of the fraction of converted methane during the different densification-experiments as a function of average temperature.

Based on the factors mentioned in the paragraph above, one can conclude that the relationship between the reaction temperature, the supply of methane-gas and the fraction of conversion of methane is highly signifficant. One can also conclude that the most deposition happens between the first and the second hour of methane-purging, given that the temperature is in the proximity of 1100 °C.

4.2 Compression-testing

This subsection shows the results of the testing of the compression-strength for the different directions for the different samples. Figure 44 shows how the compression strength develops when more and more carbon is deposited to the charcoal. The values at 0 % deposition is from the sample that is just heated with Ar. As one can see, there is a lot of uncertainties regarding the values, and one of the reasons to this is the big variations in surface texture, fiber arrangement and pore-pattern in each sample specimen. One thing that is the same for all deposition-degrees is that the compression-strength parallel to the fiber-direction seems to be greater than the strength of the perpendicular to the fiber-direction.

The results from Figure 45, which shows the compression-strength values for raw charcoal and heated charcoal, is perhaps more interesting than the results of Figure 44. This is because the increase of strength is more visible here, compared to the other figure, when it comes to both directions relative to the fibers. Based on this information it may be possible to conclude that the heating-process is more important than the densification-process, when it comes to the compressive strength of the charcoal.

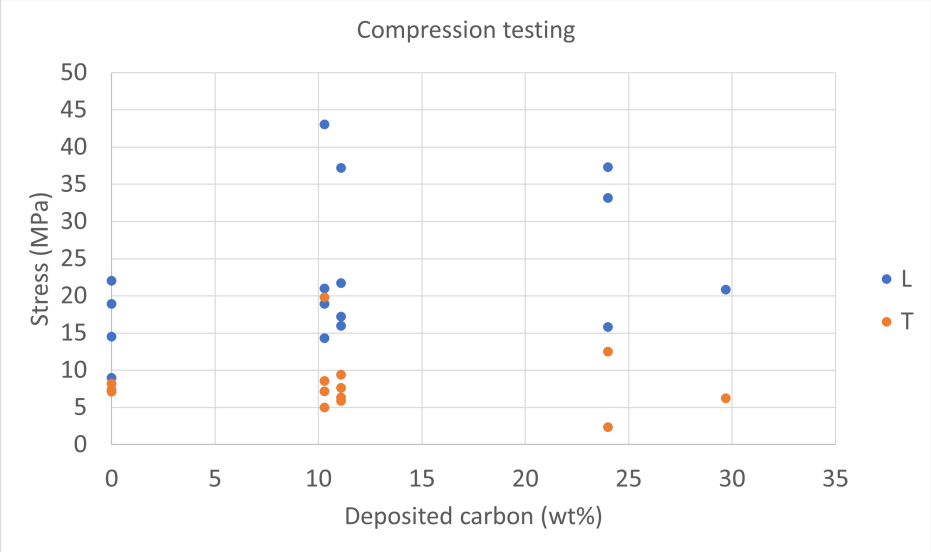

Figure 44: The figure shows the different values of compression strength as a function of increased carbon-deposition. The letter T and L refers to when the compression-stress is directed perpendicular and parallel to the fiber-direction in the material, respectively.

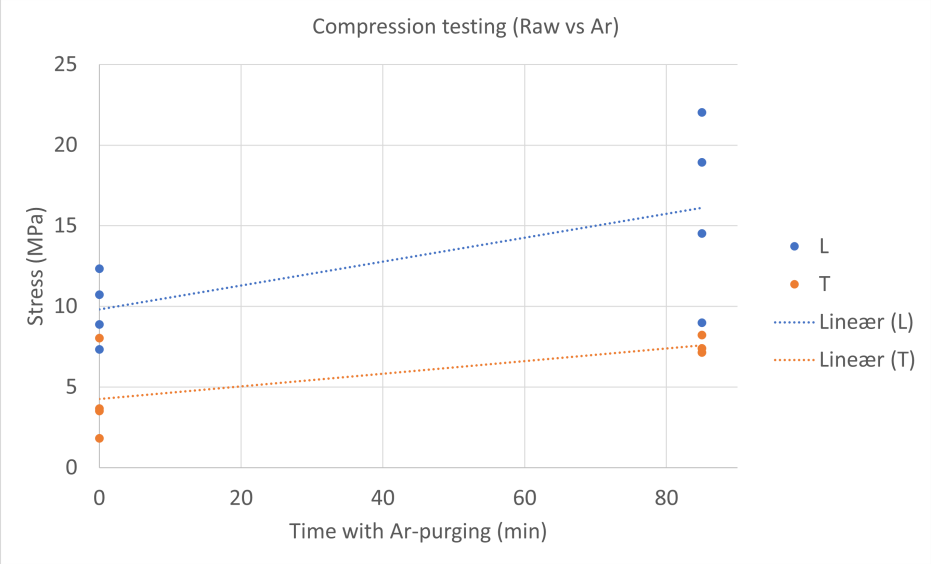

Figure 45: The figure shows the different values of compression strength for both raw charcoal and charcoal that is purged with argon-gas. The letter T and L refers to when the compression-stress is directed perpendicular and parallel to the fiber-direction in the material, respectively.

4.3 Abrasive strength-testing

Figure 46 shows how the different size-intervals contributes to the total mass of the different samples. Figure 47 shows the same results, but with a more enlarged focus on the upper size-intervals. Based on the these figures, it is easy to see that there is a big difference between the raw-material and the rest of the samples when it comes to fines, that is particles with a size of 1,25 mm or less. The results show that for raw charcoal, about 20 wt% of the total mass consists of fines, while this number is as low as 5 wt% for the sample which is heated with argon. This small value is similar to the densified samples. The low fraction of fines for the densified samples may indicate that the deposited carbon has a great ability to stick to the material and withstand the forces of the milling-process, which is performed in this experiment. The enlarged picture of Figure 47 shows a relative big gap between the raw-material and the argon-purged material and the densified samples, but since the latter samples have a higher increase between the size of 10 and 12,5 mm, it is right to assume that these samples posses the highest fractions of samples in this size-range. Based on all this information about the abrasive-test, one can conclude that there is no clear change as the degree of densification increases, but that the densified samples in general have a lower fraction of fines than the sample that is just heated with Argon. This could be due to the densification process itself, or that the densified samples are exposed to a high temperature for much longer time than the sample with just Ar. The greatest change is, however, between the

raw-material and the rest of the samples.

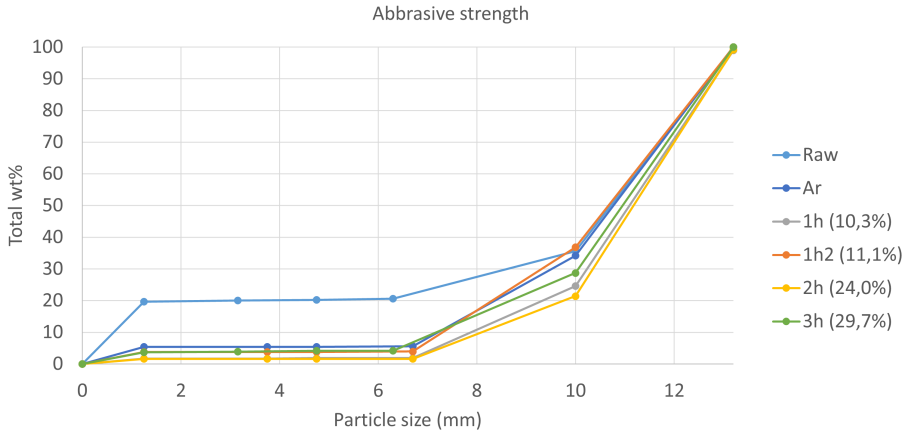

Figure 46: The figure shows the resulting values of the abrasive strength testing. The figure is an overview of total size distribution of all the samples.

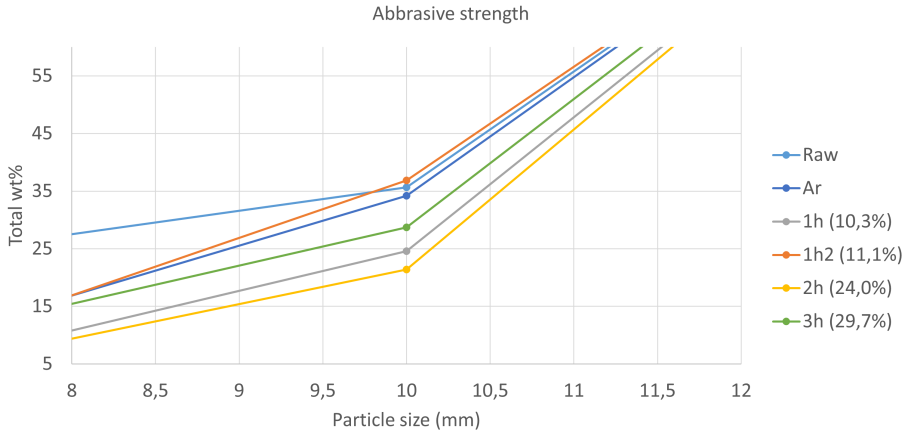

Figure 47: The figure is an enlarged figure of Figure 46 with a greater focus on the highest size-intervals.

4.4 Norlab-results

The table below (Table 5) shows the results of the ordered chemical analysis for the three samples that were performed by Sintef Norlab. The results t

	Raw	Ar	3h
Volatiles (%)	14,31	1,97	0,96
Ash (%)	2,09	1,57	2,04
Fix C (%)	83,6	96,46	97,0

Table 5: Results from the chemical analysis that was ordered by Sintef Norlab

4.5 BET surface area

The figure (Figure 48) and the table below (Table 6) shows the results of the BET-experiment with the one sample that managed to not get a error regarding pressure-fail. The actual session with BET, after the 24 hours of degassing, took about 5-6 hours. This is a relatively short time compared to other materials, often in the form of powders.

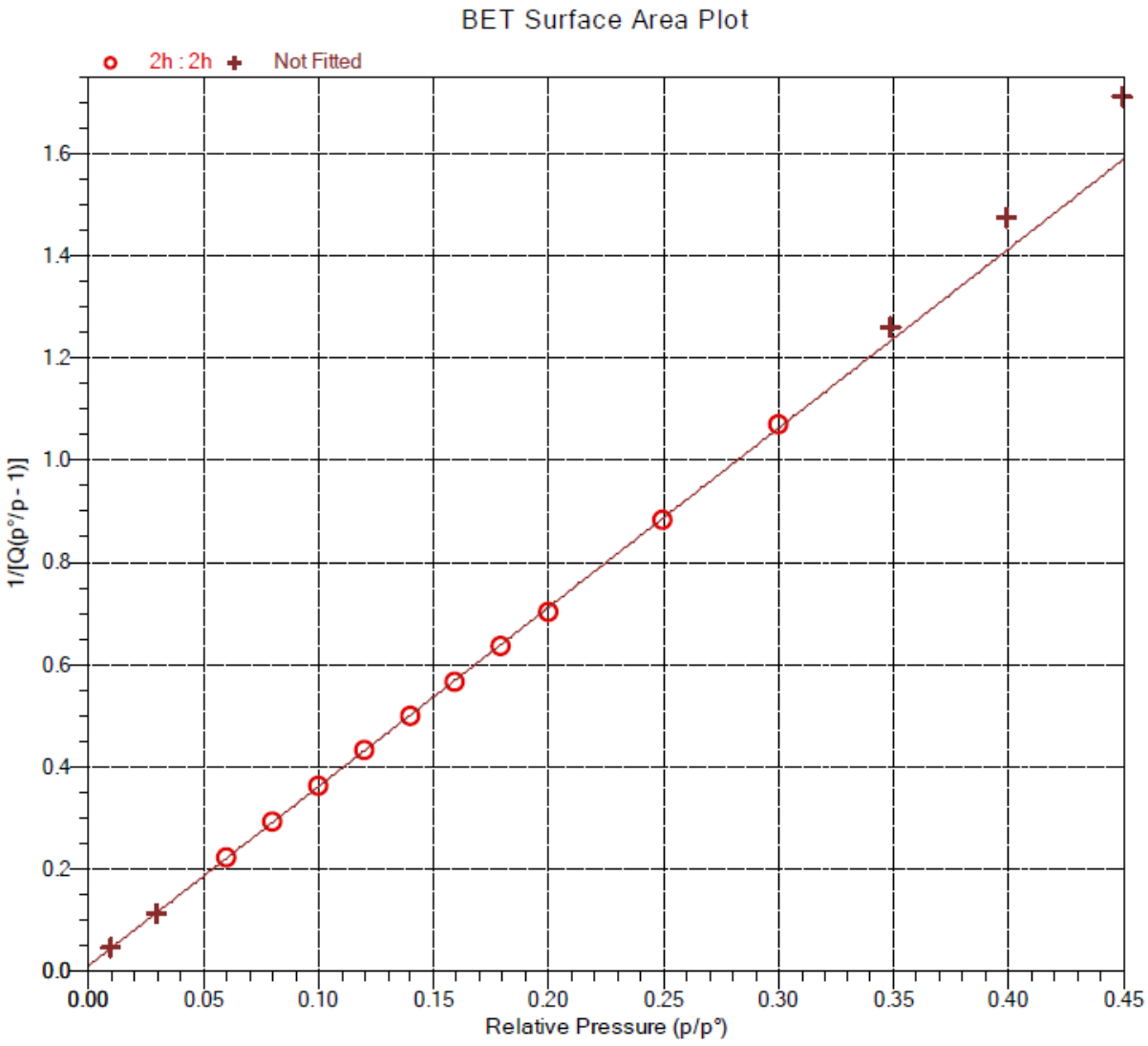

Figure 48: The figure shows the BET surface plot for the charcoal-sample with 24 wt% deposition

	Value	Unit
BET surface area	1,2375 $\pm 0,0075$	m^2/g
Slope (s)	3,506277 $\pm 0,021074$	g/cm^3
Y-intercept (i)	0,010947 $\pm 0,003669$	g/cm^3
C	321, 292523	-
Q_m	0,2843	cm^3/g STP
Molecular cross-sectional area (A_m)	0,1620	nm^2

Table 6: The table shows important parameters for the calculations of the BET plot in Figure 48. All the parameters are already accounted for and elaborated in the experimental section

4.6 Porosity

Figure 53 shows the calculated porosity of the different samples with the different degree of carbon deposition. Figure 54 shows the same porosity values for the raw charcoal that was used and the charcoal that was heated only with argon-gas. The values of the two types of densities that were used to calculate these porosity-values, are shown in Figure 49, Figure 50, Figure 51 and Figure 52. In the four figures of the densities, their respective standard deviations are also calculated and added on. As one can see in the figures of the densities, the uncertainties and the standard deviations of the measurements of the apparent densities are much higher than for the absolute densities. However, the apparent density is not significant. Both density-curves shows trends towards increasing with increased deposition. If one looks at Figure 50 The results in Figure 53 and Figure 54 are found using constant values for the absolute density. The constant values are 1,6 for the raw-material, 2,01 for the samples heated with only argon and 1 for the densified materials. By doing this it was possible to calculate several values for the porosity within each degree of densification. Even though there is a wide range in the results, one can see that the average value tends to decrease when the densification increases.

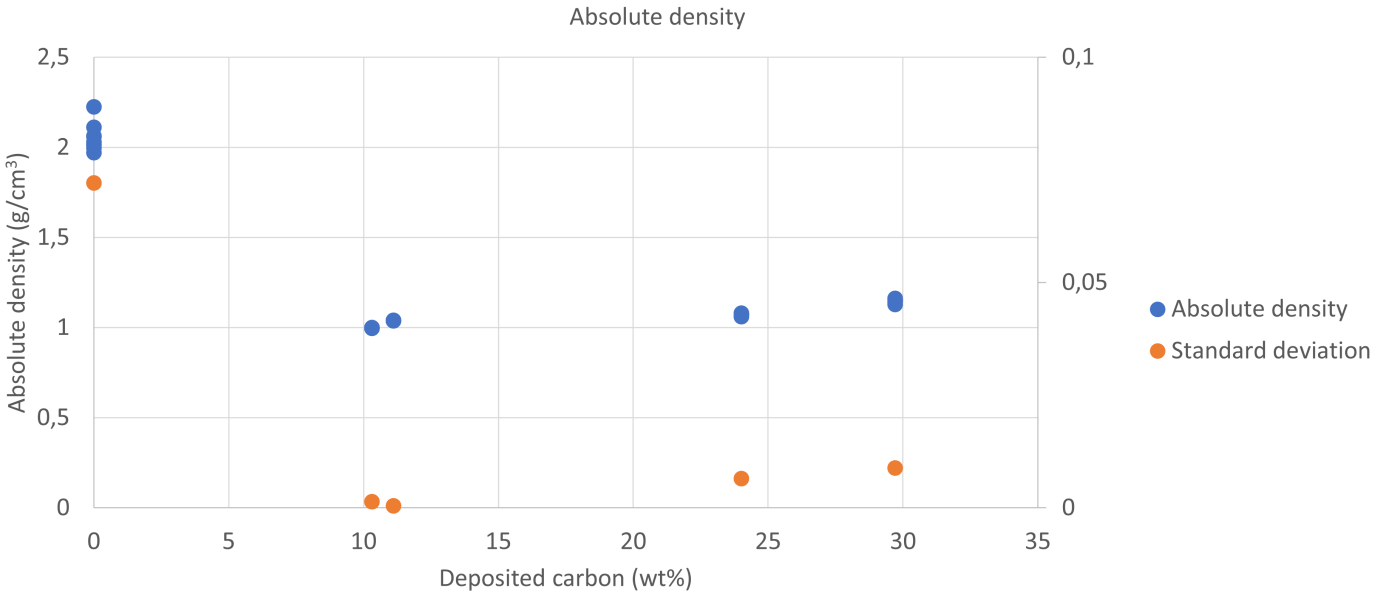

Figure 49: The figure show the different values of absolute/skeletal density as a function of wt% of deposited carbon, together with the respective values of standard deviation (right vertical axis)

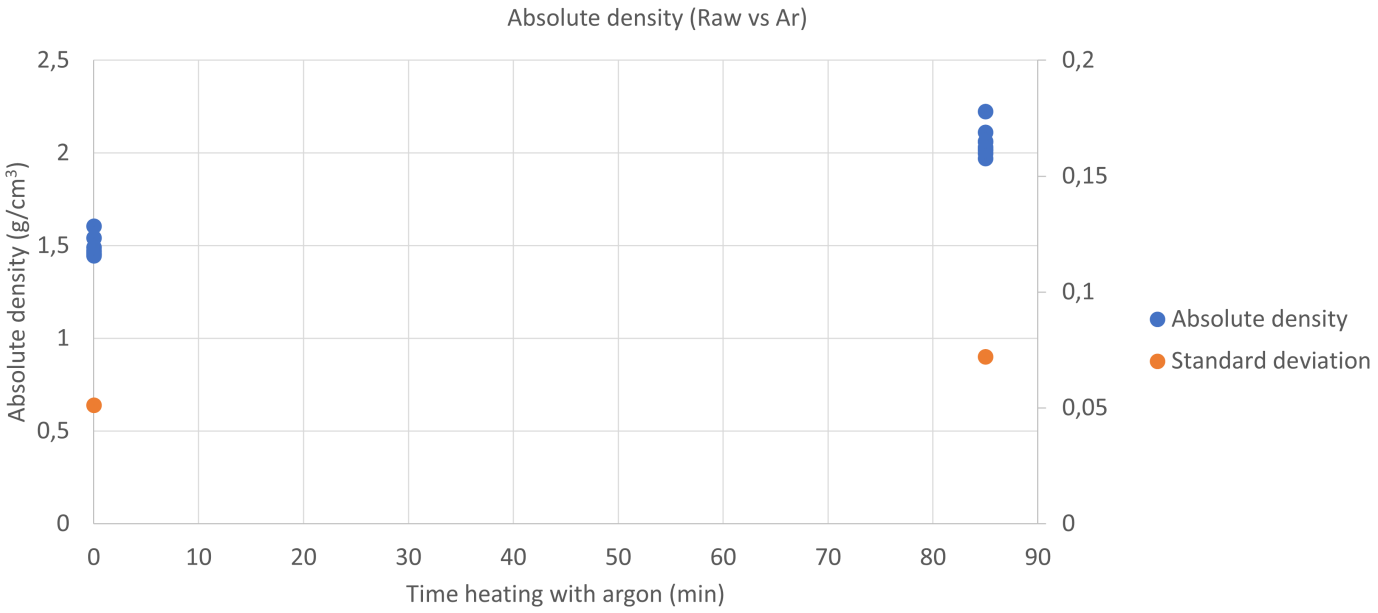

Figure 50: The figure show the different values of absolute/skeletal density for raw charcoal and for the argon-heated sample, together with their respective values of standard deviation (right vertical axis)

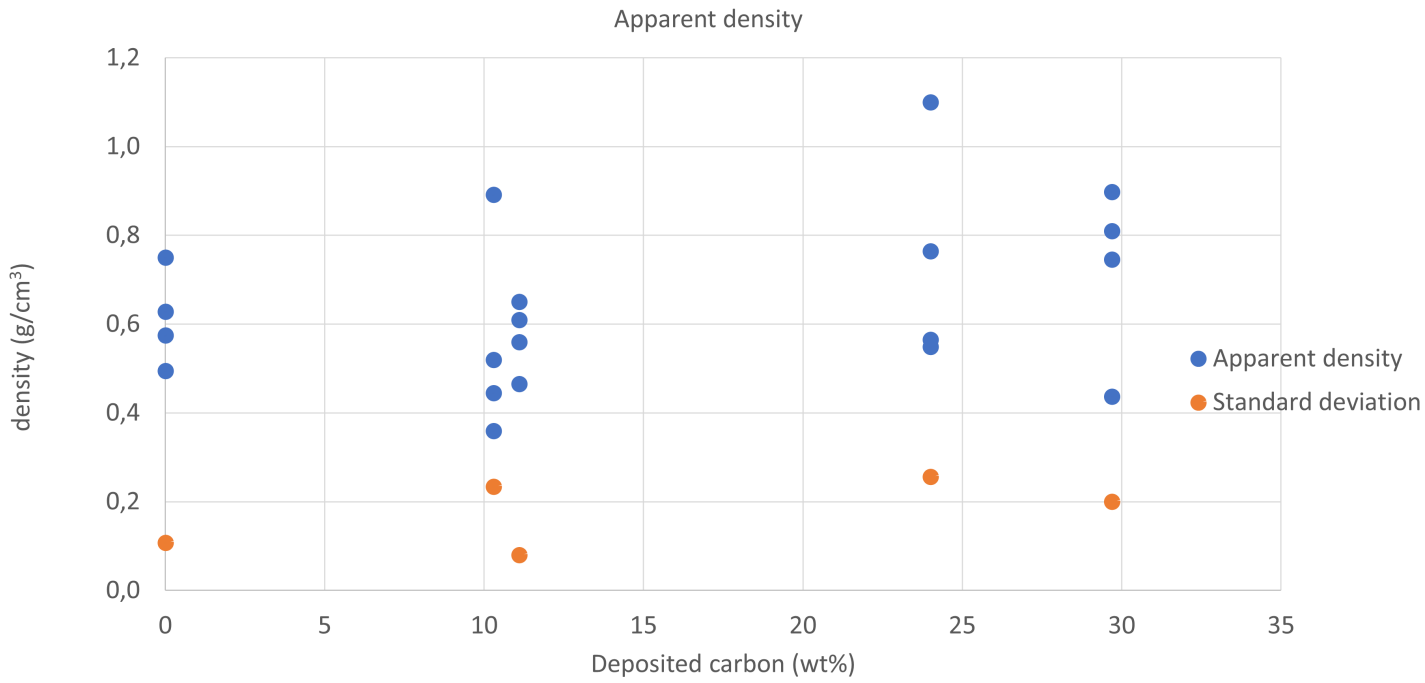

Figure 51: The figure show the different values of apparent density as a function of wt% of deposited carbon, together with the respective values of standard deviation.

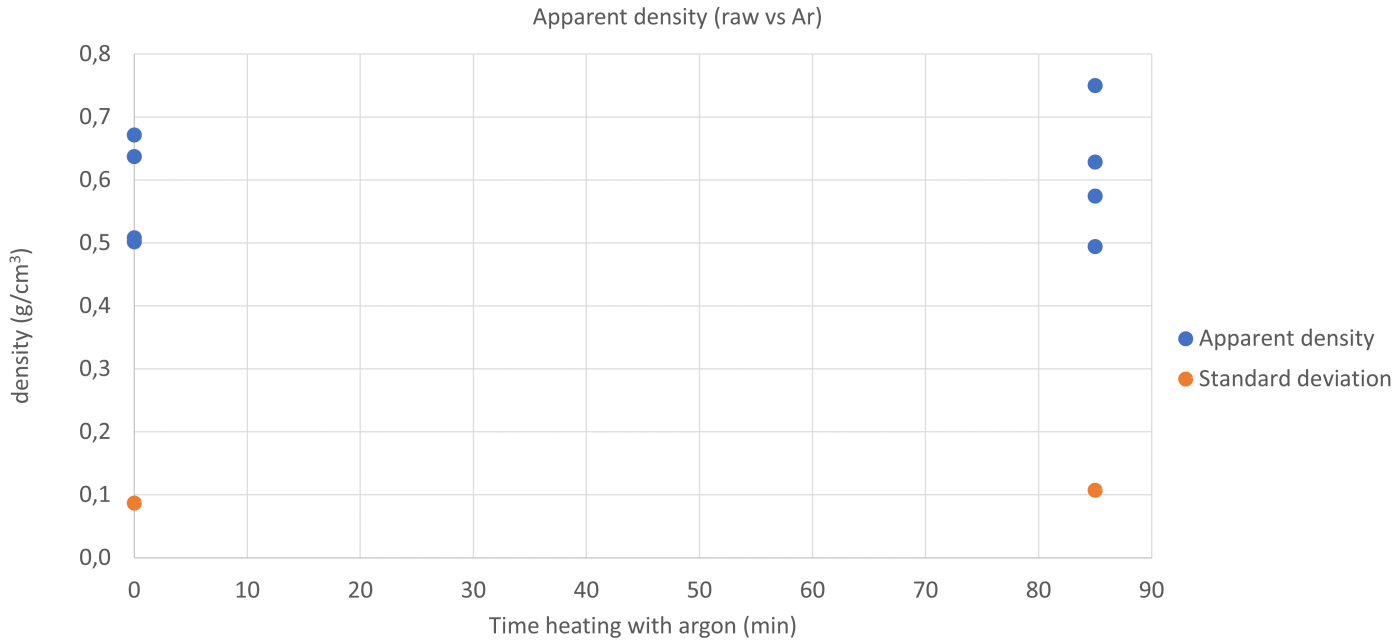

Figure 52: The figure show the different values of apparent density of raw charcoal and the sample heated with argon, together with their respective values of standard deviation.

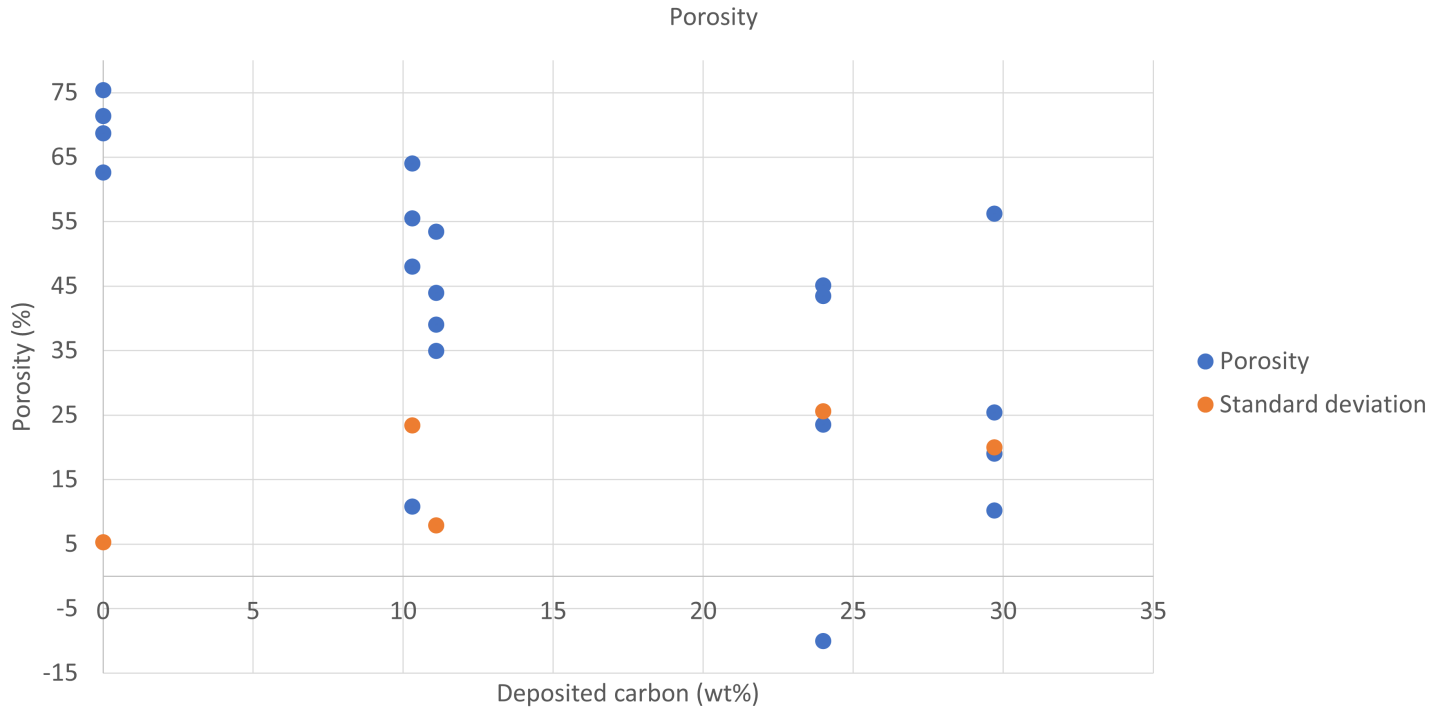

Figure 53: The figure shows porosity-values as a function of amount of deposited carbon by calculation with apparent and absolute density, together with their standard deviations.

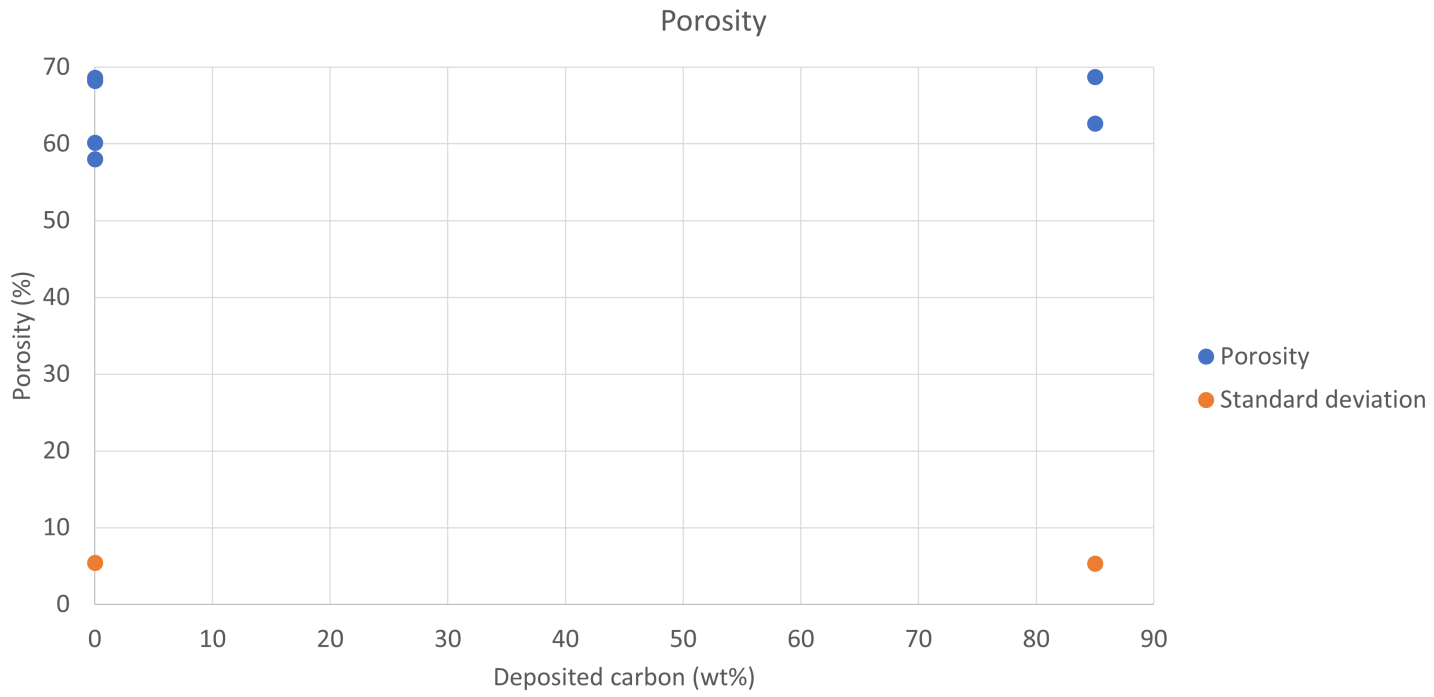

Figure 54: The figure shows porosity-values for raw charcoal and the sample heated with argon by calculation with apparent and absolute density, together with their standard deviations.

4.7 SEM/ImageJ

The SEM-images below shows how the porosity is developing throughout the cross-section of the investigated sample. The figures shows one of the three samples that were examined from each of the five sample-sets. After every overview-picture of the surface, the respective points are shown with a greater magnification to show the variation in the surface-structure. From Figure 55 one can see that there is a relatively high porosity throughout the surface, which is demonstrated in the enlarged sub-pictures (Figure 56a-Figure 58b). These pictures show clear pore-pattern with almost no misfits or particles in the pores. If one looks on the sample that has been heater with only argon (Figure 59) one can see that the porosity is significantly lower. The figure showing the sample that is densified with 10,3 wt% (Figure 63) is showing a higher porosity compared with the sample purged with only argon deposition is showing a higher value of overall porosity. Based on this development, there might be challenging to see a specific development or pattern for the porosity. It might also be difficult to see any pattern for how the porosity develops as the examination proceeds into the material.

4.7.1 Raw

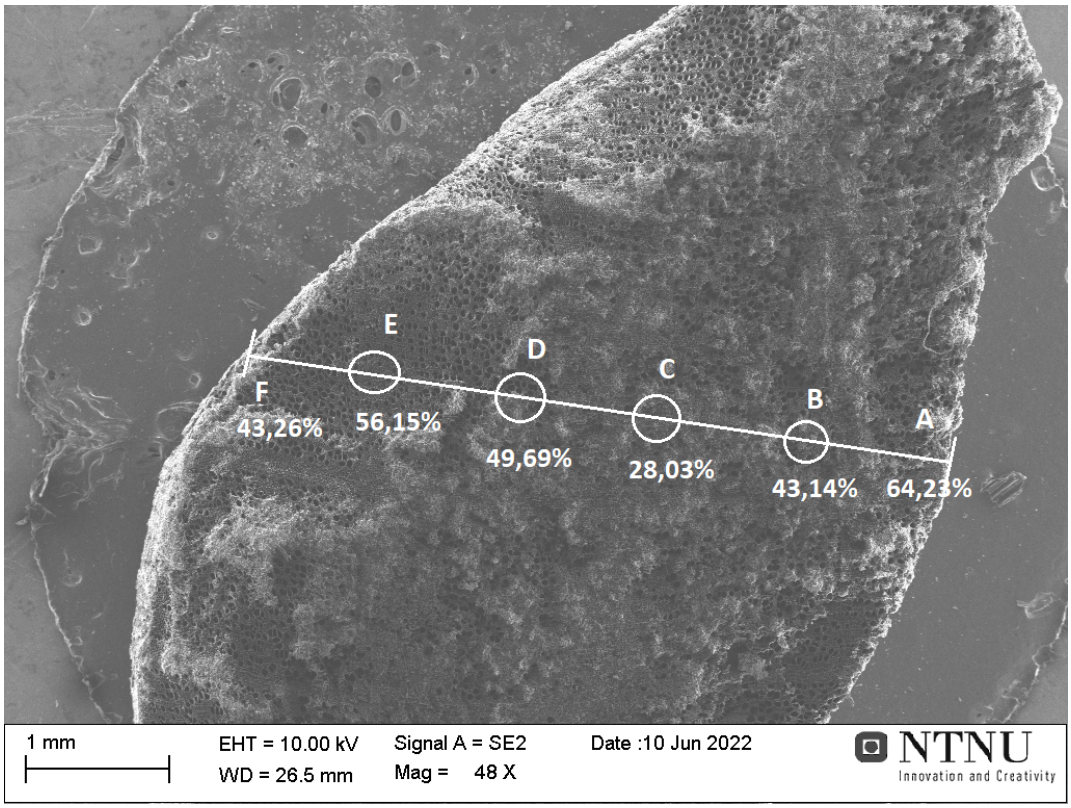

Figure 55: Overview of Sample 1 for raw charcoal

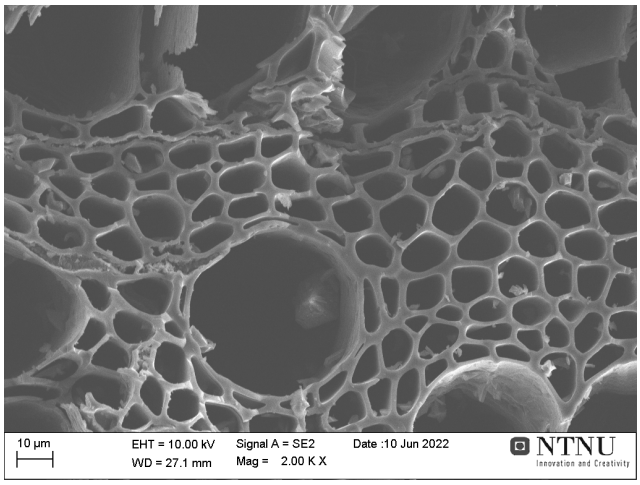

(a) A

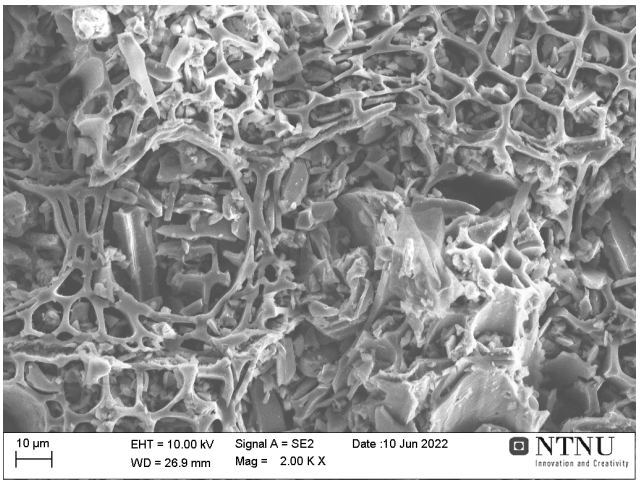

(b) B

Figure 56: The pictures are showing area 1A and 1B for raw charcoal

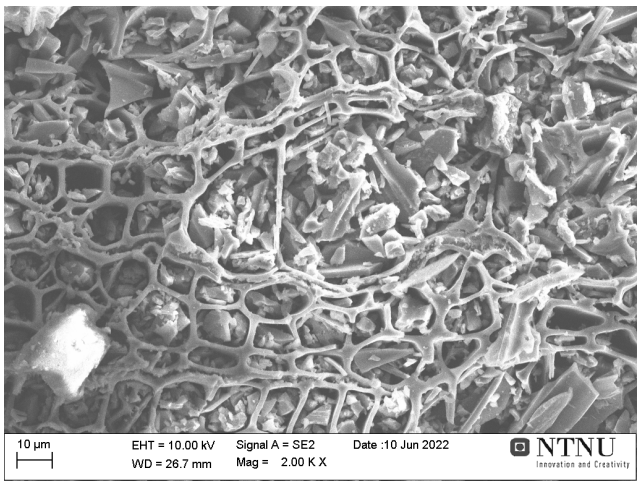

(a) C

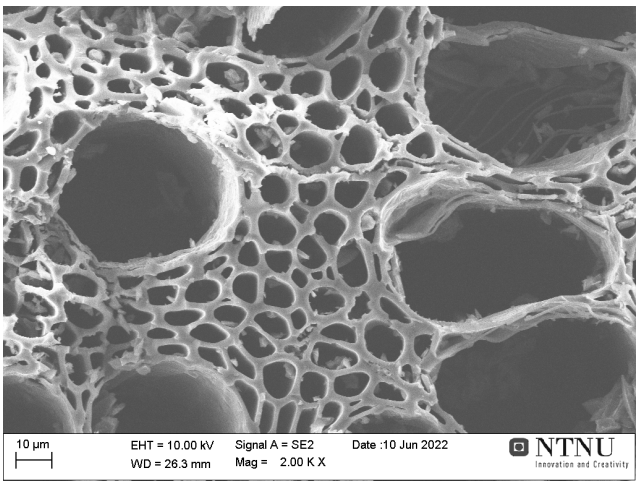

(b) D

Figure 57: The pictures are showing area 1C and 1D for raw charcoal

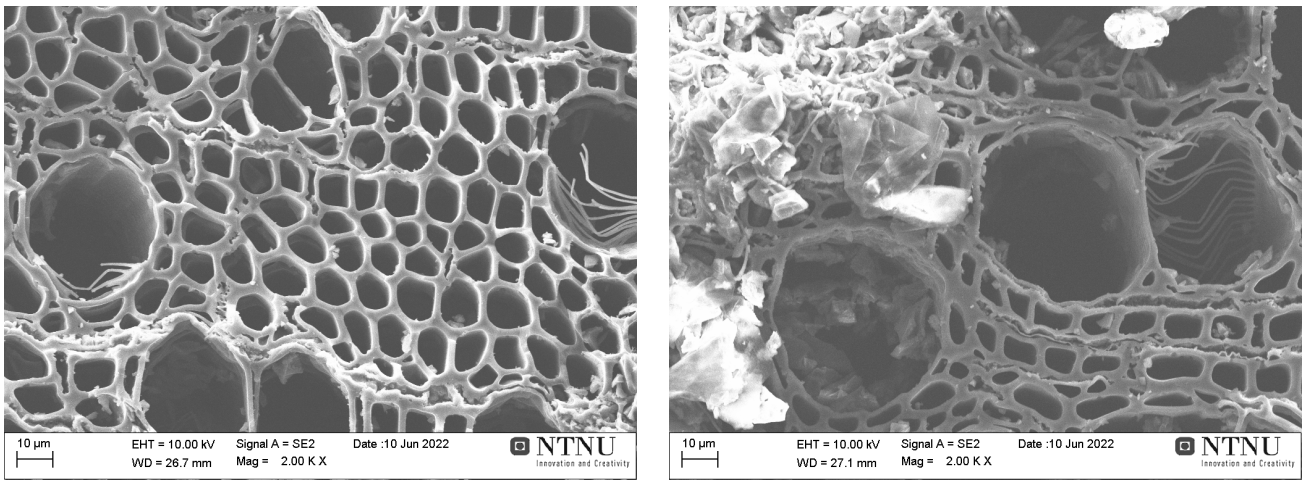

(a) E **(b)** F

Figure 58: The pictures are showing area 1E and 1F for raw charcoal

4.7.2 Ar

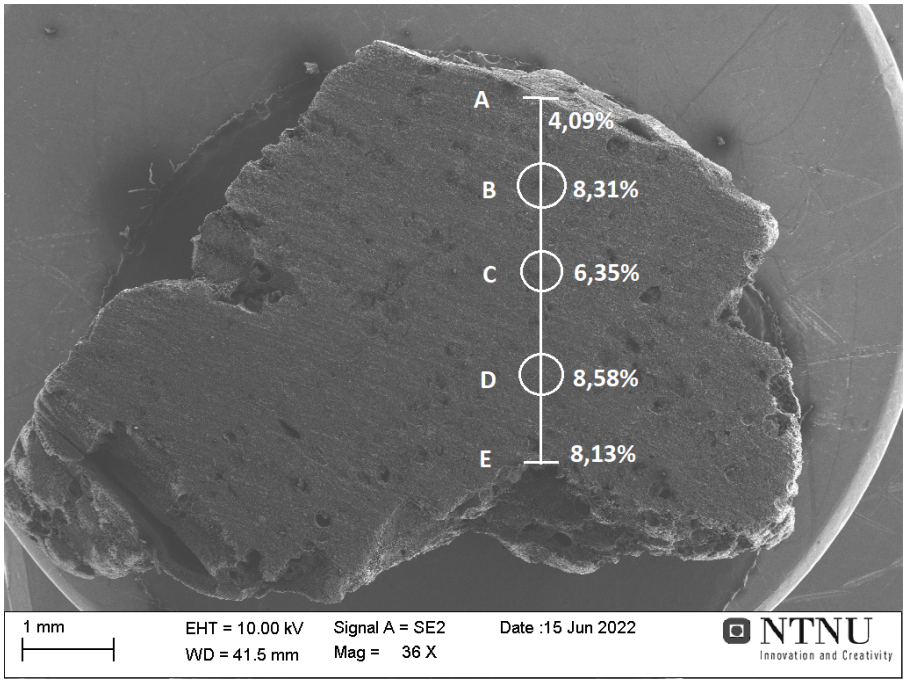

Figure 59: Overview of Sample 1 for ar-heated charcoal

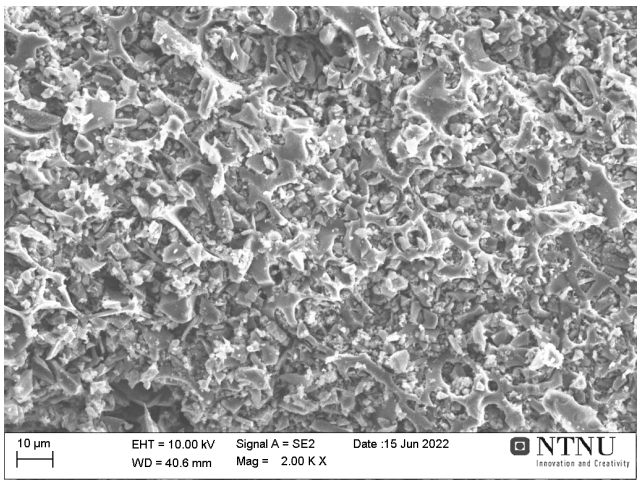

(a) C

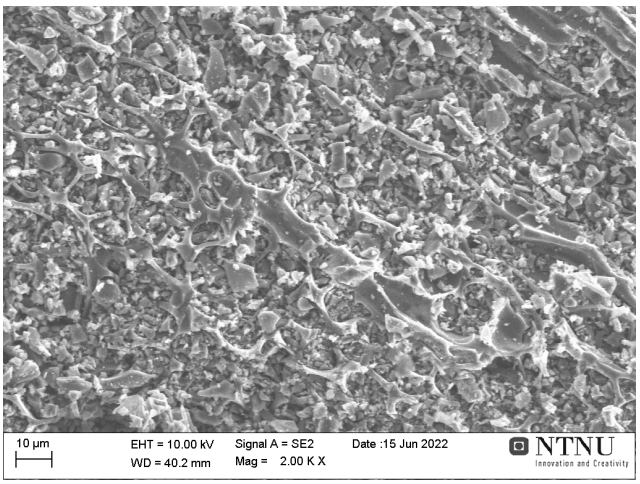

(b) D

Figure 61: The pictures are showing area 1C and 1D for ar-heated charcoal

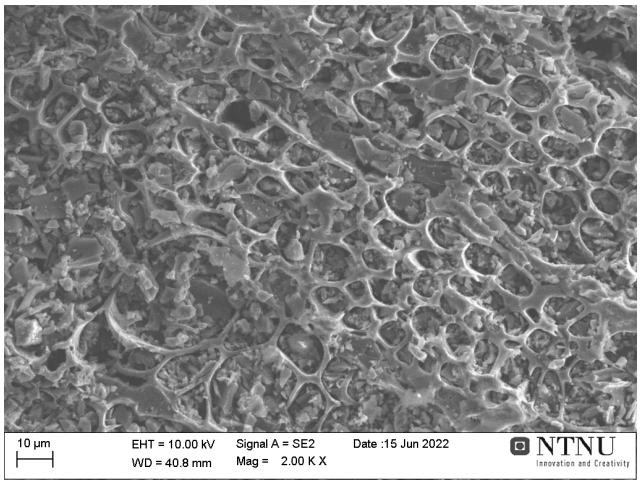

(a) A

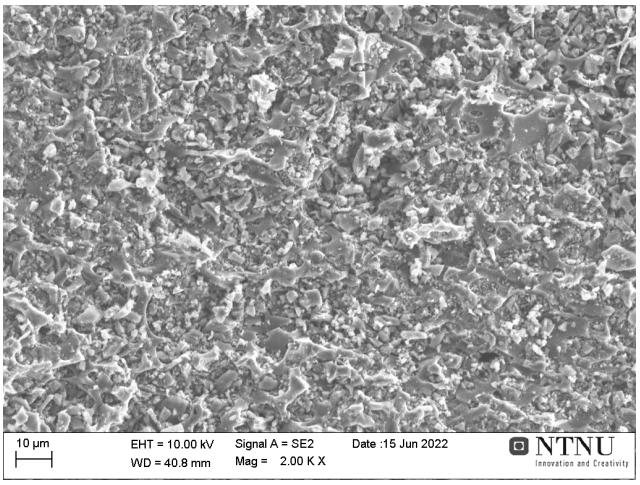

(b) B

Figure 60: The pictures are showing area 1A and 1B for ar-heated charcoal

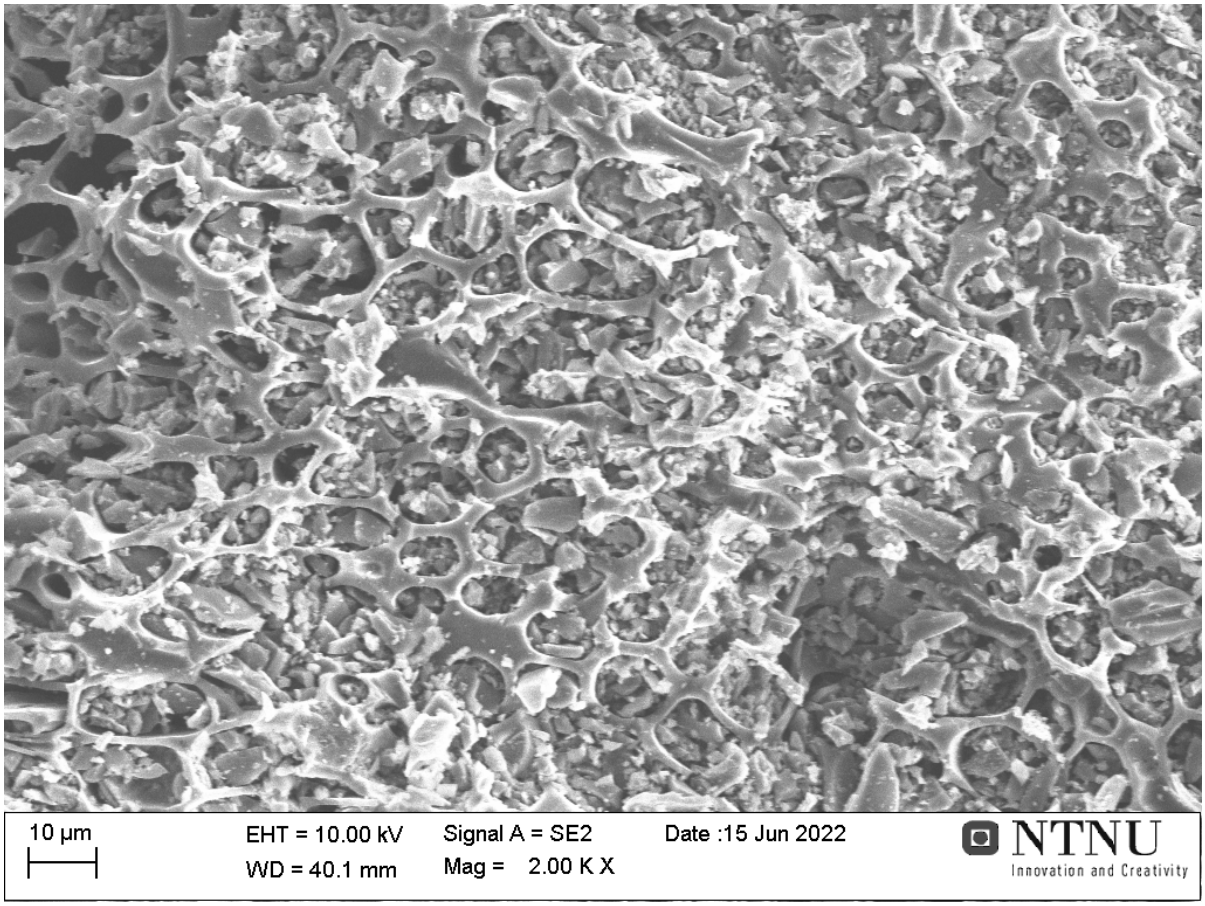

Figure 62: The picture is showing area 1E for ar-heated charcoal

4.7.3 1h (10,3 wt%)

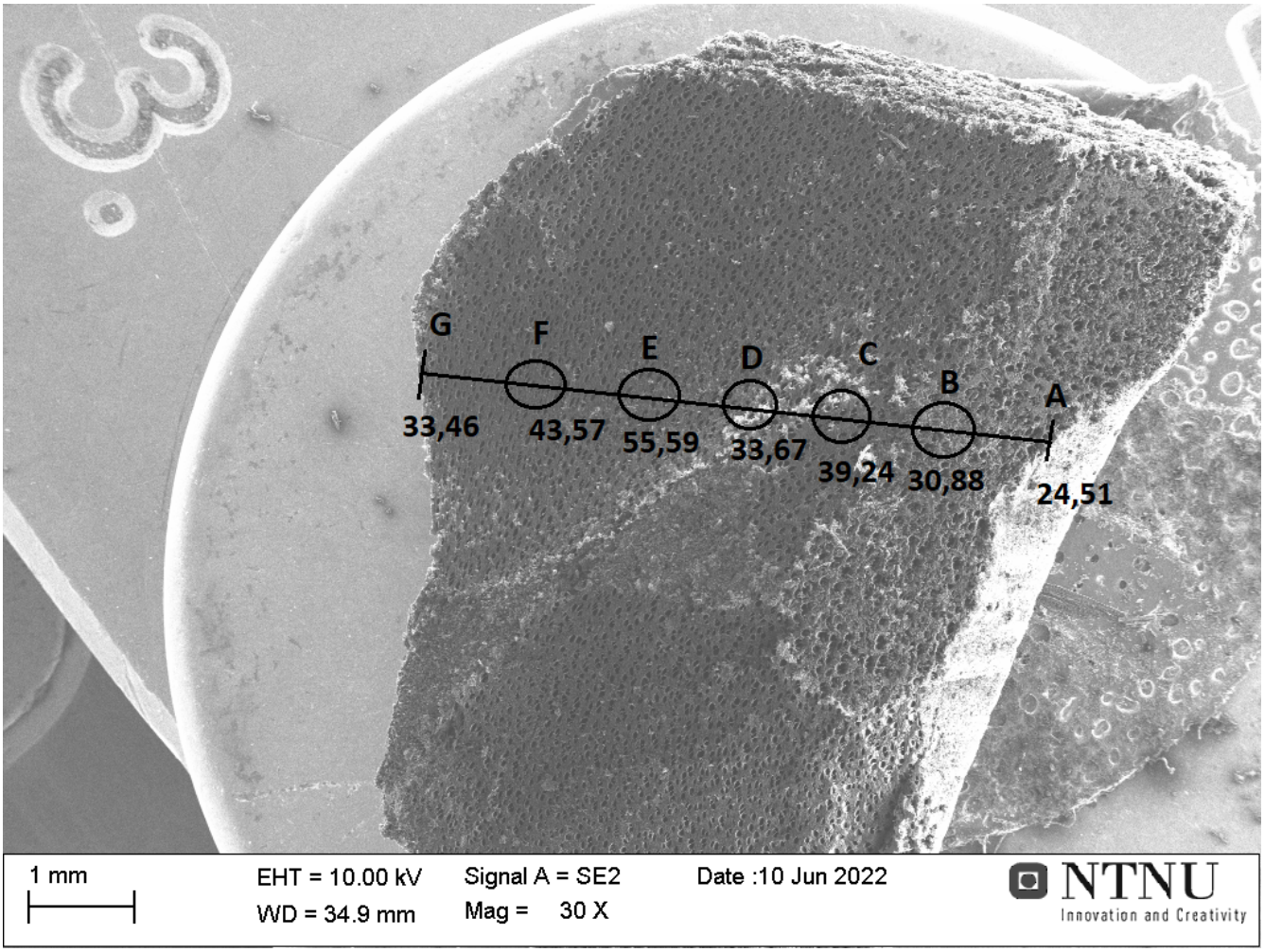

Figure 63: Overview of Sample 1 for charcoal with 10,3 wt% carbon deposition

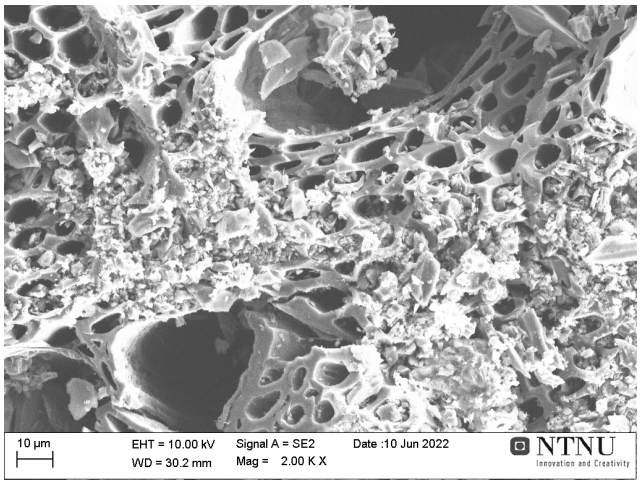

(a) A

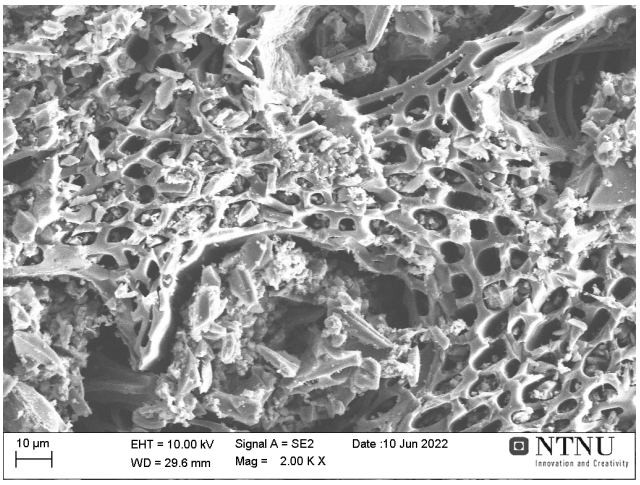

(b) B

Figure 64: The pictures are showing area 1A and 1B for charcoal with 10,3 wt% deposition

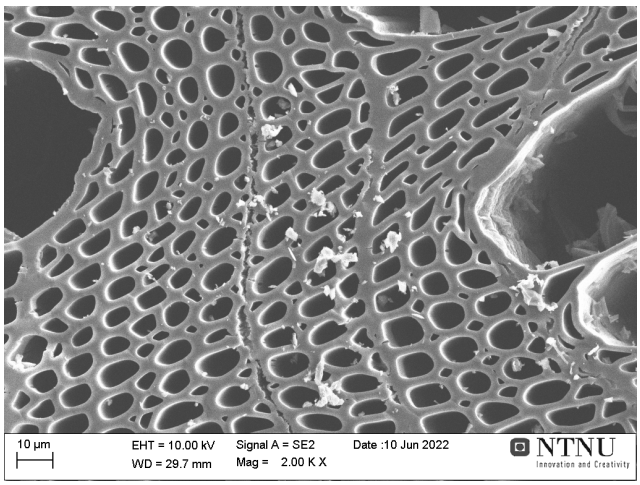

(a) C

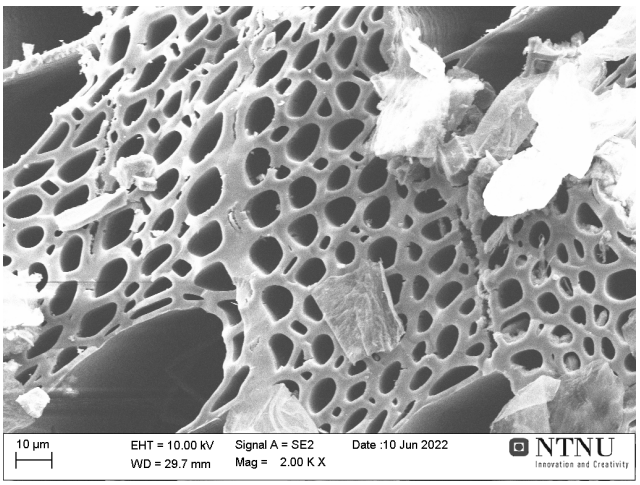

(b) D

Figure 65: The pictures are showing area 1C and 1D for charcoal with 10,3 wt% deposition

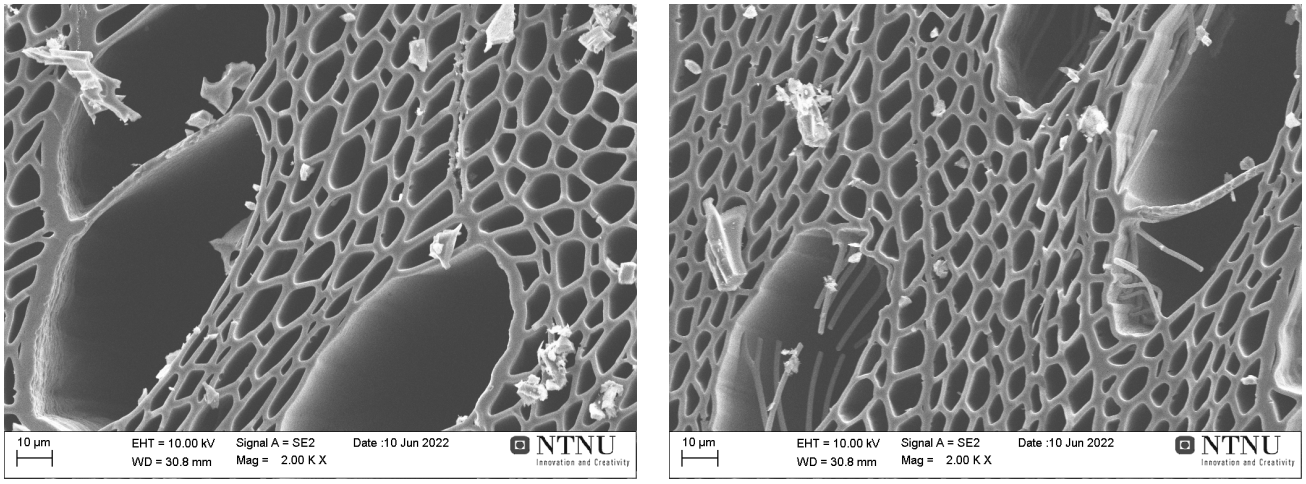

(a) E **(b)** F

Figure 66: The pictures are showing area 1E and 1F for charcoal with 10,3 wt% deposition

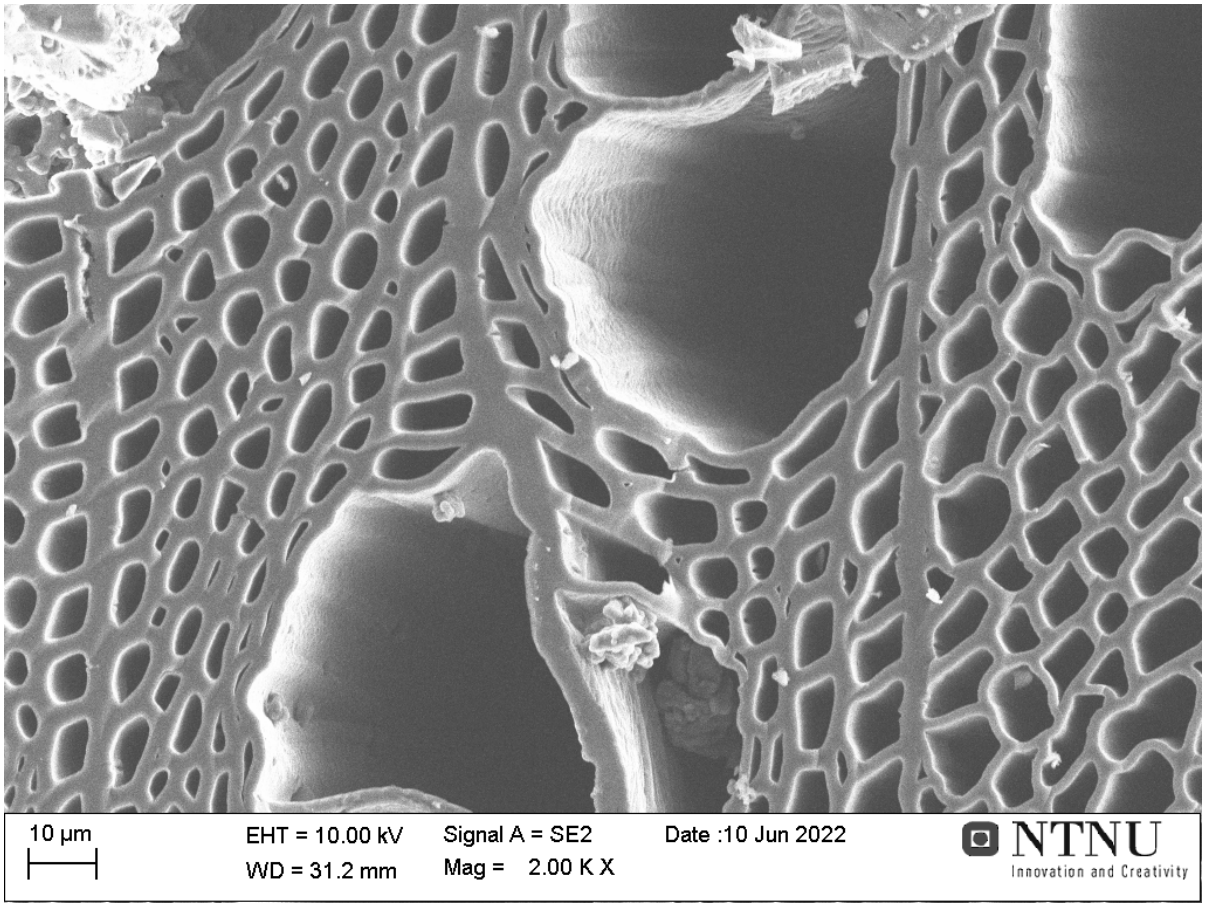

Figure 67: The picture is showing area 1G for charcoal with 10,3 wt% deposition

4.7.4 2h (24,0 wt%)

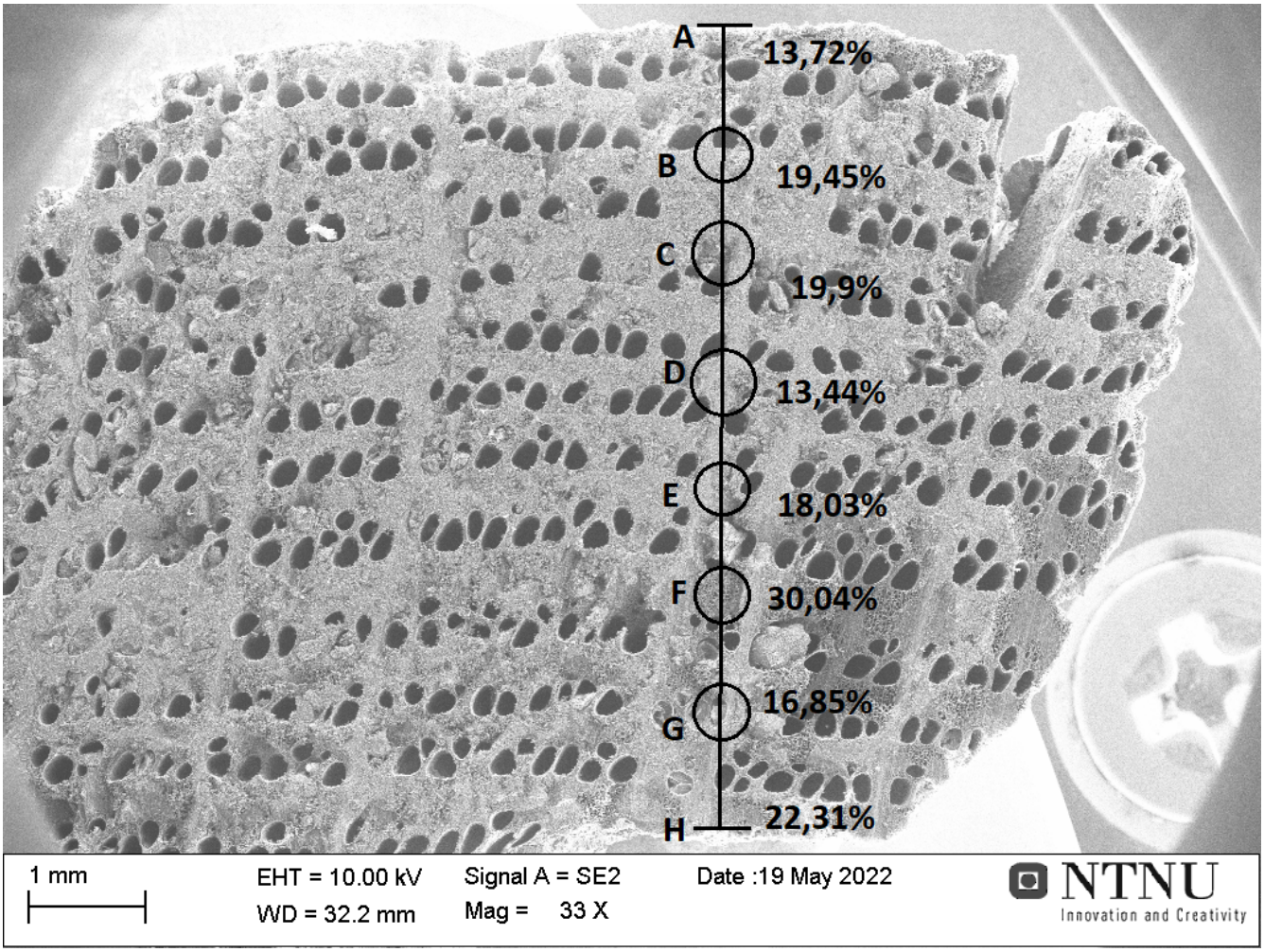

Figure 68: Overview of Sample 2 for charcoal with 24,0 wt% carbon deposition

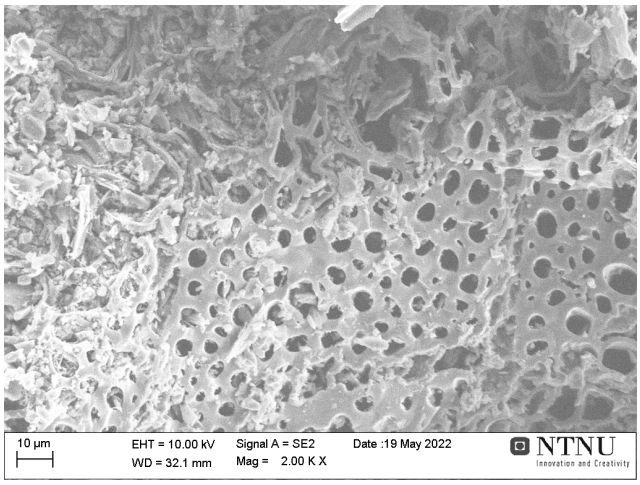

(a) A

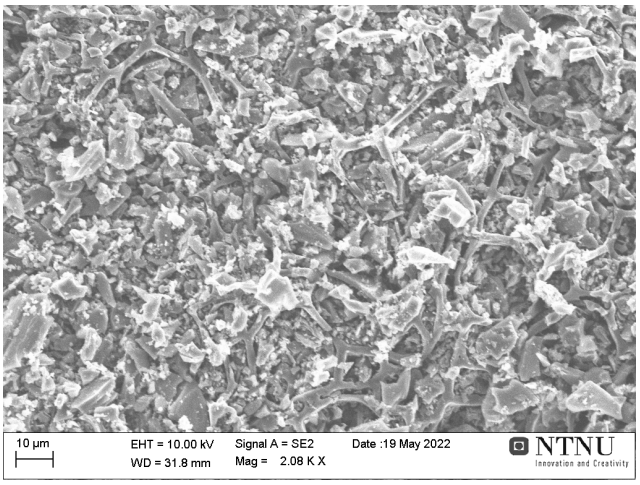

(b) B

Figure 69: The pictures are showing area 2A and 2B for charcoal with 24,0 wt% deposition

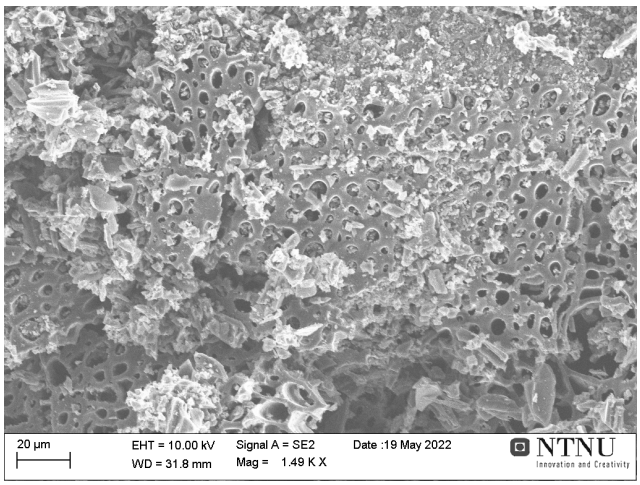

(a) C

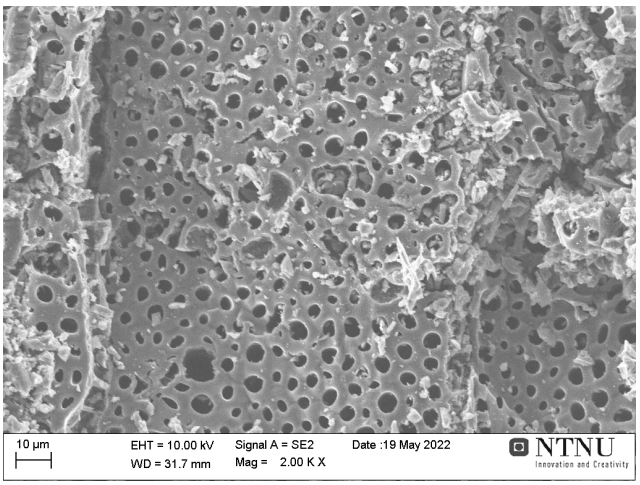

(b) D

Figure 70: The pictures are showing area 2C and 2D for charcoal with 24,0 wt% deposition

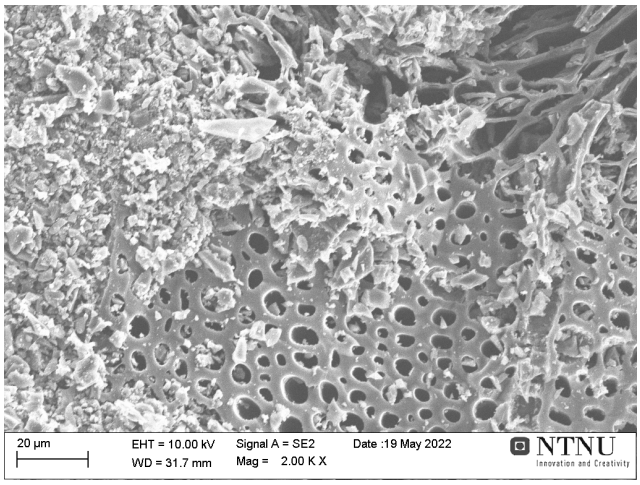

(a) E

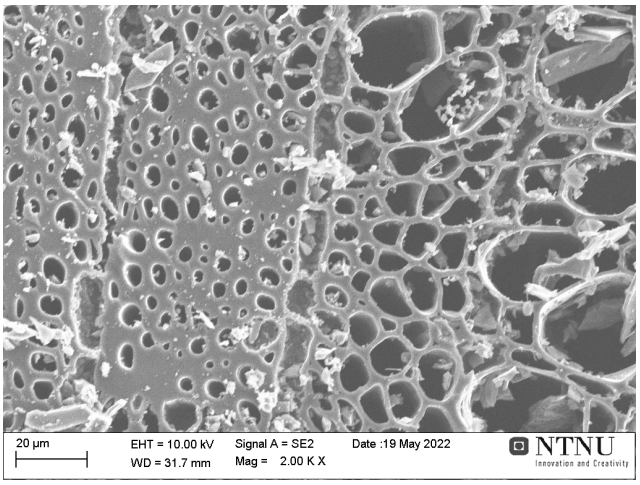

(b) F

Figure 71: The pictures are showing area 2E and 2F for charcoal with 24,0 wt% deposition

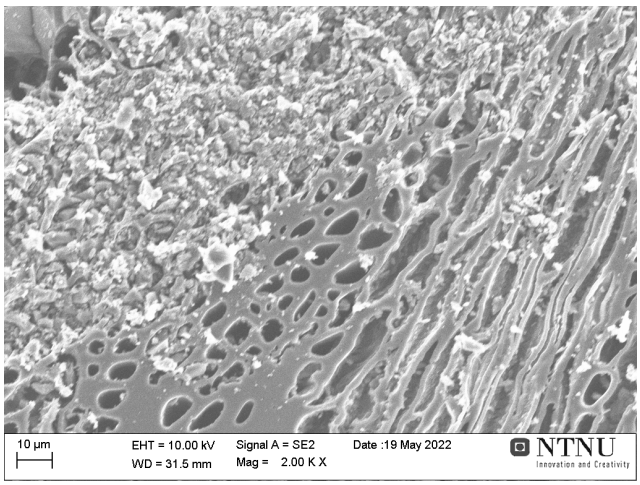

(a) G

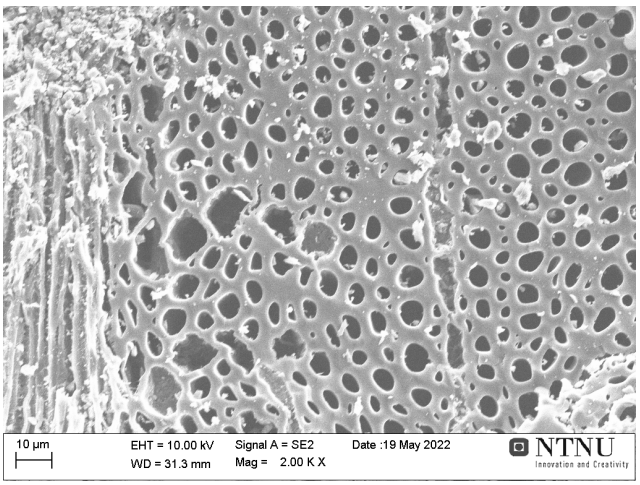

(b) H

Figure 72: The pictures are showing area 2G and 2H for charcoal with 24,0 wt% deposition

4.7.5 3h (29,7 wt%)

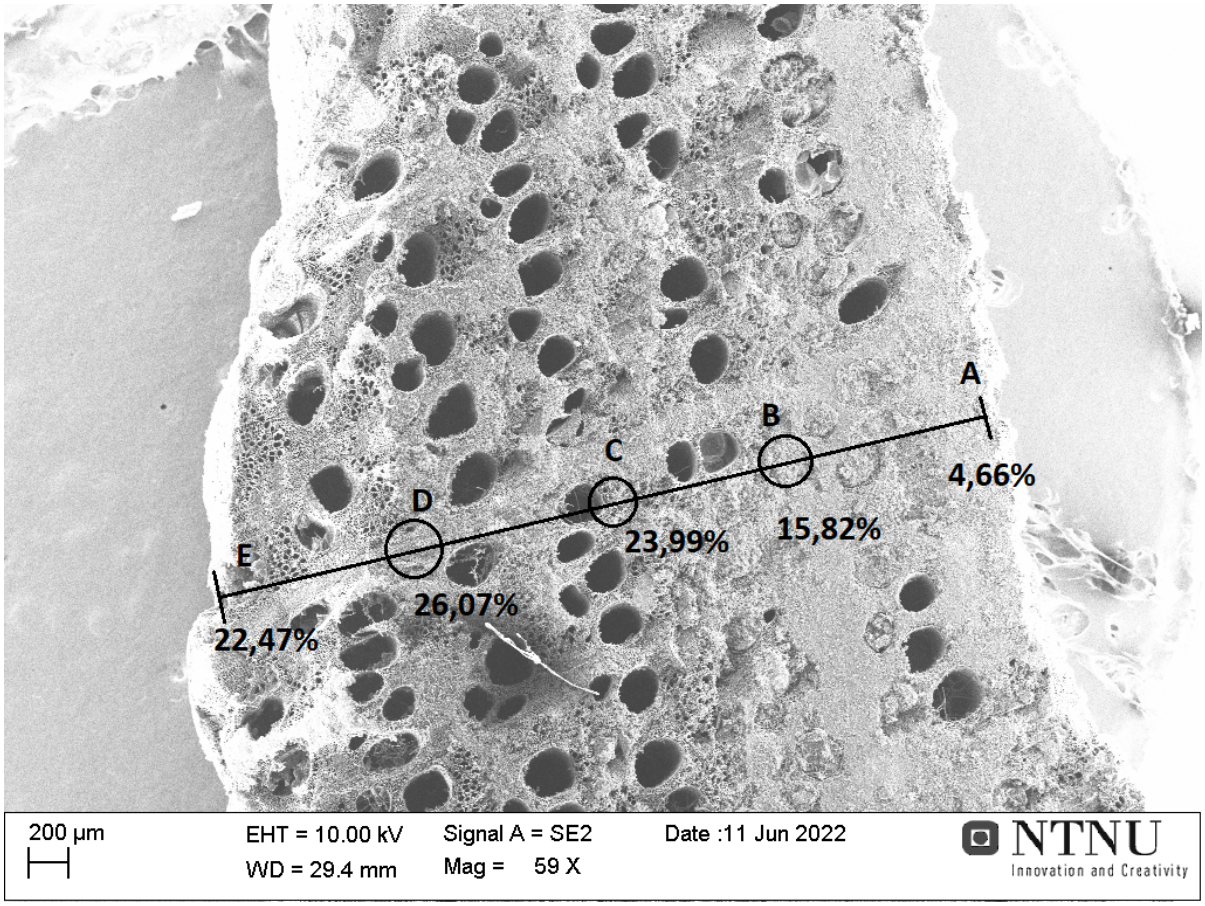

Figure 73: Overview of Sample 1 for charcoal with 29,7 wt% carbon deposition

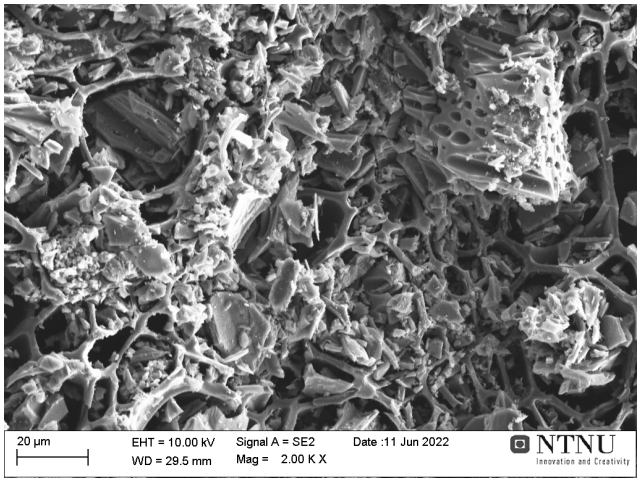

(a) C

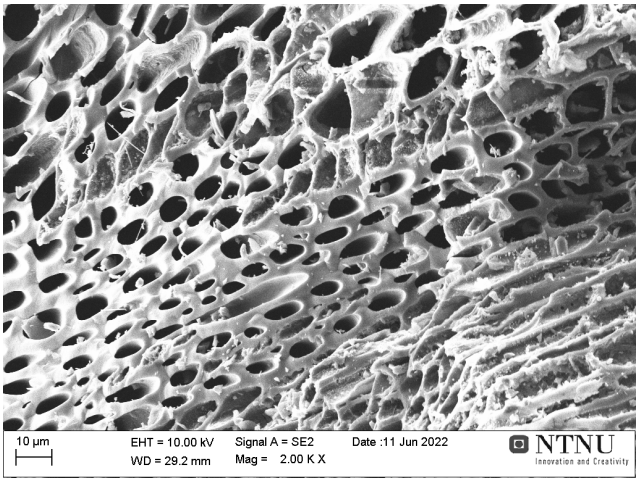

(b) D

Figure 75: The pictures are showing area 1C and 1D for charcoal with 29,7 wt% deposition

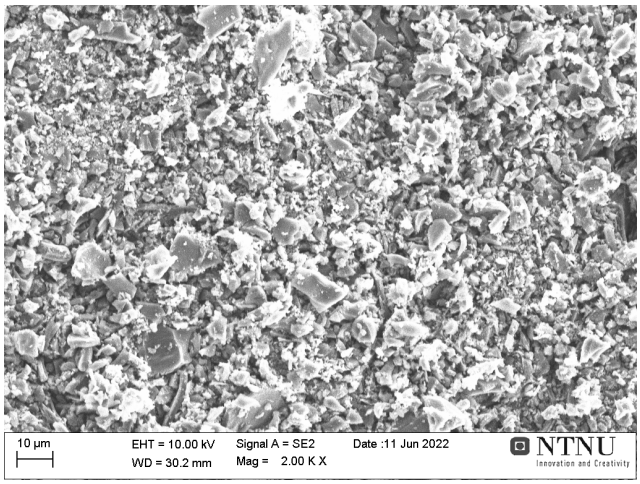

(a) A

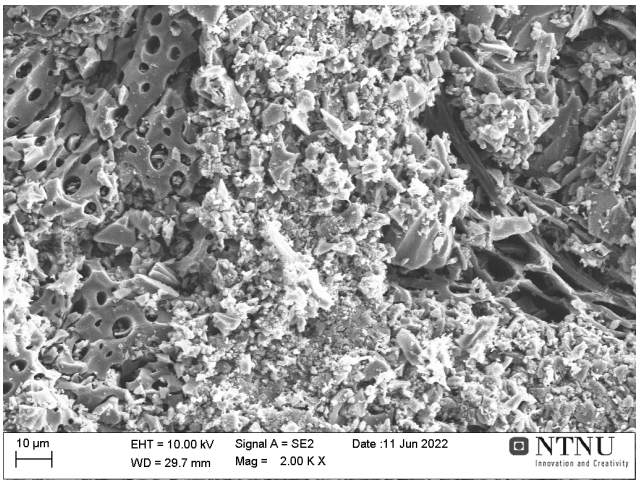

(b) B

Figure 74: The pictures are showing area 1A and 1B for charcoal with 29,7 wt% deposition

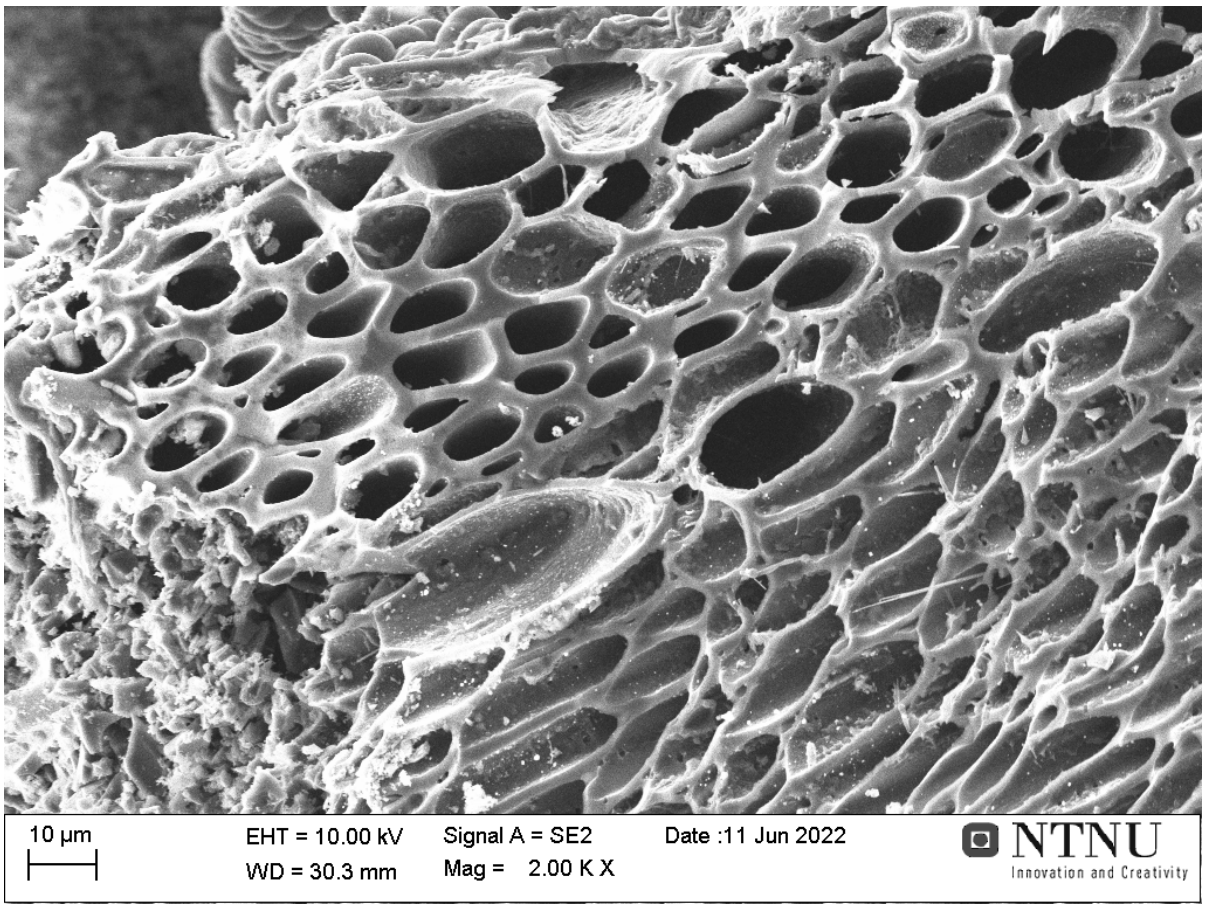

Figure 76: The picture is showing area 1E for charcoal with 29,7 wt% deposition

The porosity-values of all the three samples in each of the sample-sets are shown in the figures below. Figure 77 shows the comparison between the sample that is heated only with argon and the samples that is densified. Figure 78 shows the values of the samples from raw charcoal and the argon-heated samples. What one can see from both these figures, and what is also indicated in the SEM-images, is that there are big variations and a very high uncertainty. As shown in the SEM-images, this might possibly come from the fact that the variations in surface-structure are very high within each sample. in Figure 77 one can see that the samples with 10,1 wt% deposition has a bit higher values than the rest of the samples. However, these values are spread over relatively higher porosity-range than the other samples, which might weaken the reliability of the results. What one can see from this figure is that the deposition of carbon does not seem to change the overall-value of porosity, according to this experimental method. A clearer development can be seen in Figure 78, where most of the values of the samples with argon-heating has a decreased porosity-value compared to the raw-material. This observations might indicate that the process of heating has a greater influence in the porosity-values than the reaction of carbon-deposition, but

the uncertainty is to high to make a proper conclusion.

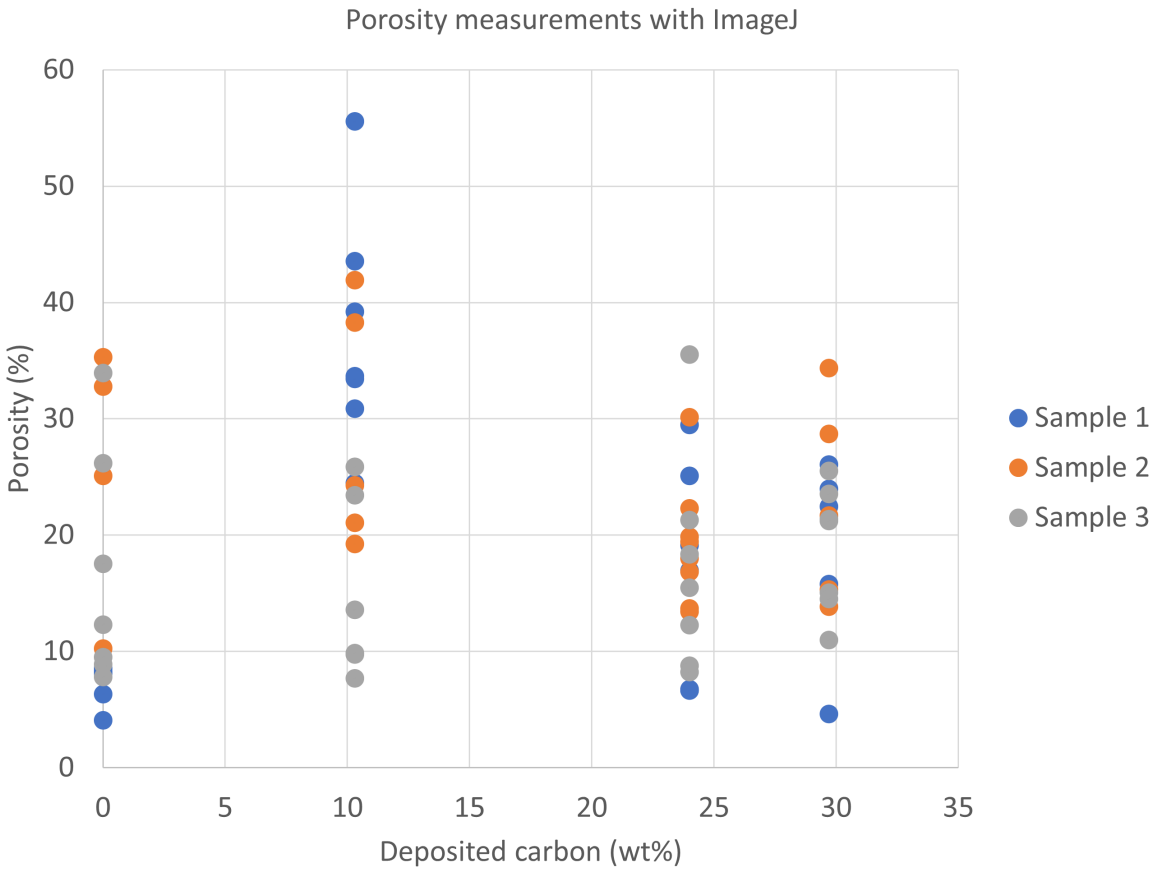

Figure 77: The figure shows the results from the porosity-measurements done with ImageJ, as a function of amount of carbon-deposition.

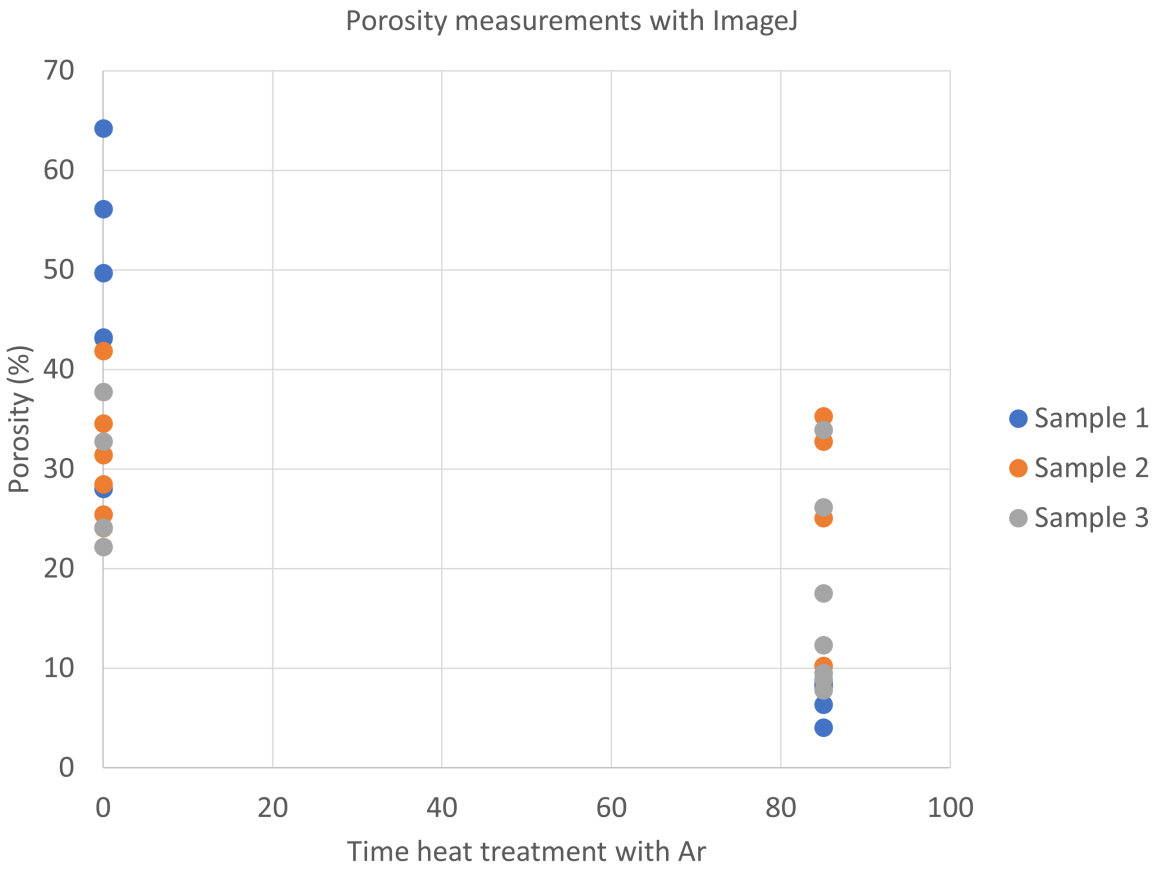

Figure 78: The figure shows the results from the porosity-measurements done with ImageJ for untreated charcoal and for charcoal heated with Argon.

5 Discussion

5.1 Densification

The densification results in the previous section (Figure 42) indicates an approximately linear relationship between the purging time and the amount of deposited carbon on the charcoal-surface. If one includes and compares with the results of the densification-experiments performed by Solhaug and Kaffash, as well as the summer-report and the specialization-project by Larsen, one gets the results as shown in Figure 79.Like in the results of this master-thesis, the average reaction-temperature is also calculated and included for the project and summer-work by Larsen. The temperature-values of the summer-work were extracted and calculated during the work of this master-thesis. In Figure 79 there are also included trend-lines for both the specialization-project of Larsen and for this master-thesis. One notices that the incline of the slopes of the two lines

are very different. If one excludes the very low value of deposition at approximately one hour of deposition (0,9wt%) one can can be able to calculate and find that the average reaction temperature for the tests of the master-thesis are slightly higher than for the specialization project by Larsen (1066 °C against 1055 °C). The big difference of decomposition is first visible after two hours of methane-purging. Here the average reaction temperature for the master results are over 50 °C higher than for the specialization-project, and this might be one of the reason for the big difference in deposition. Another reason might be the difference in size-distribution; the size-range of the samples in the project varied from 10-20mm, while this size-range is narrowed down to just 10-13,2 mm, as mentioned in the experimental-section. This may lead to less variations in surface-area and less void-fraction, which again would lead to less variations in deposition within each sample-batch. From 2 to 3 hours of methane purging, the difference between the project and master-results does not increase significantly, and here the average temperature of the project is actually over 20 °C higher than the temperature of the master-thesis. This shows that the charcoal of the master-thesis still manages to achieve almost twice as much deposition as for the project, even with lower reaction-temperature. These observations might indicate that the average reaction-temperature plays a less crucial role for methane-purging at 3 hours compared to 2 hours. Other observations that can be seen in Figure 79 is that most of the results of Kaffash and Solhaug, which is purged at 90 minutes, is placed between the densification-values for 1 and 2 hours of purging for the works of Larsen.

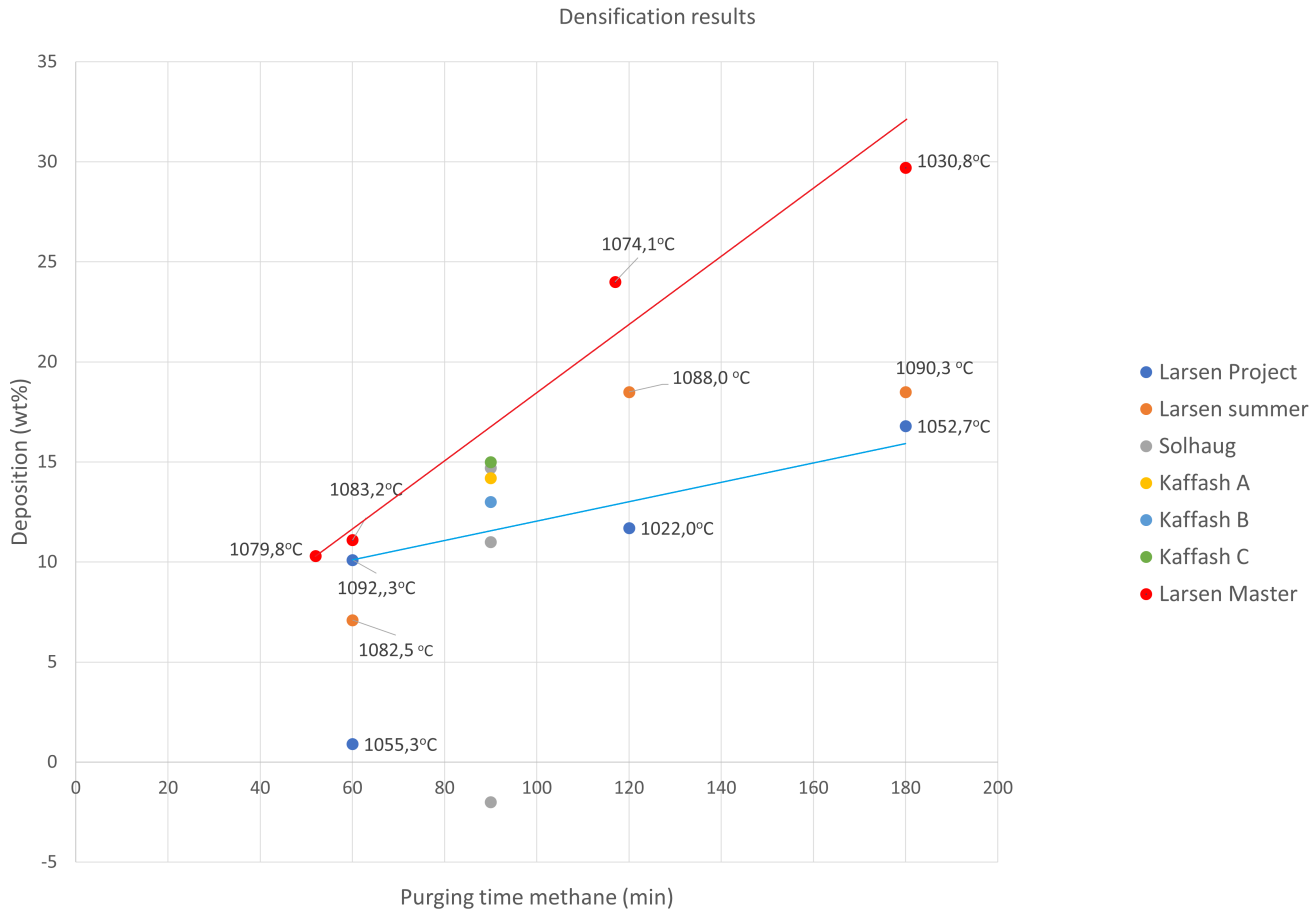

Figure 79: The figure shows a comparison of the different densification-experiments done by Larsen ([22][21]), Solhaug ([36]) and [19] (the type of charcoal used in the work by Kaffash, is not the same as used in the works of Larsen and Solhaug).

To summarize the subsection regarding the densification-discussion, the variations in the amount of carbon deposition can vary significantly, due to temperature, but maybe more to the charcoal particles size and other experimental differences. If the charcoal forms gas channels, all particles will not experience the same amount of methane, and hence the % C deposited will overall be lower.

5.2 Methane conversion

Figure 80 shows a comparison of the methane-conversion as a function of average reaction temperature for both the previous works by Larsen, in addition to the values of this master-thesis. The values of the specialization-project is calculated and shown in the report [22], while the values for the summer-project was extracted and calculated during the work of this master-thesis. From the

results of the work with the master-thesis, one saw that most of the samples followed the trend with decreasing reaction-temperature with increasing purging-time. This observation is not the fact if one include the other experiments, as the summer-experiments show an increasing temperature with increasing purging-time, while there in the specialization-project is no pattern in that matter. While the master-experiments show that 3 out of four samples suggests an increased conversion with increasing temperature, this is also the case with the specialization-project. However, an outlier in both of the mentioned works opposes this trend, which is also the case when you look at the result of the summer-work. One of the easiest things to notice in Figure 80 is the relatively substantial collection of values that are assembled in the upper right corner of the diagram. Of all the samples with a reaction temperature above 1070 °C, it is shown that 5 out of 7 experiments have a methane conversion higher than 35 %. This might have industrial relevance when it comes to yield-limits and temperature-limits.

If one compares the findings of Figure 80 with other densification-experiments in the literature, one can see that the trend of decreasing methane-conversion with increasing purging-time is found in the works of Nishii and co-workers in the report from 2019 (Figure 8). This is however not the case in this work, and up to 30% carbon deposition one can not see this trend. It should be noted that in the work of Nishii, the temperature in this experiment is set to 1173 K or 900 °C, with a space-velocity at 360 h^{-1} (space velocity, SV , is defined as the amount of gas per hour passing through the reactor divided by the volume of the catalyst in the reactor [31]). These factors, and the fact that this experiment is performed on four materials that are not charcoal, makes it challenging to make a proper comparison, but might give a good indication since they are all carbon-based materials.

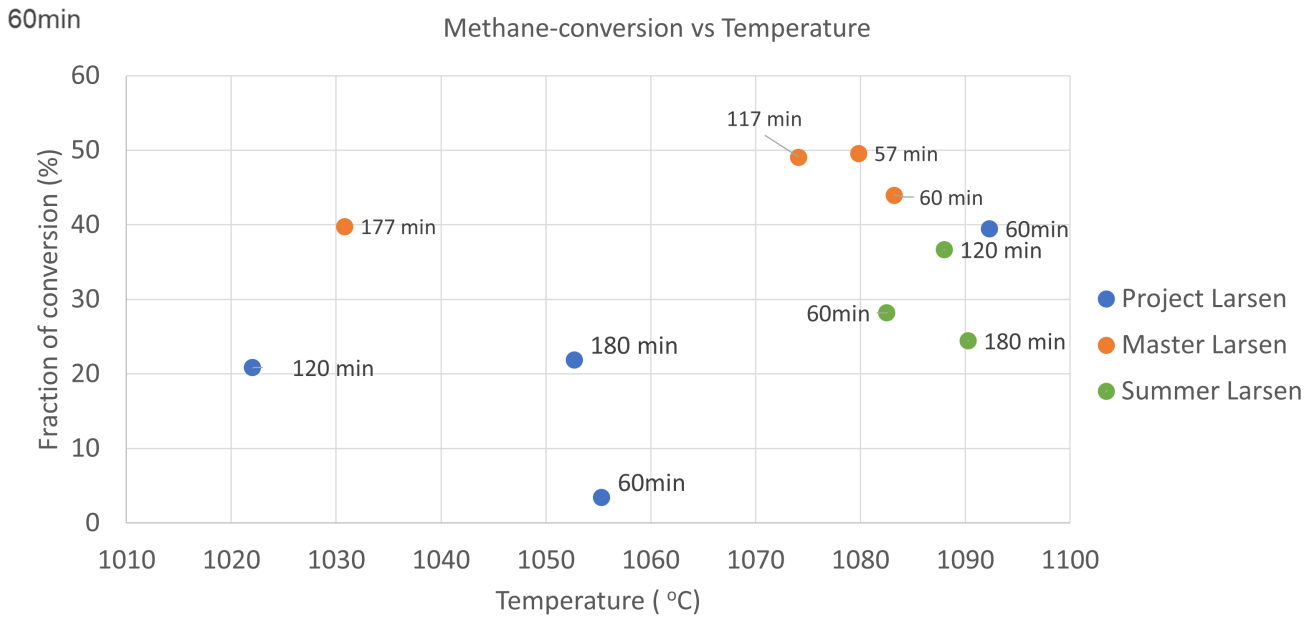

Figure 80: The figure shows a comparison of the relationship between the average reaction temperature and the methane-conversion for the experiments done by Larsen ([22][21]), in addition to the results of this master-thesis.

5.3 Compression-testing

The figures below (Figure 81, Figure 82, Figure 83 and Figure 84) show the different values of the compression-strength for the different fiber-directions. The letters "L" and "T" represent the strength when the force is directed in parallel and perpendicular to the fiber direction in the material, respectively. In Figure 81 and Figure 82 the values with 0 wt% carbon deposition are the samples that are heated with only argon. The first two images show that there is no clear relationship between the amount of deposited carbon and compression strength. However, it can be interesting to notice that the most distinctive increase in strength comes during the first 90 minutes of heat-treatment, as shown in Figure 83 and Figure 84. There is also a very clear increase from the argon-purged samples to the first hour of methane-purging in Figure 81. These observations might indicate that the heat-treatment of the material is just as important for strength-increase as the densfication-process, maybe even more important.

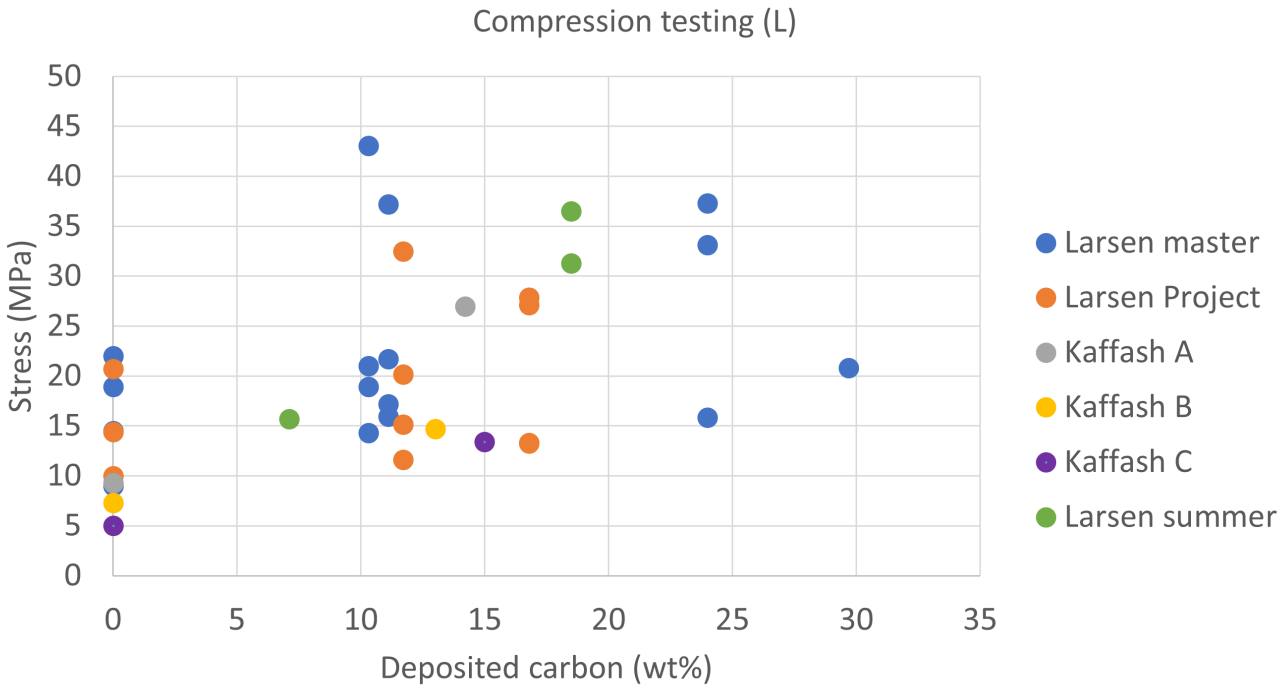

Figure 81: The figure shows the comparison of the compression-strength as a function of amount of deposited carbon for the experiments of both Larsen and Kaffash when the direction of the force is parallel to the fiber-direction.

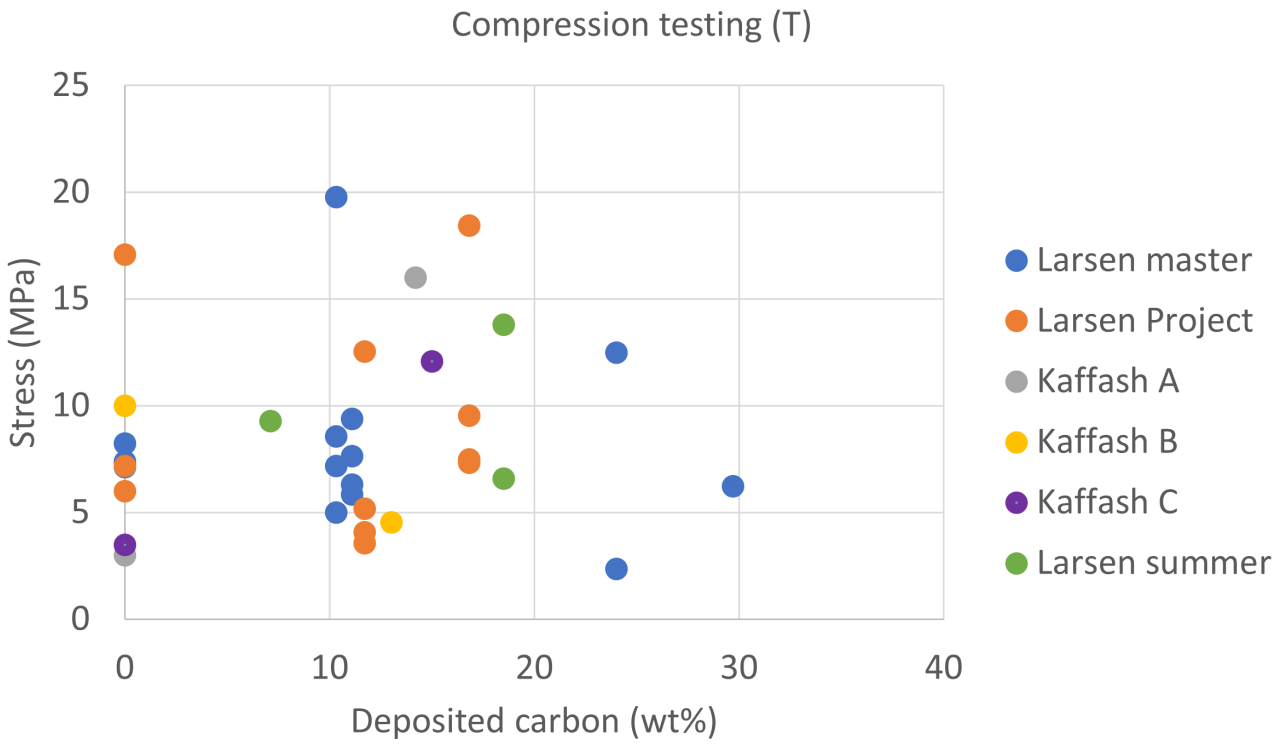

Figure 82: The figure shows the comparison of the compression-strength as a function of amount of deposited carbon for the experiments of both Larsen and Kaffash when the direction of the force is perpendicular to the fiber-direction.

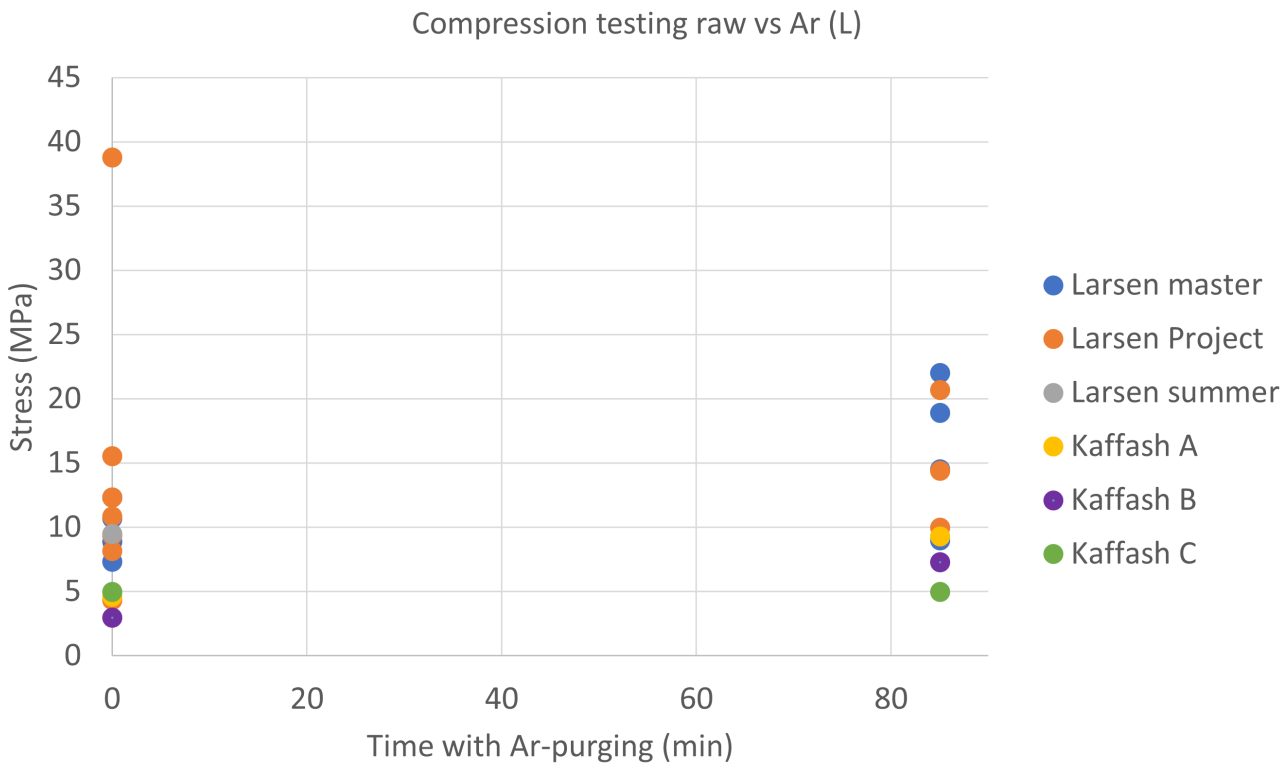

Figure 83: The figure shows the comparison of the compression-strength between raw-material and Ar-purged samples for the experiments of both Larsen and Kaffash when the direction of the force is parallel to the fiber-direction.

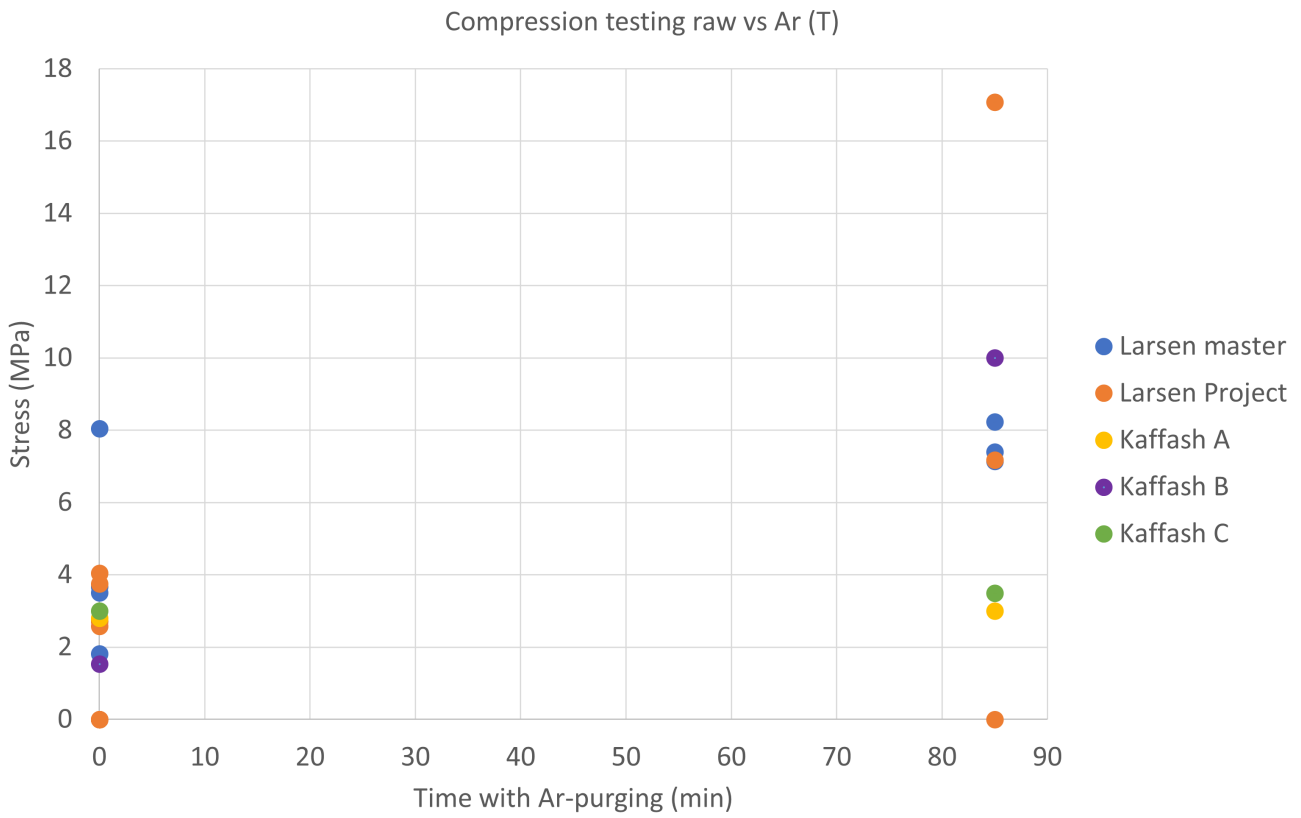

Figure 84: The figure shows the comparison of the compression-strength between raw-material and Ar-purged samples for the experiments of both Larsen and Kaffash when the direction of the force is perpendicular to the fiber-direction.

5.4 Abrasive strength

As shown in the results (Figure 46 and Figure 47) the highest change of fraction of fines is between the raw charcoal and the sample heated with argon. As in the results of the compression-testing, it seems also here that the heating-process is a big contributor to the strength-increase of the material. When one in addition considers the fact that the samples were exposed to a sieving-process after the milling, this strength is highly emphasized. One can of course consider the possibility that the values for the raw-material is an "outlier", since there were only ran one test per sample. However, this is an assumption not considered her, but can maybe be the scope in future research.

5.5 Porosity

The calculating of porosity can as mentioned, be done according to this equation:

$$p = (1 - \frac{\rho_{app}}{\rho_{abs}}) \cdot 100 \tag{5.1}$$

where ρ_b and ρ_m denotes the apparent and absolute densities, respectively. When one calculates the following porosity, this can be done in several ways, depending on how many values one wants with regard to uncertainty and standard deviation. This subsection provides two models for the calculation of porosity, and a comparison of the mentioned methods and their respective standard deviations:

5.5.1 Model 1: Fixed absolute density and variable apparent density

This model is the one that was already used in the results, with fixed absolute densities for raw charcoal (1,6 g/cm^3), ar-purged sample (2,01 g/cm^3) and for the densified samples (1 g/cm^3). These exact values were chosen because they were approximate average-values, så that the deviation would be as low as possible.

5.5.2 Model 2: Average values and error propagation

In this model the average values for both absolute and apparent densities were used, together with their respective standard deviations. these values were again used to calculate single average values for the porosity by the use of the equation above (Equation 5.1). To determine the resulting standard deviation of the porosity (σ_p), the formula of error propagation was used:

$$(\frac{\sigma_{\mathrm{p}}}{\overline{\mathrm{p}}})^2 = (\frac{\sigma_{\mathrm{abs}}}{\overline{\rho}_{\mathrm{abs}}})^2 + (\frac{\sigma_{\mathrm{app}}}{\overline{\rho}_{\mathrm{app}}})^2 \tag{5.2}$$

$$\sigma_{\mathrm{p}} = \sqrt{(\frac{\sigma_{\mathrm{abs}}}{\overline{\rho}_{\mathrm{abs}}})^2 + (\frac{\sigma_{\mathrm{app}}}{\overline{\rho}_{\mathrm{app}}})^2} \cdot \overline{\mathrm{p}} \tag{5.3}$$

in the equations $\overline{p}$ is the average porosity-value, while $\overline{\rho}_{abs}$ and $\overline{\rho}_{a}pp$ are the average values for the absolute and apparent densities, respectively. The parameters of σ_{abs} and σ_{app} denotes the standard deviation of the average absolute and apparent density, respectively.

5.5.3 Comparison of methods

Figure 85 and Figure 86 shows a comparison of the methods mentioned above, for both the porosity-values and the standard deviations. If one studies these figures, one can see that the standard deviations are a smaller for method 2 than for method 1, especially in Figure 85. One can also see that the porosity seems to decrease with increasing deposition, until it reaches 24 wt%, from which it increases a little. In Figure 86 one can see that the porosity shows a slight decrease after being heated with argon for 85 minutes, and this is the case for both methods. The standard deviations for both methods also seems to be approximately the same, even though a slight increase for method 2. The fact that the second method has a decreased standard deviation compared to the first method might seem odd. This is because while only one variable parameter is introduced in the first method (the apparent density) the second method introduces one more (absolute density). The inclusion of an additional parameter would normally increase the resulting standard deviation, according to the formula of error propagation. A possible explanation for the higher standard deviations for method 1 is the contribution of the fixed values of absolute density. A constant value of 1 for the densified samples, 1,6 for the raw samples, and 2,01 for the argon-heated samples may in fact introduce more variable parameters than for the second method, since all these fixed absolute densities has a relatively high standard deviation in itself, as shown in Figure 49 and Figure 50.

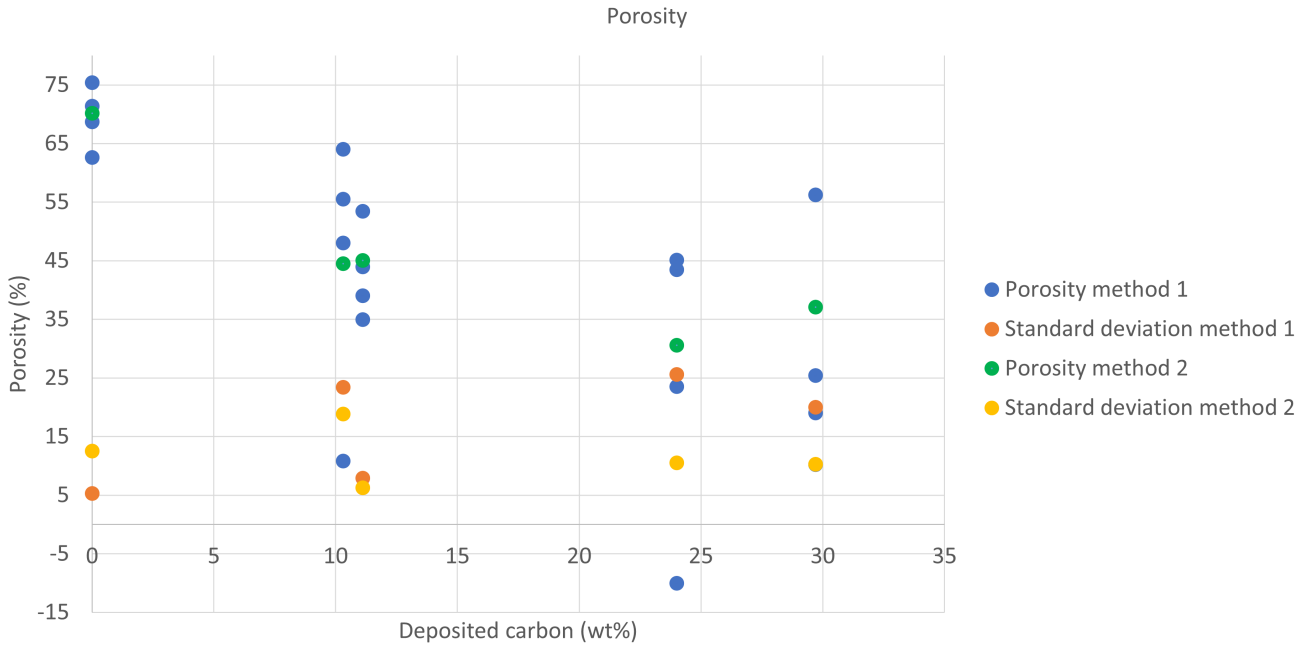

Figure 85: The figure shows a comparison of the two methods which is used to calculate porosity as a function of deposited carbon, in addition to their standard deviations.

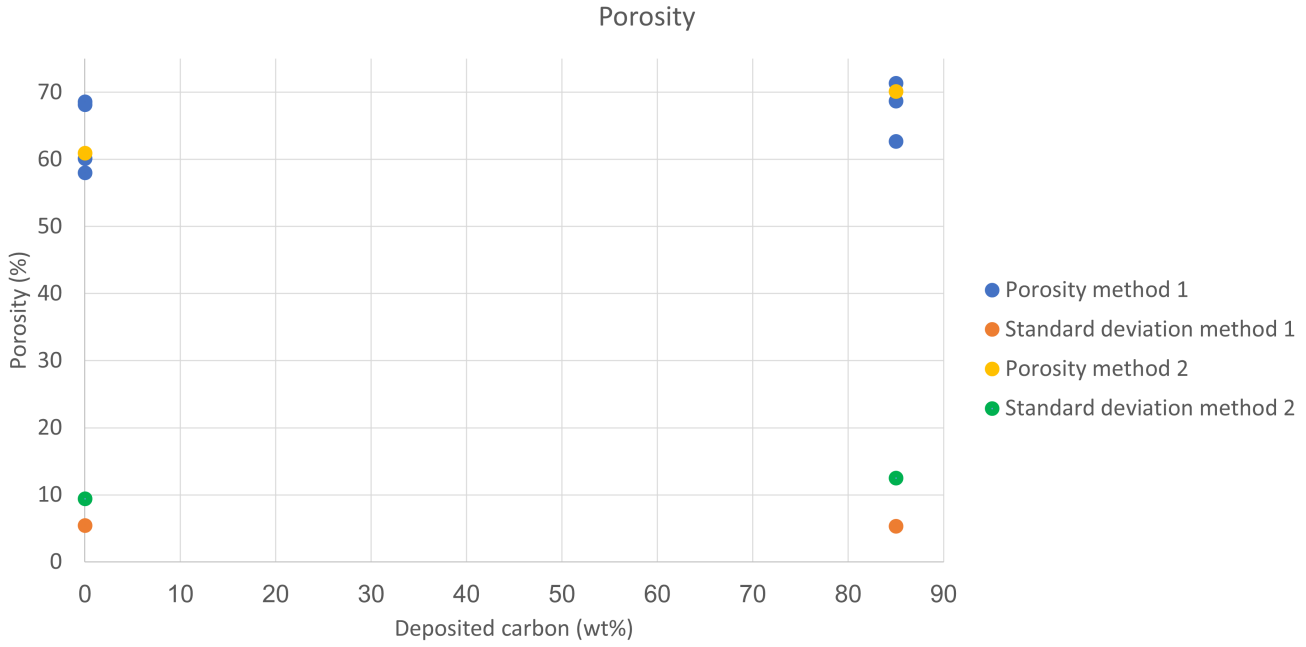

Figure 86: The figure shows a comparison of the two methods which is used to calculate porosity for raw charcoal and for the ar-heated sample, in addition to their standard deviations.

The two figures below compares the porosity-values from this master-thesis with the values of the earlier works done by Larsen ([21], [22]) and the works of Kaffash and Tangstad ([19]). Figure 87 shows the porosity-values as a function of amount of deposited carbon, while Figure 88 shows the porosity for the raw charcoal and for charcoal heated with argon. Except for the third method of the specialization project by Larsen, all the porosity-values are obtained by the same method, that is by the calculation using absolute and apparent density. This makes the values easier to compare and analyze. One can see from Figure 87 that even though there are a high range of uncertainty for the different degrees of deposition, one can see a trend towards decreased porosity with increasing deposition. This trend is especially relevant in the area between 10 and 18,5 wt%. When it comes to the porosities for raw charcoal and heated charcoal in Figure 88, one can see that the porosities varies from 60-80% for raw charcoal, depending on the experiment. The reason for the high variance in porosity for the raw material might not always be as easy to identify. As an example one can looks at the difference between one of the charcoals studied by Kaffash, called "Charcoal B Kaffash" and the charcoal in the specialization-project by Larsen called "Method 1 Project Larsen". As one can see in Figure 87, the porosity-value for charcoal B is 80 %, while it is down to 70,88% for Larsens sample. As can be shown in Table 1 and Table 5, the respective fractions of volatile-content are approximately the same. The fraction of Kaffash is 2,44% higher than for the charcoal from Larsen. The ash-content is also approximately the same, so this wont influence the high difference in porosity. If one in addition looks to one of the parameters used to calculate the porosity, the absolute density, one discovers that also these values are approximately the same. The charcoal of Kaffash has a density of 0,44 g/cm^3, while Larsens charcoal has an average apparent/skeletal density of about 0,44 g/cm^3. These observations show just how much physical variations that can occur for this kind of material, even though the chemical composition is approximately the same.

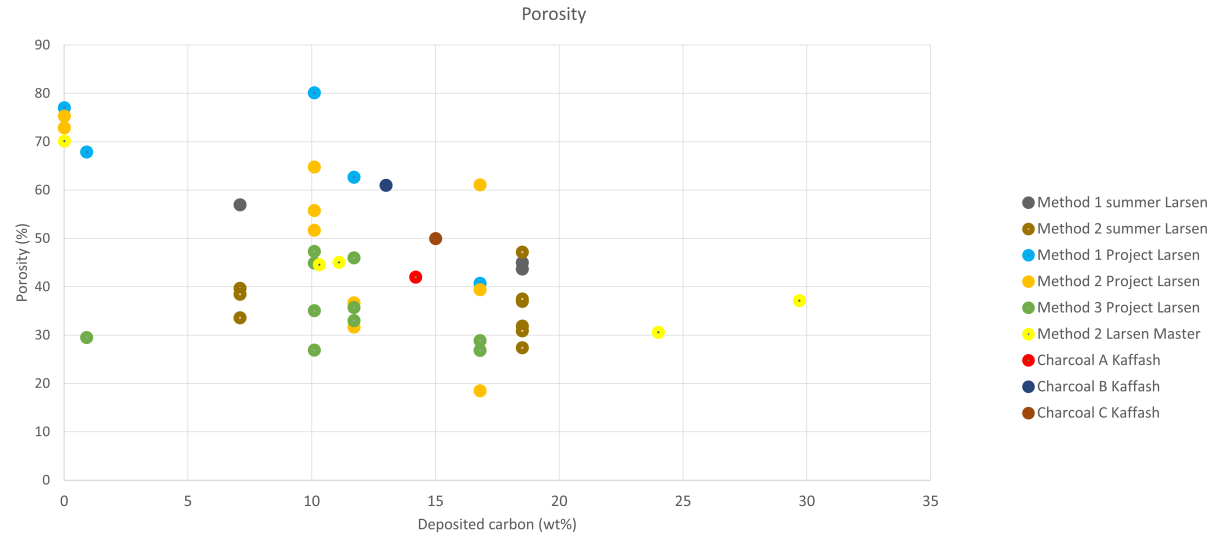

Figure 87: The figure shows an overview of the different values of porosity from the experiments of both Larsen (project and summer report [22] [21]) and Kaffash [19]

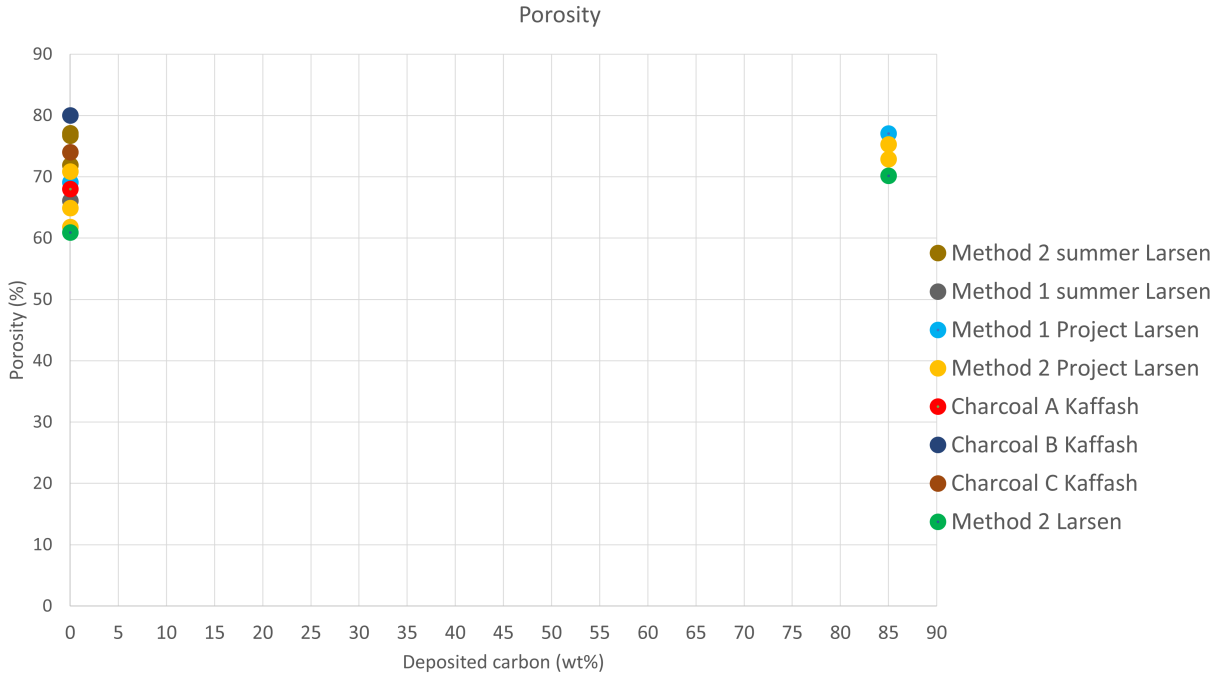

Figure 88: The figure shows an overview of the different values of porosity from the experiments of both Larsen (project and summer report [22] [21]) and Kaffash [19]

5.5.4 Carbon depositions effect on absolute and apparent density

The two important parameters for the calculation of porosity is shown below. Figure 89 and Figure 90 shows a comparison of the absolute densities that was measured for both the specialization-project and the master-thesis by Larsen, while Figure 91 and Figure 92 shows the apparent densities for the same works by Larsen, in addition to the works of Kaffash and Tangstad [19]. For the absolute density, one can see that the results from the specialization-project and the master-thesis is rather alike. This can be stated if one looks away from the values at 10,1 wt% deposition, which have a value of approximately 3 g/cm^3. One sees that the absolute density is relatively high when only exposed to heating with argon, but then decreases rapidly once it is exposed to carbon deposition. The density then flattens out relatively fast as the carbon deposition goes on. The fact that the absolute density decreases once the new carbon-material deposits on the charcoal surface, suggests that the density of the deposited carbon is lower than the density of the charcoal. For both the specialization project and master-thesis of Larsen, the absolute density increases when exposed to heat-treatment with argon-gas compared to raw charcoal. This trend is the same as it is shown in the work of Hussein with co-workers in Figure 23 [Hussein et.al 2016] [12] As claimed in this article, this increase in absolute density could be due to the growing of more ordered structures at the expense of more amorphous structures.

The development of the apparent density according to Figure 91 and Figure 92 is not as easy to interpret. The uncertainties are high for all degrees of densification, and there is no clear indication of either increased or decreased density as the deposition goes on. There is also no clear difference between the raw charcoal and the heated charcoal in Figure 92. Given that the apparent density or envelope density is defined as the density in which the volume of the pores and the small cavities are included [15], one would think that this type of density should increase as the carbon penetrates the pores, but this trend is not so easy to conclude with for the figures below.

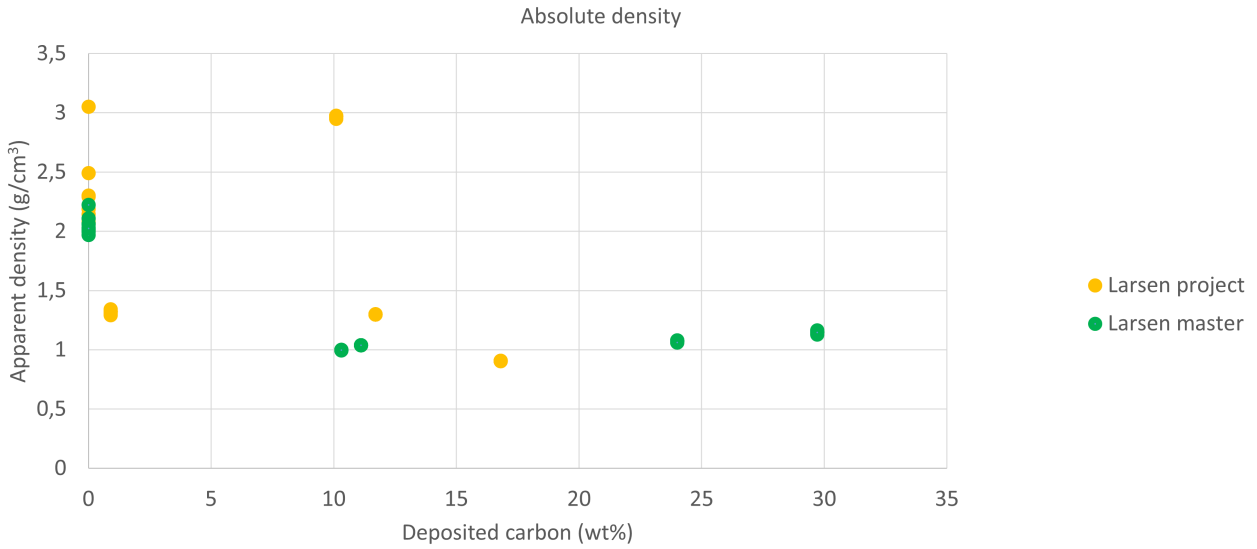

Figure 89: The figure shows a comparison of the absolute density-values for the master-thesis and the specialization-project by Larsen, as a function of carbon deposition.

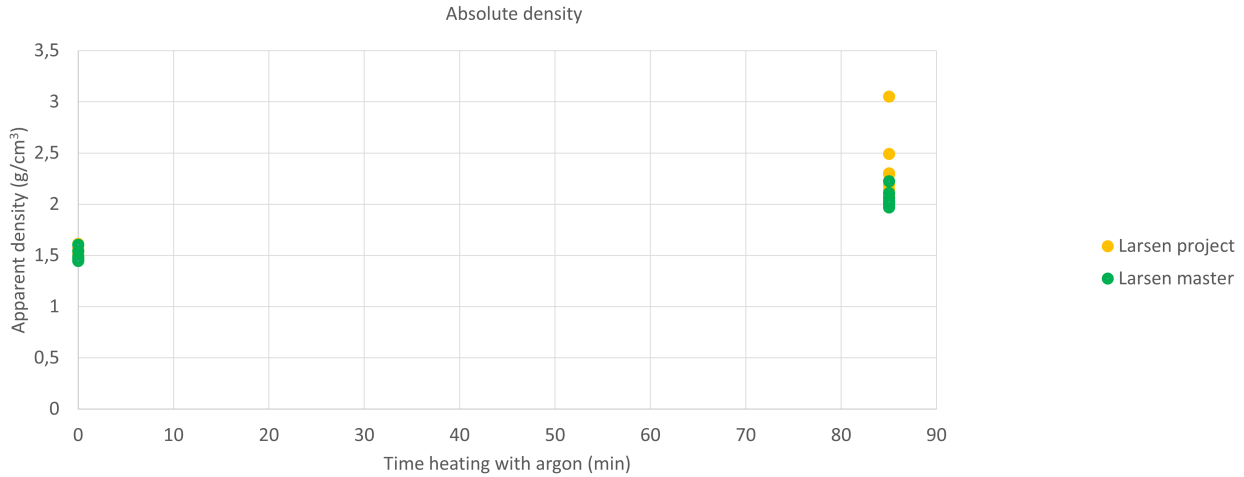

Figure 90: The figure shows a comparison of the absolute density-values for the master-thesis and the specialization-project by Larsen, for the raw charcoal and the charcoal heated with argon.

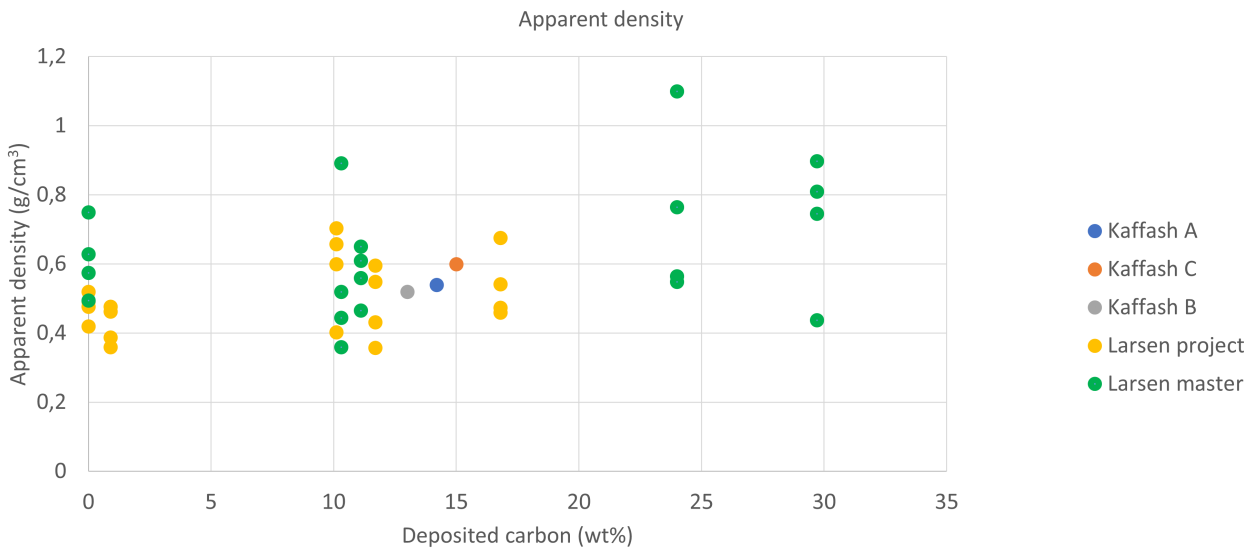

Figure 91: The figure shows a comparison of the apparent density-values for the master-thesis and the specialization-project by Larsen and the works of Kaffash and Tangstad, as a function of carbon deposition.

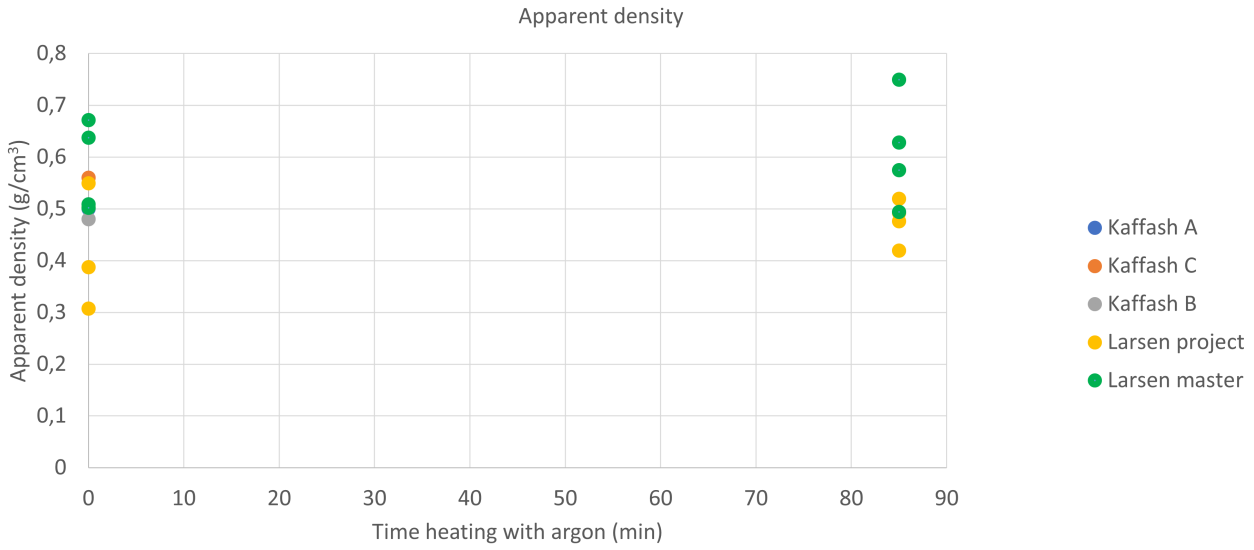

Figure 92: The figure shows a comparison of the apparent density-values for the master-thesis and the specialization-project by Larsen and the works of Kaffash and Tangstad, for the raw charcoal and the charcoal heated with argon.

5.6 SEM

By studying SEM-images of raw charcoal and charcoal that is heated with argon-gas, one can see differences with respect to surface-, and pore-structure. An example of this is the already shown images from the result-section. The images below (Figure 93) shows the surface-images of raw charcoal (left) and argon-heated charcoal (right). One can see that the pores in the charcoal that is heated are rather shallow. Whether this comes from the already existing surface structure prior to the heating or because of the heating-process itself is hard to say, but it definitely decreases the porosity-values compared to the left sample (raw) when it comes to the measurement with ImageJ.

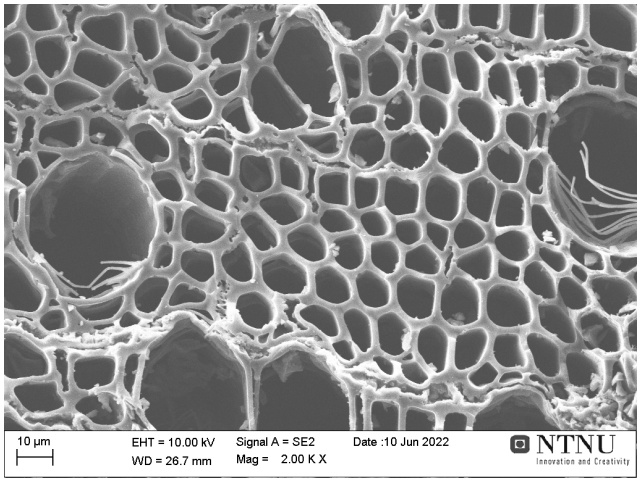

(a) Raw charcoal

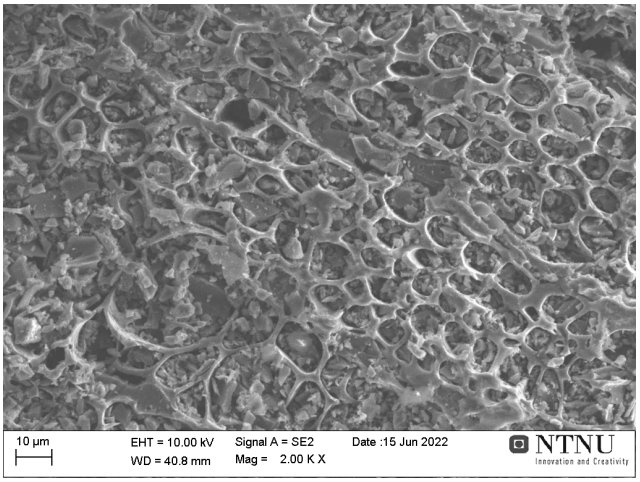

(b) Ar-heated sample

Figure 93: The figure shows examples in the structure between raw charcoal (left) and ar-heated charcoal (right)

The structure and the value of porosity can also vary from sample to sample, as is shown in Figure 94 and Figure 95. From the four pictures below, the two on the left shows images with 2000X magnification of specific areas of two different samples, while the tow images on the right shows an overview of these two respective samples. As one can see, the two investigated areas are very different when it comes to pore-structure. Because they are both located approximately in the centre of each of the sample-surfaces, it makes it easier to compare without thinking about internal differences throughout the thickness in each sample.

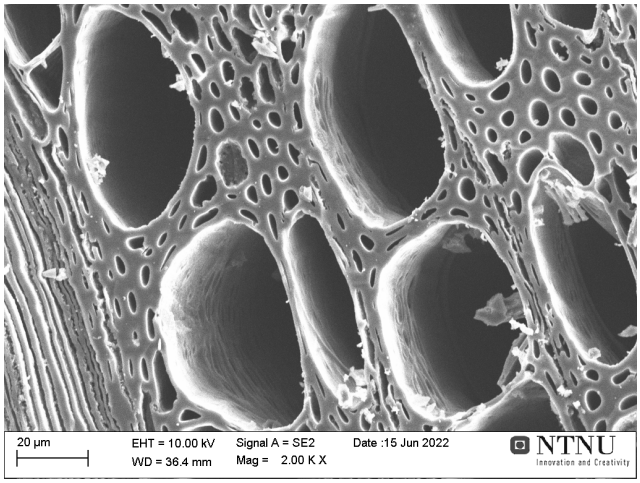

(a) Ar-heated charcoal sample 2B

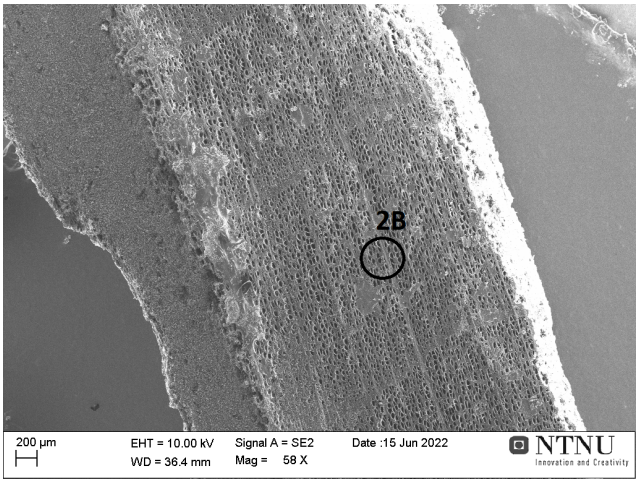

(b) Overview of the sample

Figure 94: The figure shows the enlarged area 2B to the left of the sample heated with argon (left), and an overview of the sample itself (right)

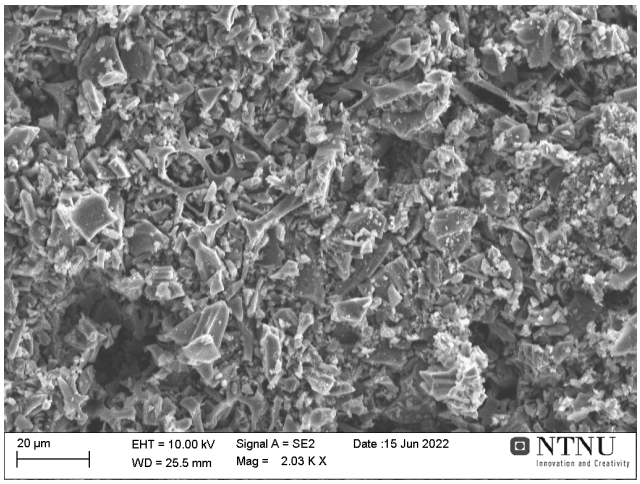

(a) Ar-heated charcoal sample 3D

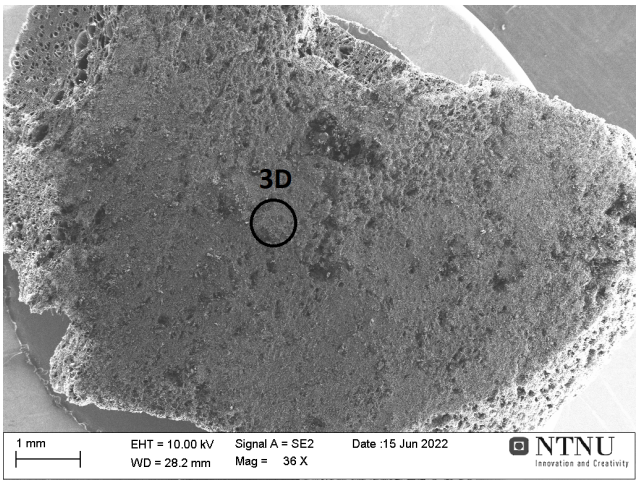

(b) Overview of the sample

Figure 95: The figure shows the enlarged area 3D to the left of the sample heated with argon (left), and an overview of the sample itself (right)

Figure 96a and Figure 96b are images that shows two different areas within the same sample-specimen for the charcoal that is exposed to 10,3 wt% deposited carbon. An overview of the entire sample-surface is shown in Figure 97. As one can see, area marked 2C contains much more unfilled pores than area 2A. The overview-image shows that 2A is located near sample-surface, while 2C is located approximately in the center. Based entirely on this result, one can believe that the porosity is lower at the sample surface than in the centre of the charcoal, and that the deposited carbon does not manage to reach the centre of the charcoal during the densification-process. If one looks at the image showing the porosity-results throughout the sample for another sample with 10,1 wt% deposition (Figure 63), one can see that this sample also experiences higher porosity in the middle, and more deposition one especially one side of the material. This could have to do with the way the sample-specimen was located in the crucible prior to the densification-process. The side of the sample that have experienced more deposition could have been the side that was located closest to the entry where the flow of methane-gas came in.

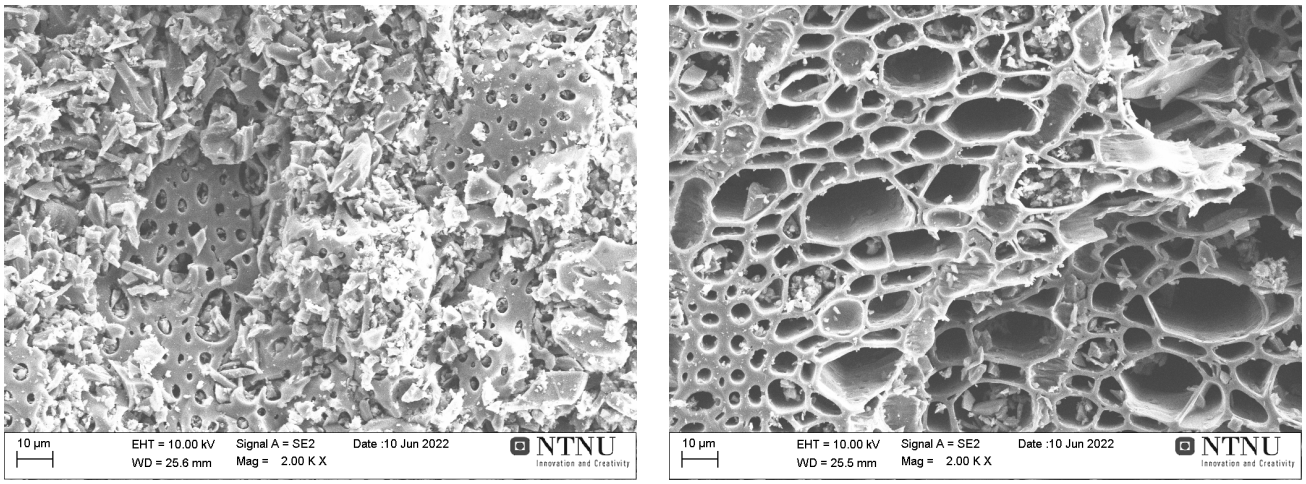

(a) 2A **(b)** 2C

Figure 96: The figure show the difference between are 2A (left) and 2C (right) for the sample with 10,1 wt% deposition

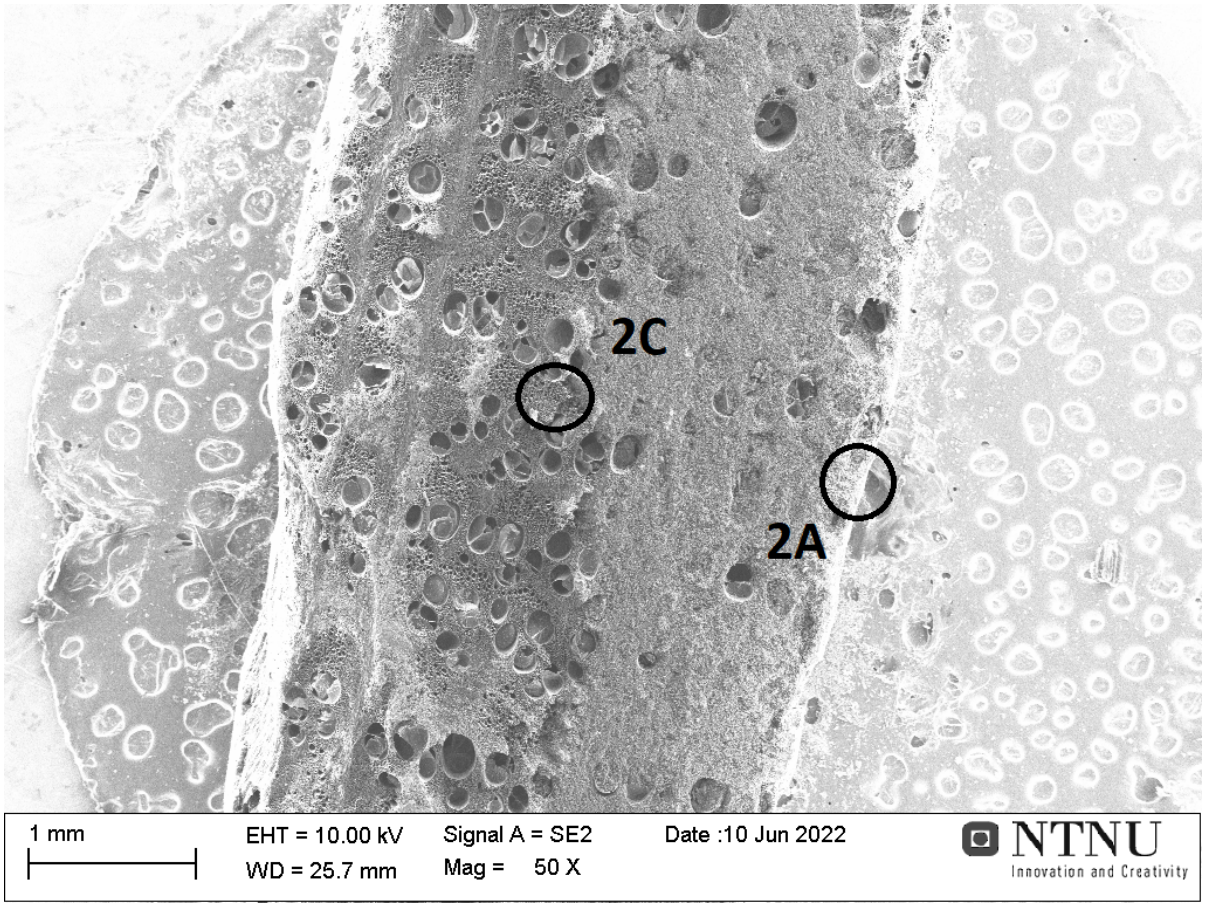

Figure 97: Overview of the sample with 10,1 wt% deposition

If one looks to the sets of charcoal that are exposed to approximately 2 and 3 hours of methane purging (24,0 and 29,7 wt%), one can see clearly that the pore-structure is influenced by the deposited carbon. This is shown in theFigure 98a which shows the magnified image to the left and the overview to the right (2h) and Figure 99 with the equivalent images of the sample with 3 hours of purging.

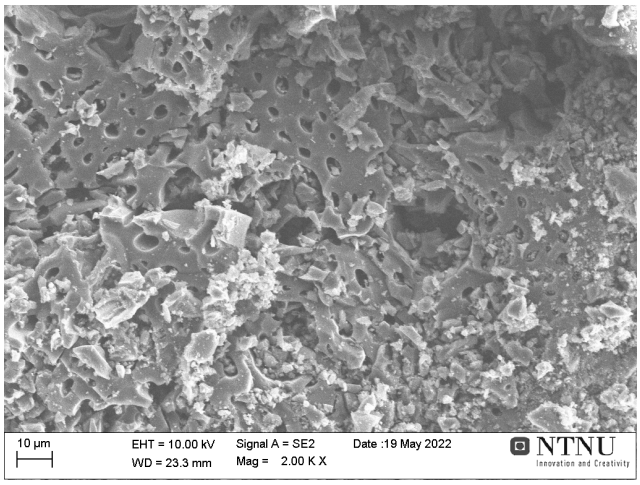

(a) 1G

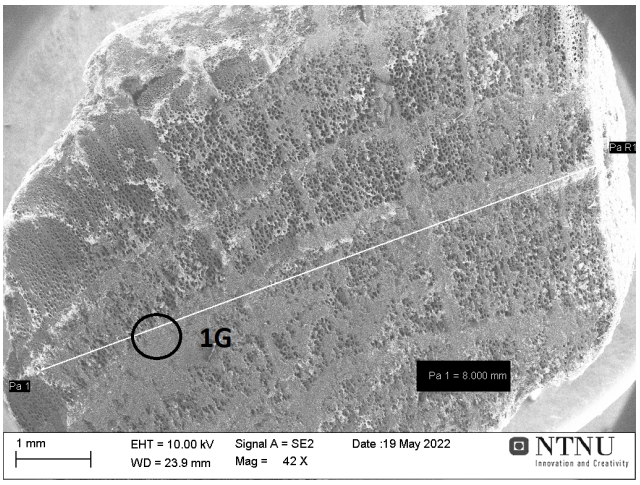

(b) Overview of the 2h-material

Figure 98

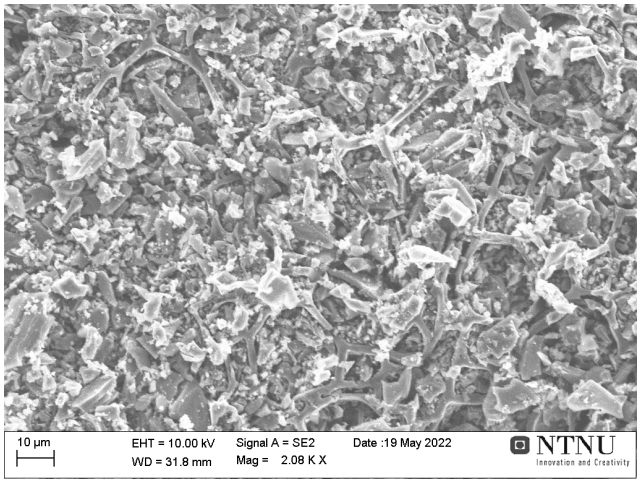

(a) 2B

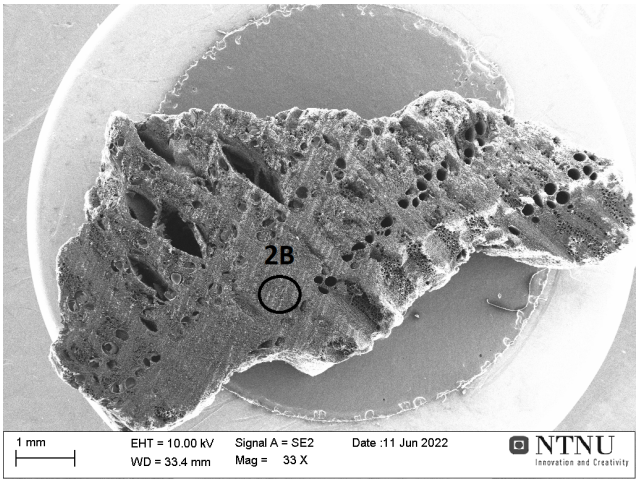

(b) Overview of the 3h-material

Figure 99

The images from the summer-report by Larsen shows how different the shape of the deposited carbon develops as the methane-purging goes on. Figure 100a, Figure 101b, Figure 101a and Figure 101 shows the SEM-images with 2000X magnification of the raw charcoal and the charcoal with 1, 2 and 3 hours of methane-purging, respectively. One can notice that the smooth and clear pore-structure in the image of the raw-charcoal ceases to exist as the methane purging goes on. This is especially clear if one looks at Figure 101b. When the methane-purging moves on to 2 and 3 hours, the deposited methane starts getting a more rounded shape, as shown in the images. In addition it looks like the amount of deposition is increasing very much. whether the rounded shape comes from more deposition of carbon or a longer amount of time at very high temperatures, is unclear.

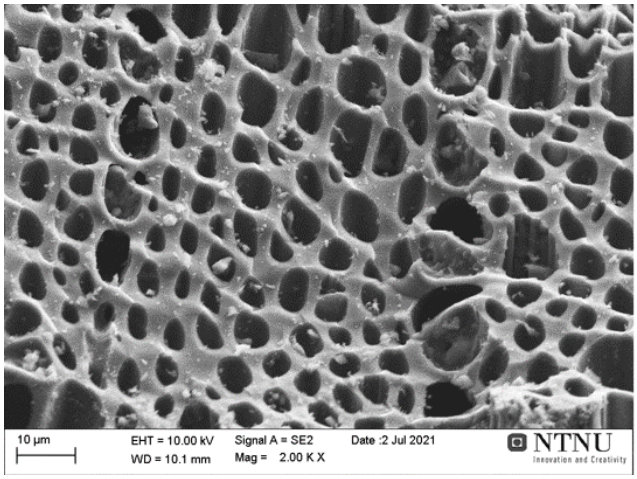

(a) Raw

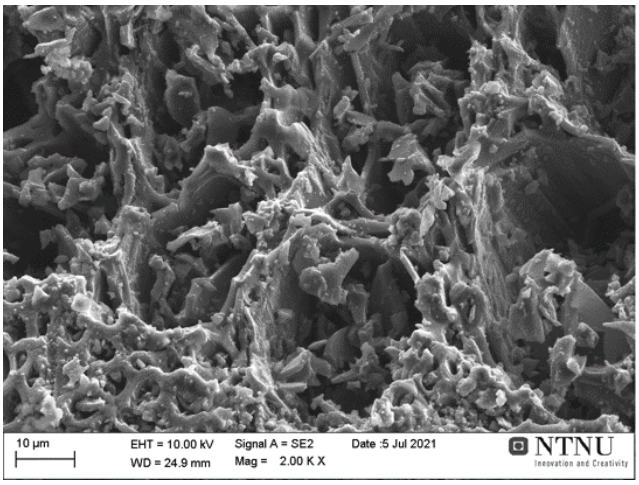

(b) 1h (7,1wt%)

Figure 100

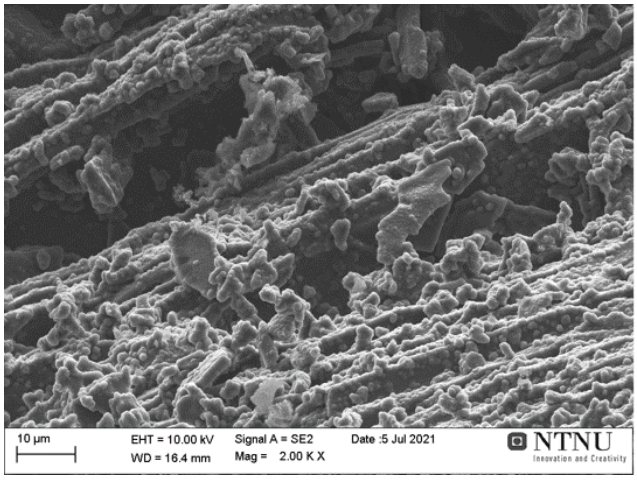

(a) 2h

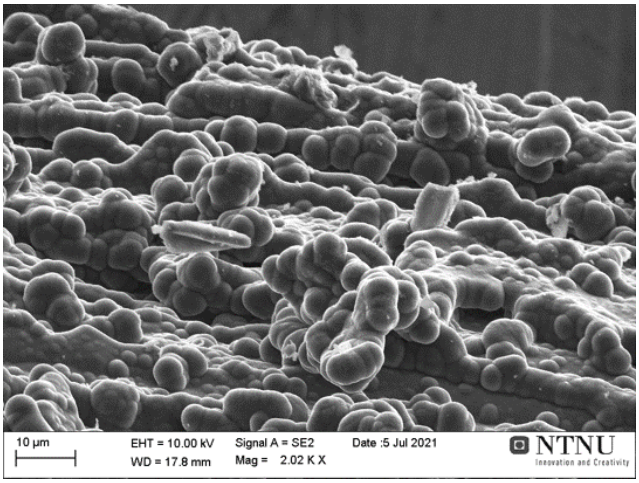

(b) 3h

Figure 101

Asa concluding remark for the discussion about SEM, one can say that there are big variations on the porosity-values for the different degrees of carbon-deposition, so to see the development as a function of purging-time with methane can be challenging. However, several of the figures indicates that the porosity is higher in the centre of the surface compared to the surface on one or both sides of the sample-specimen. This could give an indication on where the sample is located relative to the outlet of the methane-purging, and that for the carbon to penetrate into the core can be challenging at even high degrees of carbon deposition.

5.7 BET surface area

The one BET-experiment performed in the result-section, with a carbon-deposition of 24 wt%, showed a specific surface area of about 1,24 m^2/g, with a relatively low standard deviation. The literature-review of this master-thesis provides a few comparisons regarding this property. If one compares with the works of Nishii [31], one can see that the densified charcoal has a very little surface-area compared to the materials studied there (Figure 7). The closest material is carbon nanofiber (CNF) with a surface area at 270 m^2/g , while materials as carbon black, mesoporous carbon and activated carbon lies in the range of 1500-2200 m^2/g. It should, however, be noted that the mentioned materials were investigated after only 5 minutes of densification at 1173 Kelvin (900 °C), while the charcoal has been purged for approximately 2 hours. As shown in Figure 102, the specific surface area drops rapidly for almost all the mentioned materials when the purging time with methane goes on. At 600 min the specific surface area of carbon nano-fibers are almost down to the level of the charcoal.

The relatively low surface area might explain some of the findings mentioned above with the comparison of the different densification-experiments (Figure 79). According to the figure, there are very small changes in carbon deposition during the first hour compared to the rest of the time-intervals. This can be explained by the literature of Muradov, Smith and T-Raissi from 2005 [29]. In this paper it was found that there was a proportional relationship between the initial rate of methane decomposition (per unit mass) and the specific surface area. It should be noted that the experiments performed in this paper were done on several carbonaceous materials that did not include charcoal, such as activated carbon and carbon black. As one can see in Figure 103, most of the rapid decrease in methane conversion happens during the first 30-40 minutes, and by the first hour, the decrease is stabilized. Although the comparison can be questioned by the fact that these are not the same materials as examined in this master-thesis, it could be interesting with regard to the general trends for carbonaceous materials.

The really low values of specific surface area can also be explained when one looks at the works of

Hussein and co-workers [Hussein et. al 2016] [12], which studied heat-treatment of small portions of charcoal with only argon to see the results in physical structure. As already shown in Figure 22, the surface area has a sudden and rapid decrease in surface area when exposed to temperatures above 800 °C. This is when investigated with N_2-gas. As this investigation was also done on charcoal, this shows that it is not only the deposition of carbon that can cause the very low specific surface area, but also a reformation of the surface-structure due to longer heat-treatments.

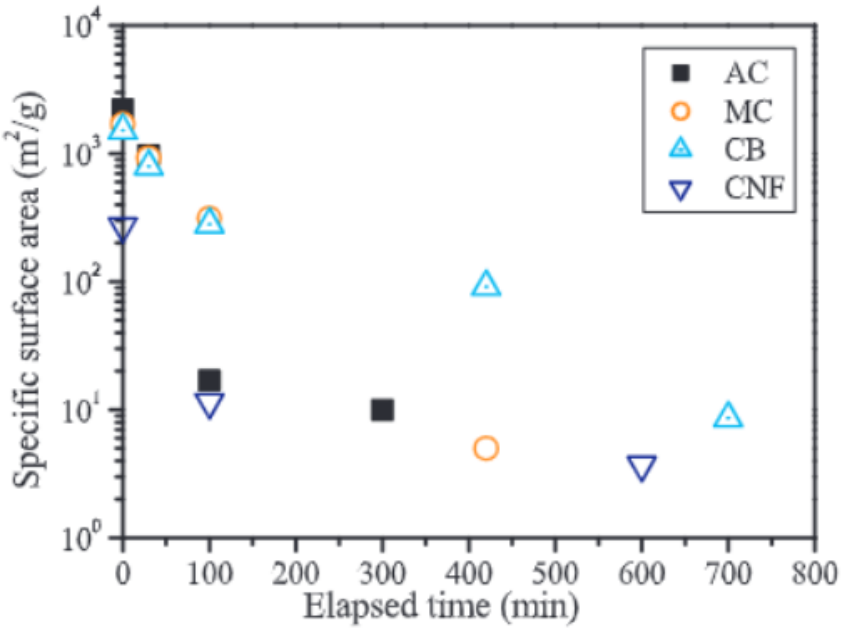

Figure 102: The figure shows the change in the specific surface area as a function of elapsed decomposition-time at 1173K, and SV = 360 h^{-1}[31]

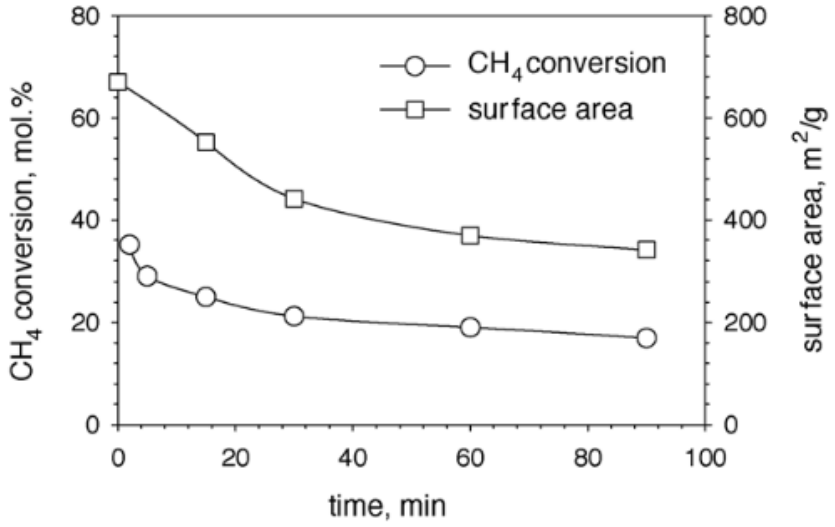

Figure 103: The figure shows the development of methane conversion and surface area as a function of reaction time for the experiments of Muradov [29]

5.8 Industrial relevance

5.8.1 Material balance

The figure below (Figure 104) shows the different outflows and inflows of materials when it comes to the densification-process with 3 hours of methane-purging (29,7wt%).

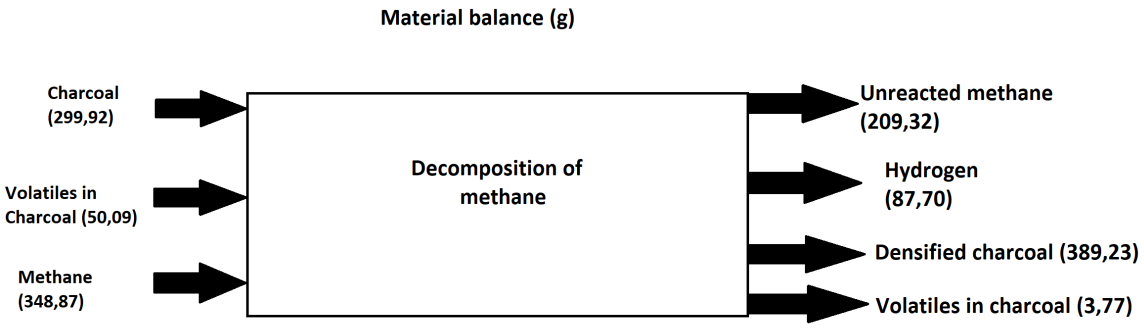

Figure 104: The figure shows the material-balance for the densification-process of the sample with 29,7 wt% deposited carbon.

As one can see in the future, the volatile-contents for both the raw charcoal and the densified charcoal are both treated as separate flows. This is done in order to get a good distinction between the different chemical compounds. These values are calculated based on the fraction-values provided by Sintef Norlab (Table 5). If one compared the total outflows with the total inflows in the process, the following equation can be made:

$$\mathrm{m_{net}} = \mathrm{m_{out}} - \mathrm{m_{in}} = 698,87\mathrm{g} - 690,02\mathrm{g} \tag{5.4}$$

$$\mathrm{m_{net}} = 8,85\mathrm{g} \tag{5.5}$$

According to this calculations, 1,27 % is lost after the densification-process. This is within the limit of the uncertainty related to the analysis and the measuring-method. In addition, carbon-dust might go out with the outlet-gas during the experiment.

5.8.2 Energy balance

As mentioned before, decomposition of methane is a highly beneficial reaction when it comes to reduction of polluting gasses. The reaction is also considered highly relevant when it comes to energy-efficiency because of its production of hydrogen. To get an overview of the inputs and outputs of the energy consumption related to the process, an energy-balance is made in the system below (Figure 105). This system is made based in the different standard formation-enthalpies of the different compounds participating in the reaction, and the different values are shown in the table (Table 7).

Table 7: Table showing the standard enthalpy of formation of the relevant compounds.

Compound	ΔH_f° (kJ/mol))
$CH_{4(g)}$	-74,0
$H_{2(g)}$	0
$C_{(s)}$	0

As can be shown in the figure, the following reaction happens:

$$CH_{4,\text{in}} + C_{(s),\text{in}} + E_{\text{el}} \rightarrow CH_{4,\text{out}} + H_2 + C_{(s),\text{out}} \tag{5.6}$$

In this reaction, $C_{(s),in}$ represents the charcoal which is placed in the proximity of the reaction, and that is meant to be densified. $CH_{4,in}$ is naturally the inlet methane, while E_{el} is the electrical energy needed for the reaction. Since the conversion of methane reacted in the experiment is not 100%, some amount of methane proceed through the furnace, and ends up as outflow, hence $CH_{4,out}$ in the reaction. H_2 and $C_{(s),out}$ represents the produced hydrogen and carbon, respectively.

In the figure, the energy-balance was performed on the sample that had been purged with methane-gas for approximately 3 hours, with a carbon deposition at 29,7 wt%. The calculations of the different energy inputs- and outputs related to this process are as follows:

$$E_{CH_{4,\text{in}}} = n_{CH_{4,\text{in}}} \cdot \Delta H_f^\circ(CH_4) \tag{5.7}$$

$$E_{C_{(s),\text{in}}} = n_{C_{(s),\text{in}}} \cdot \Delta H_f^\circ(C_{(s)}) \tag{5.8}$$

$$E_{CH_{4,\text{out}}} = (1-\eta) \cdot n_{CH_{4,\text{in}}} \cdot \Delta H_f^\circ(CH_4) \tag{5.9}$$

$$E_{H_2} = 2 \cdot \eta \cdot n_{CH_{4,\text{in}}} \cdot \Delta H_f^\circ(H_2(g)) \tag{5.10}$$

$$E_{C_{(s),\text{out}}} = n_{CH_{4,\text{in}}} \cdot \eta \Delta H_f^\circ(C_{(s)}) \tag{5.11}$$

All these calcualtions can then be used to calculate the electric energy needed to be supplied:

$$E_{\text{el}} = E_{CH_{4,\text{out}}} + E_{C_{(s),\text{out}}} + E_{H_2} - E_{CH_{4,\text{in}}} - E_{C_{(s),\text{in}}} \tag{5.12}$$

In the calculations n_x represents the amount of mole of the chemical compound x, while η represents the fraction of methane that reacts and decomposes in the process.

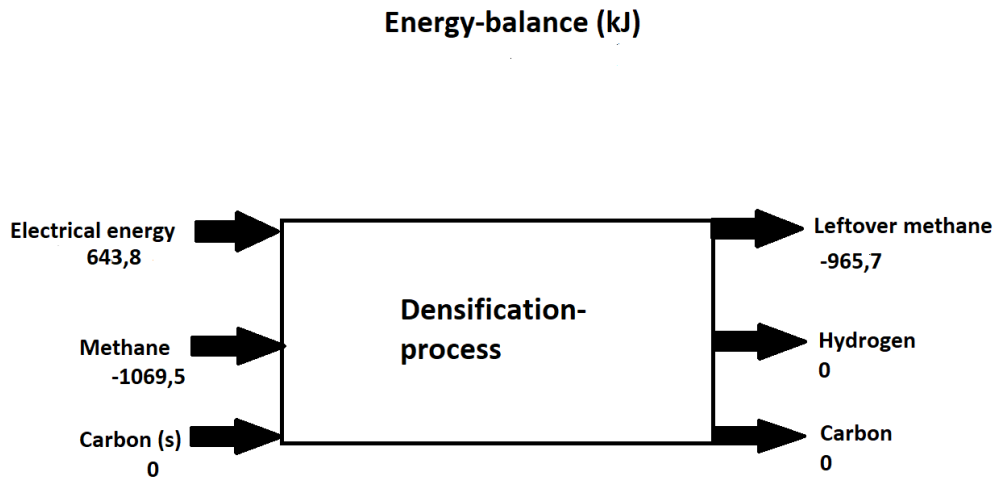

Figure 105: The figure shows the energy-balance for the densification-process of the sample with 29,7 wt% deposited carbon.

The values shown in Figure 105 corresponds to an electric input-energy of **0,52 kwh / kg C input in the furnace**

To get an overview of the relationship between the energy used in the process and the potential energy that can be extracted from the produced hydrogen, is made. To do these calcualtions, the value of the higher heating value (HHV) for hydrogen. For hydrogen, this value is 887 kJ/mol CH_4[38]. To calculate the total combustion energy of the hydrogen (E_C) the following equation was used.

$$\mathrm{E_C} = \mathrm{n_{CH_{4,in}}} \cdot \eta \cdot \mathrm{E_{HHV,H_2}} \tag{5.13}$$

$$\mathrm{E_C} = 21,75\mathrm{mol} \cdot 0,4 \cdot 887\mathrm{kJ/molCH4} \tag{5.14}$$

$$\mathrm{E_C} = 7716,9\mathrm{KJ} \tag{5.15}$$

The total energy gain (E_{gain}) of the reaction is then:

$$\mathrm{E_{gain}} = \mathrm{E_C} - \mathrm{E_{el}} = 7073,1\mathrm{kJ} \tag{5.16}$$

This is equivalent to **5,58 kwh/kg C input in the furnace.**

The decomposition of methane is a process that can have both advantages and limitations seen from an energetic point of view. The advantages are :

- Deposited C will be a more environmental-friendly choice compared to metallurgical coke. The methane could come from biogas, but even if it came from fossil natural gas, it would still have been better, since one then can avoid the coke-process, which leads to great emissions of CO_2
- Better raw materials with less CO_2-reactivity.

However, one of the main disadvantages to this process is increased energy consumption and increased cost. The main conclusion regarding energy-balance is that the densification-process creates better charcoal, creates hydrogen-gas, but will lead to increased energy-consumption and cost.

6 Conclusion

What has been shown in this article is that heat-treatment and densification through methane decomposition has various effects on some of the physical properties of charcoal. The highest degree of densification that was achieved in this work was an increase of mass of 29,7 wt% due to methane deposition. For this sample, methane was purging for 177 minutes. The experimental results of these experiments seem to have a linear relationship between the purging-time and the amount of deposited carbon, but if one compares with literature, one can see that the variations of carbon deposition can be substantial due to variations in reaction temperature. Another important factor seems to be the distribution of particle-size, because of variations in access to the purged methane due to locations, which again will affect the overall carbon-deposition. When it comes to the fraction of methane-conversion, it is difficult to draw a conclusion based on purging-time, reaction temperature and size-distribution. But the fact that at temperatures above 1070 °C, 5 out of 7 experiments show a conversion-value higher than 35 % tell something about the lower limit of temperature for this range of conversion-fraction. The results of the compression-testing showed big variations, both parallel and perpendicular to the fiber-direction, but based on the graphs one were able to see that the effect on compression strength of heating with argon was greater and more substantial than of the densification-process, possibly due to rearrangement in the structure, which increased the strength of the material. The effect of argon-heating had a greater impact on the abrasive strength as well, compared to the effect of methane-decomposition. The results of porosity by measuring absolute and apparent density show a trend towards decreasing porosity with increasing carbon-deposition, although big variations. The difference in porosity between raw charcoal and argon-heated charcoal is not so easy to see, because of the relatively high standard deviation. One can see that the ar-heating and the methane decomposition has an decreasing

effect on the absolute density, which rearrangement in the structure due to heating, but it also indicates that the density of the deposited carbon is lower than the density of the raw charcoal. The porosity-values with respect to SEM and ImageJ show big variations for the different degrees of densification and heating. However, there might be possible to see indications that the porosity increases towards the centre of the material, compared to the edges. There might also be possible to see that some sides of the material receives more methane-purging than the opposite side, which indicates something about the location of the samples in the furnace. The porosity also depends of the different structures within each material. Due to experimental challenges, only one of the samples were exposed to BET surface-examination, and this sample showed a very low value of specific surface area (1,24 m^2/g). This is very low compared to value in the literature, although these values were from other carbonaceous materials. Regarding the material- and energy-balances, the results showed us that the densification-process experienced a loss of mass of about 1,3 %, which was within the limits of uncertainty. The energy-balance show that the densification-process creates better charcoal, creates hydrogen-gas, although it demands an electric energy-consumption of 0,52 kwh / kg C input in the furnace.

7 Further work

As apart of the future works it would be interesting to examine the long time effects of densification of chacoal using decomposition of methane. That is, to let the methane-purging go one for more than 3 hours to see if one can reach the so-called saturation-time. Another thing that would be interesting to examine is how the process for examination of the BET surface-are could be improved, so that the leak-error that has occurred in this work could be avoided.

References

[1] Hazzim F Abbas and WMA Wan Daud. "Hydrogen production by thermocatalytic decomposition of methane using a fixed bed activated carbon in a pilot scale unit: apparent kinetic, deactivation and diffusional limitation studies". In: *International journal of hydrogen energy* 35.22 (2010), pp. 12268–12276.

[2] Michael Jerry Antal and Morten Grønli. "The art, science, and technology of charcoal production". In: *Industrial & Engineering Chemistry Research* 42.8 (2003), pp. 1619–1640.

[3] A.G. Blackman et al. *SI Chemical Data , 7th edition*. John Wiley Sons Australia, Ltd, 2014.

[4] PR Blankenhorn, GM Jenkins, and DE Kline. "Dynamic mechanical properties and microstructure of some carbonized hardwoods". In: *Wood and Fiber Science* 4.3 (1972), pp. 212–224.

[5] Tony J Collins. "ImageJ for microscopy". In: *Biotechniques* 43.S1 (2007), S25–S30.

[6] AR Coutinho, JD Rocha, and CA Luengo. "Preparing and characterizing biocarbon electrodes". In: *Fuel processing technology* 67.2 (2000), pp. 93–102.

[7] Halvor Dalaker and Pål Tetlie. "Decomposition of methane during oxide reduction with natural gas". In: *Celebrating the Megascale*. Springer, 2014, pp. 537–546.

[8] Zeyu Fan et al. "Catalytic decomposition of methane to produce hydrogen: A review". In: *Journal of Energy Chemistry* 58 (2021), pp. 415–430.

[9] Laurent Fulcheri and Yvan Schwob. "From methane to hydrogen, carbon black and water". In: *International journal of hydrogen energy* 20.3 (1995), pp. 197–202.

[10] Morten G Groenli. "A theoretical and experimental study of the thermal degradation of biomass". In: (1996).

[11] Jeffrey R Hook. "An introduction to porosity". In: *Petrophysics-The SPWLA Journal of Formation Evaluation and Reservoir Description* 44.03 (2003).

[12] Asem Hussein et al. "Effects of heat treatment and acid washing on properties and reactivity of charcoal". In: *Biomass and Bioenergy* 90 (2016), pp. 101–113.

[13] Nina Hwang and Andrew R Barron. "BET surface area analysis of nanoparticles". In: *The Connexions project* (2011), pp. 1–11.

[14] Micrometrics Inc. *AccuPyc II: Gas Displacement Pycnometry System*. 2022. URL: https://www.micromeritics.com/accupyc-ii/ (visited on 04/26/2022).

[15] Micrometrics Inc. *Density*. 2022. URL: https://www.micromeritics.com/particle-testing/analytical-testing/density/ (visited on 06/26/2022).

[16] Micrometrics Inc. *Flex 3Flex - Surface Area, Porosity, Chemisorption, and Temperature Programmed Methods*. 2022. URL: https://www.micromeritics.com/3flex/ (visited on 04/26/2022).

[17] BJ Inkson. "Scanning electron microscopy (SEM) and transmission electron microscopy (TEM) for materials characterization". In: *Materials characterization using nondestructive evaluation (NDE) methods*. Elsevier, 2016, pp. 17–43.

[18] Hamideh Kaffash, Gerrit Ralf Surup, and Merete Tangstad. "Densification of Biocarbon and Its Effect on CO2 Reactivity". In: *Processes* 9.2 (2021), p. 193.

[19] Hamideh Kaffash and Merete Tangstad. "The Effect of Densification on Compressive Strength of Charcoal". In: *Available at SSRN 3926700* (2021).

[20] Andrew K Kercher and Dennis C Nagle. "Microstructural evolution during charcoal carbonization by X-ray diffraction analysis". In: *Carbon* 41.1 (2003), pp. 15–27.

[21] Marius Larsen. "Densification of charcoal and its characterization". In: *Summerjob-report, Department of Materials Science and Engineering (NTNU)* 08.01 (2021).

[22] Marius Larsen. "TMT4500 - Materials Technology, Specialization Project: Densification of charcoal". In: *Specialization project, Department of Materials Science and Engineering (NTNU)* 47.01 (2021).

[23] Aik Chong Lua, Fong Yow Lau, and Jia Guo. "Influence of pyrolysis conditions on pore development of oil-palm-shell activated carbons". In: *Journal of analytical and applied pyrolysis* 76.1-2 (2006), pp. 96–102.

[24] DM Mackay and PV Roberts. "The influence of pyrolysis conditions on yield and microporosity of lignocellulosic chars". In: *Carbon* 20.2 (1982), pp. 95–104.

[25] T Marquardt, A Bode, and S Kabelac. "Hydrogen production by methane decomposition: Analysis of thermodynamic carbon properties and process evaluation". In: *Energy Conversion and Management* 221 (2020), p. 113125.

[26] William Shu Lai Mok et al. "Formation of charcoal from biomass in a sealed reactor". In: *Industrial & engineering chemistry research* 31.4 (1992), pp. 1162–1166.

[27] B Monsen et al. "Charcoal for manganese alloy production". In: *Proceedings of the INFACON XI, New Delhi, India* (2007), pp. 18–21.

[28] N1 Muradov. "Catalysis of methane decomposition over elemental carbon". In: *Catalysis communications* 2.3-4 (2001), pp. 89–94.

[29] Nazim Muradov, Franklyn Smith, T Ali, et al. "Catalytic activity of carbons for methane decomposition reaction". In: *Catalysis Today* 102 (2005), pp. 225–233.

[30] Nazim Muradov et al. "Production and characterization of Lemna minor bio-char and its catalytic application for biogas reforming". In: *Biomass and Bioenergy* 42 (2012), pp. 123–131.

[31] Haruki Nishii et al. “Catalytic activity of several carbons with different structures for methane decomposition and by-produced carbons”. In: *Applied Surface Science* 473 (2019), pp. 291–297.

[32] Adetoyese Olajire Oyedun, Ka Leung Lam, and Chi Wai Hui. “Charcoal production via multistage pyrolysis”. In: *Chinese Journal of Chemical Engineering* 20.3 (2012), pp. 455–460.

[33] Webb P. and Orr C. *Analytical methods in Fine Particle Technology*. Micrometrics Instrument Corporation, 1997.

[34] Helmut Schwarz. “Chemistry with methane: concepts rather than recipes”. In: *Angewandte Chemie International Edition* 50.43 (2011), pp. 10096–10115.

[35] F Shimazu and C Sterling. “Effect of wet and dry heat on structure of cellulose”. In: *Journal of Food Science* 31.4 (1966), pp. 548–551.

[36] Emma Solhaug. “Densified biocarbon and the effect of potassium on the CO $_2$-reactivity”. In: *Specilization-project, Department of Materials Science and Engineering (NTNU)* 88.01 (2021).

[37] Emma Solhaug. “Different methods for K-impregnation of Charcoal and the effect on the CO_2 reactivity”. In: *Summer-project, Department of Materials Science and Engineering (NTNU)* 32.01 (2021).

[38] Meyer Steinberg. “The HY-C process (thermal decomposition of natural gas:) Potentially with the lowest cost source of hydrogen with the least $CO_2 - emission$”. In: *Brookhaven national laboratory Upton, NY 11973* (1994).

[39] I Suelves et al. “Carbonaceous materials as catalysts for decomposition of methane”. In: *Chemical Engineering Journal* 140.1-3 (2008), pp. 432–438.

[40] Gerrit Surup et al. “Characterization of renewable reductants and charcoal-based pellets for the use in ferroalloy industries”. In: *Energy* 167 (2019), pp. 337–345.

[41] Javier I Villacampa et al. “Catalytic decomposition of methane over Ni-Al2O3 coprecipitated catalysts: Reaction and regeneration studies”. In: *Applied Catalysis A: General* 252.2 (2003), pp. 363–383.

A Appendix

A.1 Apparent density

% deposition	volume (cm)	mass (g)	density (g/cm^3)
0	0,576	0,293	0,509
0	0,81	0,544	0,672
0	0,56	0,357	0,638
0	0,48	0,241	0,502
10,3	0,65	0,289	0,445
10,3	0,57	0,508	0,891
10,3	0,42	0,151	0,360
10,3	0,72	0,374	0,519
11,1	0,384	0,215	0,560
11,1	1,296	0,79	0,610
11,1	0,792	0,515	0,650
11,1	0,432	0,201	0,465
24,0	0,91	0,514	0,565
24,0	1,19	0,653	0,549
24,0	0,637	0,487	0,765
24,0	0,22	0,242	1,1
29,7	0,264	0,237	0,898
29,7	0,42	0,34	0,81
29,7	0,33	0,246	0,745
29,7	0,462	0,202	0,437
0	0,56	0,352	0,629
0	0,32	0,24	0,75
0	0,36	0,207	0,575
0	0,36	0,178	0,494

Table 8: Results from the calculations of the apparent densities. The four last rows are the values for argon-heated charcoal

A.2 BET surface plot values

Relative Pressure (p/p^0)	Quantity Adsorbed ($cm^3/gSTP$)	$1/[Q(p^0/p-1)]$
0,059690206	0,2842	0,223390
0,079793432	0,2957	0,293203
0,099679188	0,3058	0,362100
0,119742661	0,3146	0,432365
0,139702748	0,3250	0,499672
0,159492476	0,3345	0,567325
0,179476740	0,3438	0,636226
0,199619916	0,3546	0,703395
0,249186810	0,3761	0,882550
0,299560138	0,3997	1.070005

Table 9: Results from the BET surface plot

Marius Larsen

Densification of charcoal by thermal decomposition of methane

NTNU
Norwegian University of
Science and Technology